

Singapore American School

# Journal of Mathematics

Vol.1

Matrices, Pixels, and RGB  
Exploring Recursive  
Sequences with Eigenvalues  
and Eigenvectors  
An Introduction to  
Combinatorial Partitions  
Calculating Implied  
Volatility using the  
Black-Scholes Model  
Countably and Uncountably  
Infinite Sets

Introduction to Chaos Theory  
Investigating the Theoretical  
and Practical Applications of  
Fractals  
Singular Value  
Decomposition and a  
Recommendation  
Algorithm  
Natural Eigenvectors in High  
Number Systems  
Evaluating Epidemiological  
Solutions through  
S-I-R Modeling



## EDITOR'S LETTER

Welcome to our groundbreaking project that brings together math enthusiasts to dive into the depths of diverse mathematical concepts and applications! This mini-mathematical journal that showcases the passion and expertise of our math club members. We want to provide an opportunity for everyone in the school community to engage with the exciting and fascinating world of math.

Through this journal, readers will discover innovative and insightful research articles that delve into a wide range of mathematical topics. We aim to make these complex ideas accessible to all, without sacrificing academic rigor.

We invite you to join us on this exciting journey as we pave the way for a vibrant and stimulating mathematics-focused community at our school!

Gyulim Jessica Kang,  
Frank Xie  
Editors-in-Chief

# CONTENTS

Singapore American School Journal of Mathematics

Editor's Letter	03	Contributors	88
Table of Contents	04	Student Authors	89

**06** **Matrices, Pixels, and RGB**  
Hyeonsoo Kwon

**11** **Exploring Recursive Sequences with Eigenvalues and Eigenvectors**  
Akshay Agarwal

**15** **An Introduction to Combinatorial Partitions**  
Akshay Agarwal

**22** **Calculating Implied Volatility using the Black-Scholes Model**  
Benjamin Cheong

**27** **Countably and Uncountably Infinite Sets**  
Benjamin Cheong

**32** **Introduction to Chaos Theory: History Examples, Applications**  
Sunghan Billy Park

**36** **Investigating the Theoretical and Practical Applications of Fractals**  
Doy Yun, Munira Takalkar

**43** **Singular Value Decomposition and a Recommendation Algorithm**  
Frank Xie

**49** **Natural Eigenvectors in High Number Systems**  
Gaurav Goel

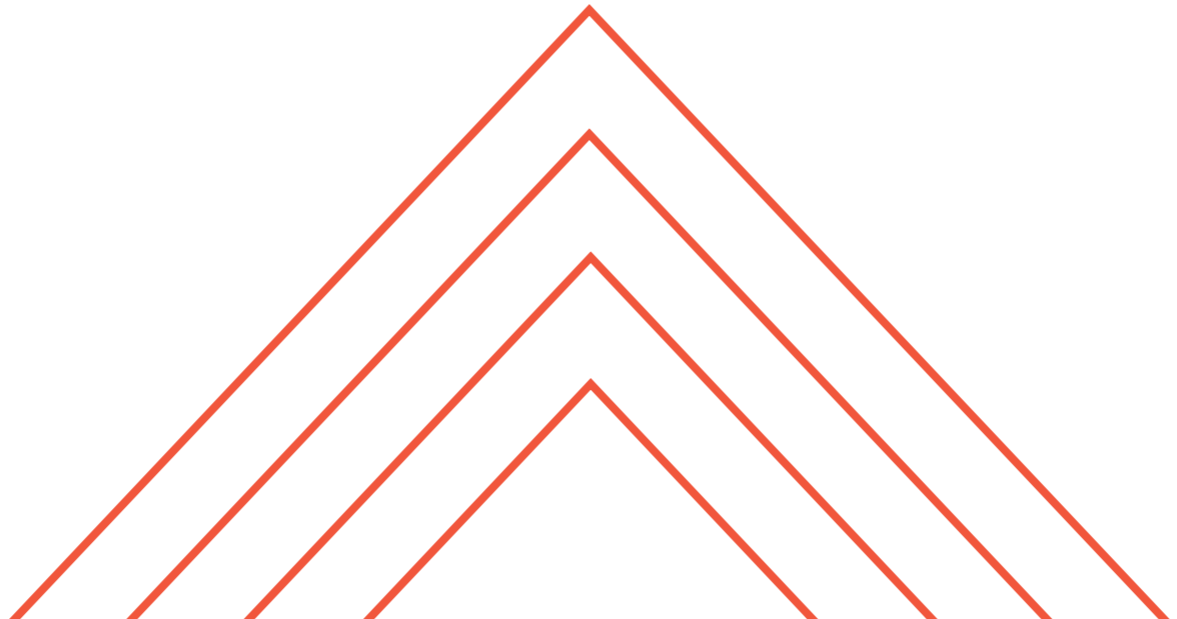
**55** **Evaluating Epidemiological Solutions through S-I-R Modeling**  
Gaurav Goel

**64** **Finding an Alternate Model to Malthusian Population Growth Model**  
Irene Choi, Morgan Ahn, Vyjayanti Vasudevan

**69** **Application of Eigenvectors and Eigenvalues: SVD Decomposition in Latent Semantic Analysis**  
Gyulim Jessica Kang

**77** **Creating a Machine Learning Pipeline to Perform Topological Data Analysis**  
Gyulim Jessica Kang

**82** **Evaluating Affirmative Action in School Choice: Comparing Mechanisms with Minority Reserves**  
Gyulim Jessica Kang



## Matrices, Pixels, and RGB (ATLA Project)

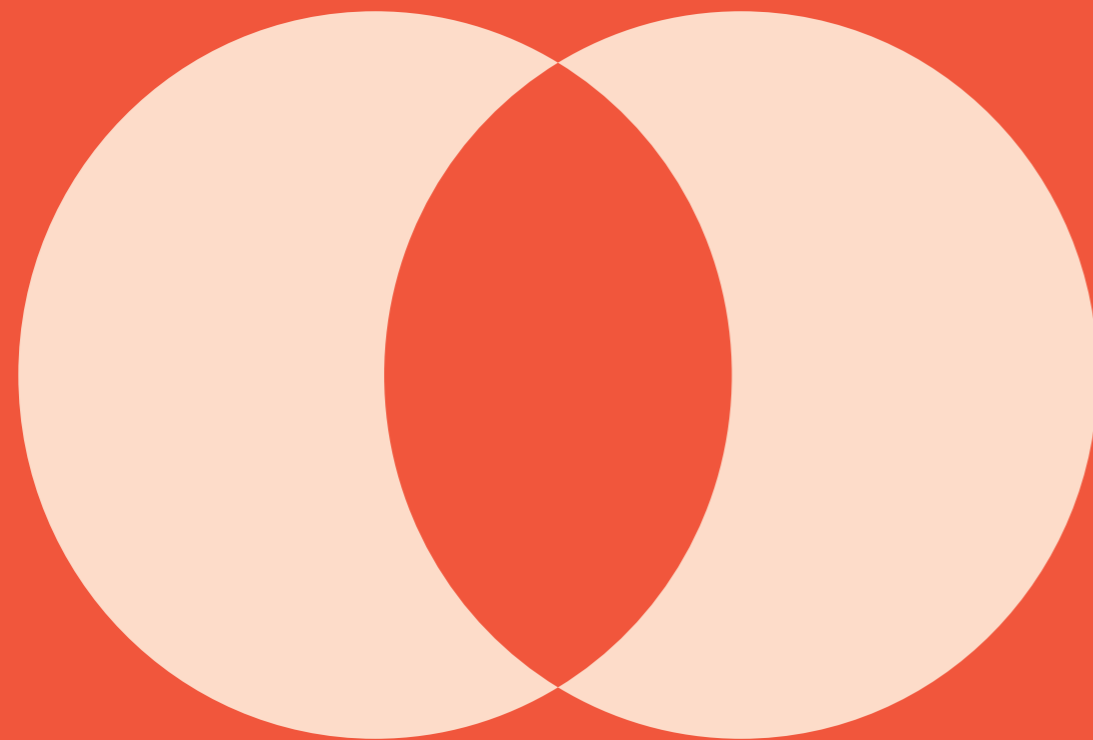
Hyeonso Kwon

kwon49627@sas.edu.sg

Teacher Reviewers:  
Mr. Zitur, Mr. Craig

# 01 Matrices, Pixels, and RGB

Written by Hyeonso Kwon



### Abstract

From Instagram to Tiktok, social media has grown to be an intrinsic part of modern society today. Out of many, one of its most prominent features that caught my attention was the different types of face filters installed in cameras of social media apps. With social media, there is no limit to how you want your photos to look. I thought this was particularly interesting. Using the concepts of matrix manipulation of RGB excel pixels, I decided to go a step further and explore the application of matrix calculations in creating face filters.

*Keywords:* matrices, RGB, Gaussian blur

### 1 Pixel Project

Let's break down the basic principles of how the pixels of images work in Excel. When digital photos are turned into excel spreadsheets, each pixel is divided into three RGB values: The amount of red, green, and blue stored in the pixel. Therefore, performing matrix multiplication to each pixel's set of RGB values allows us to manipulate the values in the photos and change how they appear on the screen.



Figure 1: Overlaying a vintage filter on an image

Here, I was able to create a color filter by breaking the image above into pixels and multiplying the portion of the values of this image by the portion of the values of the original image. The formula used to perform this calculation was  $DA1\$A\$228 + (1 - \$A\$228) HA1$ , where DA1 was the location of the first pixel of the original image and HA1 was the location of the first pixel of the "filter." Essentially, what

this calculation is doing is scaling down the RGB matrix of the original image to a certain level (for example, 0.5), scaling down the RGB matrix of the filter to a number that is the scale factor of the RGB matrix of the original image subtracted from 1 (which in this case would be 0.5), and adding the two matrices together to create a new matrix that is the result of the matrix calculation. To put this into the perspective of number calculations, let's say one of the pixel values of the original image has an RGB matrix of [206, 192, 175], and one of the pixel values of the filter has an RGB matrix of [189, 131, 120].

$$A = \begin{pmatrix} 206 \\ 192 \\ 175 \end{pmatrix}, B = \begin{pmatrix} 189 \\ 131 \\ 120 \end{pmatrix};$$

$$0.5 \cdot A = \begin{pmatrix} 103 \\ 96 \\ 87.5 \end{pmatrix}$$

$$0.5 \cdot B = \begin{pmatrix} 94.5 \\ 65.5 \\ 60 \end{pmatrix}$$

$$0.5 \cdot A + 0.5 \cdot B = \begin{pmatrix} 197.5 \\ 161.5 \\ 147.5 \end{pmatrix}$$

206	189	197.5
192	131	161.5
175	120	147.5

Figure 2:  $A$ ,  $B$ , and  $0.5 \cdot A + 0.5 \cdot B$

I wanted to use these concepts to create filters that somewhat imitate the actual filters that can be seen in social media apps.

### 2 Extension 1

I first converted two photos into RGB pixels and pasted them onto Excel.

I decided to set the opacity to 50% as it made the most sense. Then, I used the formula



Figure 3: 2 images of Audrey Hepburn

$A1 * \$A\$611 + (1 - \$A\$611) * HA1$  (the column and row number changes for each pixel) which sets the opacity of the photos to 50% and combine them together to create a single image. This process allowed me to generate an average face between the younger and older version of Audrey Hepburn. I was aiming to imitate the filters that take your baby face and create a hypothetical version of your older self.



Figure 4: Blended image of Audrey Hepburn

### 3 Investigation 2/Extension 2 (Coding)

For my second extension, I wanted to create a filter with coding that imitates the Photoshop filters like face brightening or mirroring effects. To achieve this, I used basic matrix calculation principles like matrix addition and multiplying the inverse of an identity matrix. For the brightening effect, I used the following formula:

$$A = \begin{pmatrix} a_{11} & \dots & a_{1n} \\ \vdots & \ddots & \vdots \\ a_{m1} & \dots & a_{mn} \end{pmatrix} + \begin{pmatrix} b_{11} & \dots & b_{1n} \\ \vdots & \ddots & \vdots \\ b_{m1} & \dots & b_{mn} \end{pmatrix}$$

$$= \begin{pmatrix} a_{11} + b_{11} & \dots & a_{1n} + b_{1n} \\ \vdots & \ddots & \vdots \\ a_{m1} + b_{m1} & \dots & a_{mn} + b_{mn} \end{pmatrix}$$

This is because the colors get brighter approach white as the RGB values get closer to 255. For example, if a pixel in the original image had the RGB values of [100 100 100], and a matrix of [30 30 30] was added, the result would be [130 130 130] pixel would achieve a greater RGB value thus a lighter color. Here, matrix **A** represents the RGB values of the original image, and matrix **B** represents the "filter". I used the inverse of the identity matrix to create a mirroring filter. This matrix allows the values in the matrix to be mirrored like the example below. Here, you can see that multiplying the inverse of the identity matrix flips the location of  $a$   $c$  and  $b$   $d$ .

$$I' = \begin{pmatrix} 0 & \dots & 0 & 1 \\ \vdots & \ddots & \ddots & \vdots \\ 0 & \dots & \dots & 0 \\ 1 & 0 & \dots & 0 \end{pmatrix}$$

$$\begin{pmatrix} a & b \\ c & d \end{pmatrix} \cdot \begin{pmatrix} 0 & 1 \\ 1 & 0 \end{pmatrix} = \begin{pmatrix} 0+b & a+0 \\ 0+d & c+0 \end{pmatrix}$$

$$= \begin{pmatrix} b & a \\ d & c \end{pmatrix}$$

I thought it was particularly interesting and decided to employ this method to try mirroring images as well using the same principle.

```
1 # Whitening skin
2 img = cv2.imread("face.jpg", cv2.IMREAD_COLOR)
3 mag = img.shape
4
5 whiten = np.zeros((mag[0], mag[1], 3))
6
7 whiten[:, :, 0] = np.ones ([mag[0], mag
8 [1]])*30
9 whiten[:, :, 1] = np.ones ([mag[0], mag
10 [1]])*30
11 whiten[:, :, 2] = np.ones ([mag[0], mag
12 [1]])*30
13
14 cv2.imwrite('whiten.jpg', whiten)
15 whiten = cv2.imread("whiten.jpg", cv2.IMREAD_COLOR)
16
17 applied = cv2.add(img, whiten)
18 cv2.imshow('original', img)
19 cv2.imshow('applied', applied)
20
21 print(mag)
22 # display image for 20 seconds
23 cv2.waitKey(20000)
24 cv2.destroyAllWindows()
25
26 (6720, 4480, 3)
```

The printed value from the second box (6720, 4480, 3) shows the size of the matrix of the photos. This means that the original photo had three matrices with the size of 6720 x 4480, each matrix being either the red, green, or

blue component of the pixels. With this original matrix, **A**, the filter matrix, **B**, would also be 6720 x 4480 with the same value (in this case, it's 30) in all entries. This snippet of code allows the image to gain higher RGB values following the matrix addition rule. Thus, the **B** matrix has to be added to all three matrices of **A**, and the three matrices altogether show the final image.



Figure 5: Original (L) After adding filter (R)

The second step was to create a mirroring filter that reverses the image. In Unit 1, while doing the cartoon project, the matrix that allowed the plots to be reflected against the  $y$ -axis was the following matrix.

$$C = \begin{pmatrix} -1 & 0 \\ 0 & 1 \end{pmatrix}$$

However, because we are dealing with RGB values in this project, this matrix can not be used (color intensity can not be negative). Therefore the alternative matrix that could be used here was the inverse of the identity matrix.

```
1 # getting mirror image
2
3 img_flip_lr = cv2.flip(img, 1)
4 cv2.imshow('flip', img_flip_lr)
5
6 #display image for 20 seconds
7 cv2.waitKey(20000)
8 cv2.destroyAllWindows()
```

This code snippet follows the same principle as the matrix calculation with the inverse of the identity matrix, which, as shown above, results in a flipped image. This code prints the following mirrored image.

The third thing I decided to add was a blurring filter that intentionally blurs the photo. This is often used to Photoshop people's skin and remove any blemishes or pimples. The formula used here was the Gaussian blur.

$$GB[I]_p = \sum_{q \in S} G_{\sigma}(\|p - q\|) I_q$$

↓  
Normalized Gaussian Function

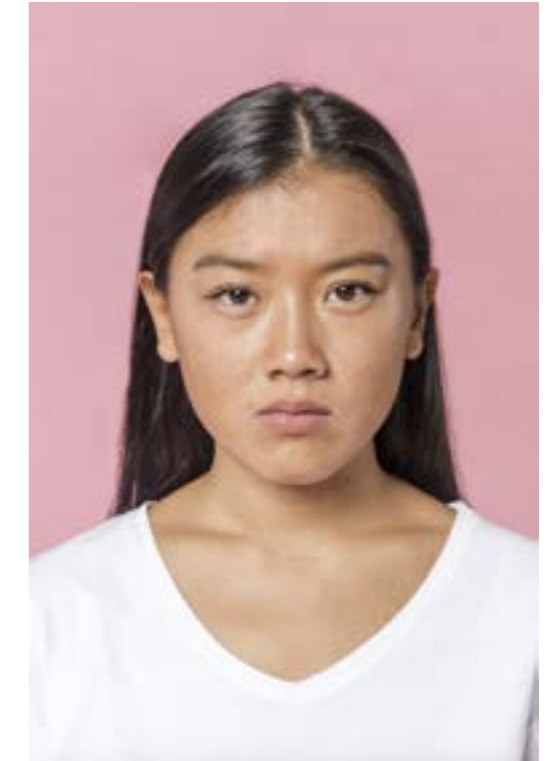


Figure 6: Original Image

The Gaussian filter formula calculates the weighted average of the current pixel and neighboring pixel values to replace the current pixel value. The closer to the current pixel, the greater the weight, and the farther, the smaller the weight. When this formula is used in images, it reduces noise and smoothens the image. However, the border of the image is also blurred. In order to preserve the borders, the original formula is modified:

$$BF[I]_p = \frac{1}{W_p} \sum_{q \in S} G_{\sigma_p}(\|p - q\|) G_{\sigma_b}(\|I_p - I_q\|) I_q$$

↓                      ↓                      ↓  
Normalization Factor      Space Weight      Range Weight

```
1 blur = cv2.bilateralFilter(applied
2 , 50, 75, 75)
3 # bilateralFilter(src, dst1, 5, 250, 10)
4 ;
5 blur2 = cv2.cvtColor(blur, cv2.COLOR_BGR2RGB)
6 plt.subplot(121), plt.imshow(img2), plt.
7 title('Original')
8 plt.xticks([], plt.yticks([]))
9 plt.subplot(122), plt.imshow(blur2), plt.
10 title('Blurred')
11 plt.xticks([], plt.yticks([]))
12 plt.show()
```

```

9
10 cv2.imshow("before", applied)
11 cv2.imshow("after", blur)
12 cv2.waitKey(3000)
13 cv2.destroyAllWindows()

```

This code snippet employs the Gaussian blur formula and blurs the photo. The (50, 75, 75) in the first line of the code represent the diameter, sigmaColor, and sigmaSpace, respectively. The larger the diameter is, the blurrier the photo gets due to the fact that larger diameters cover larger areas.



Figure 7: Original (L) After the blur filter (R)

#### 4 Summary

Overall, I really enjoyed the freedom of choosing the topic and tinkering with different types of computer software. Coming up with an idea was definitely challenging at first, but I was eventually able to generate original ideas that really helped me propel the project forward. Although my extensions were not perfect, I genuinely enjoyed the process and was satisfied with my product. To summarize, this project uses the basic principles of matrix calculation and applies them in a broader context from the perspective of images. The main theme of this project was face filters, and I aimed to imitate popular filters on social media or camera apps on my own using Excel and Jupyter notebook. It was a very interesting experience being able to merge visuals with math together and understand how there is always some sort of math beneath everything.

#### References

Applications of Linear Algebra in Image Filters [Part I]- Operations. (2020). Retrieved 31 January 2023, from <https://medium.com/swlh/applications-of-linear-algebra-in-image-filters-part-i-operations-aeb64f236845>  
 opencv-python. (2022). Retrieved 31 January 2023, from <https://pypi.org/project/opencv-python/>  
 Python — Bilateral Filtering - GeeksforGeeks. (2019). Retrieved 31 January 2023, from <https://www.geeksforgeeks.org/python-bilateral-filtering/>  
 Rosebrock, A. (2021). OpenCV Load Image (cv2.imread) - PyImageSearch. Retrieved 31 January 2023, from <https://pyimagesearch.com/2021/01/20/opencv-load-image-cv2-imread/>

Zitur Linear Algebra - 1.7.6 Pixel Pictures. (2023). Retrieved 31 January 2023, from <https://sites.google.com/a/sas.edu.sg/zitur-linear-algebra/home/unit-1/1-2-5-pixel-into-pictures?authuser=0>  
 아름다움의 정상, 오드리 햅번의 생애 . (2013). Retrieved 31 January 2023, from <https://parklanda.tistory.com/15761458>

# 02 Exploring Recursive Sequences with Eigenvalues and Eigenvectors

Written by Akshay Agarwal

## Abstract

Recursive sequences are well-known and well-studied. Generally, when learning about them in earlier math classes such as Precalculus and Algebra, the only way they were computed were...recursively. For instance, the fibonacci sequence tends to be calculated by manually adding the terms  $0+1 = 1+1 = 2+1 = 3...$  However, representing recursive sequences in this manner hides a lot of the intricacies and beauty in recursive sequences...especially the fibonacci sequence. After exploring the fibonacci sequence, we go on to generate our own spirals with complex eigenvalues and calculate the transformations that form the spiral.

*Keywords:* Fibonacci sequence, eigenvalues, eigenvectors, complex numbers, transformations, matrices

# Exploring Recursive Sequences with Eigenvalues and Eigenvectors

**Akshay Agarwal**

agarwal45366@sas.edu.sg

**Teacher Reviewer:**

Mr. Son

## 1 The Fibonacci Sequence

The Fibonacci sequence is a well-known sequence, which consists of:

0, 1, 1, 2, 3, 5, 8, 13, 21,...

where each  $F(n)$  is the sum of the two previous terms:  $F(n) = F(n-1) + F(n-2)$ , and  $F(0) = 0, F(1) = 1$ .

When graphing the sequence on the x-y plane, where the x-coordinate of each point is  $F(n-1)$ , and the y-coordinate is  $F(n)$ , one gets:



Figure 1: Points of the fibonacci sequenced graphed on the x-y plane, where the x-coordinate is  $F(n-1)$  and the y-coordinate is  $F(n)$

When fitting a curve, a line in this case, on the graph, one gets:



Figure 2: Curve fit through the Fibonacci Sequence points

Where the equation of the line is  $y = 1.618x$ ,  $1.618 = \phi$ , the golden ratio!

This is a known property of the fibonacci numbers, if you list enough numbers, the ratio of two consecutive terms in the sequence gets closer and closer to  $\phi$ . But how to prove this?

### Proving $\phi$ as the Fibonacci Ratio

If we write a term of the Fibonacci sequence as a vector, namely

$$\begin{pmatrix} F_n \\ F_{n-1} \end{pmatrix}$$

then the sequence can be rewritten as a matrix:

$$\begin{pmatrix} F_n \\ F_{n-1} \end{pmatrix} = \begin{pmatrix} 1 & 1 \\ 1 & 0 \end{pmatrix} \cdot \begin{pmatrix} F_{n-1} \\ F_{n-2} \end{pmatrix}$$

As by matrix multiplication,

$$\begin{pmatrix} F_n \\ F_{n-1} \end{pmatrix} = \begin{pmatrix} F_{n-1} + F_{n-2} \\ F_{n-1} \end{pmatrix}$$

Next, as we have a matrix, and every point on the graph showed above comes from multiplying the previous point by the matrix, we can deduce some interesting observations. Namely, whenever we multiply by the matrix, the point vector is being scaled on the same line...which is exactly what an eigenvalue and eigenvector is supposed to do. Therefore, if we can find the eigenvalue,  $\lambda$ , that should hopefully be the slope of the line,  $\phi$ .

The eigenvalue can be calculated routinely, where the determinant of the matrix

$$\begin{pmatrix} 1-\lambda & 1 \\ 1 & -\lambda \end{pmatrix} = 0$$

Thus, finding and solving the characteristic polynomial yields:

$$(1-\lambda) \cdot -\lambda - 1 = \lambda^2 - \lambda - 1 = 0$$

By the quadratic formula,

$$\lambda = \frac{1 \pm \sqrt{(-1)^2 + 4}}{2} = \frac{1 \pm \sqrt{5}}{2} = \phi$$

Which IS the golden ratio!

### Fibonacci Sequence isn't Unique?

As we've already found the eigenvalues of the fibonacci matrix, it naturally follows to find the eigenvectors

Reducing the matrix:

$$\begin{pmatrix} 1-\lambda & 1 & 0 \\ 1 & -\lambda & 0 \end{pmatrix} = \begin{pmatrix} 1-\phi & 1 & 0 \\ 1 & -\phi & 0 \end{pmatrix} \sim \begin{pmatrix} 1 & -\phi & 0 \\ 0 & 0 & 0 \end{pmatrix}$$

Means that the eigenvector is  $\begin{pmatrix} \phi \\ 1 \end{pmatrix}$ .

As the eigenvalue is also  $\phi$ , that means that it should be an eigenvector for any starting value, as the y-coordinate will eventually become  $\phi$  times the x-coordinate. Let's test this:

Fibonacci Sequence: 0, 1, 1, 2, 3, 5, 8, 13, 21, 34, 55, 89, 144

Random Sequence 1: 5, 6, 11, 17, 28, 45, 73, 118, 191, 309

Random Sequence 2: -1, 3, 2, 5, 7, 12, 19, 31, 50, 81, 131

$\frac{144}{89} = 1.618$  and  $\frac{309}{191} = 1.618$  and  $\frac{131}{81} = 1.618$ , they all equal  $\phi$ !

## 2 Recursive Sequences with Complex Eigenvalues

### Generating the Recursive Sequence

As calculating the eigenvalue,  $\lambda$ , for a 2x2 matrix requires using the quadratic formula, if the characteristic polynomial of the matrix's discriminant is negative,  $\lambda$  will be complex.

I had to find a matrix with complex eigenvalues that still functioned as a series, which meant that my matrix  $\mathbf{A}$  had to be in the form:

$$\begin{pmatrix} a & b \\ 1 & 0 \end{pmatrix} \text{ as when multiplying } \begin{pmatrix} a_n \\ a_{n-1} \end{pmatrix} = \begin{pmatrix} a & b \\ 1 & 0 \end{pmatrix} \cdot \begin{pmatrix} a_{n-1} \\ a_{n-2} \end{pmatrix},$$

the bottom value of the resultant matrix will be  $a_{n-1}$ , which creates the ideal sequence.

Next, the matrix needs to have complex eigenvalues, the characteristic polynomial of the matrix  $\begin{pmatrix} a-\lambda & b \\ 1 & -\lambda \end{pmatrix}$  is  $\lambda^2 + \lambda a - b = 0$ .

The discriminant of this polynomial is  $a^2 + 4b$ , where  $a^2 + 4b < 0$  needs to be satisfied. I chose a simple solution where  $a = 2, b = -2$ , such that  $a^2 + 4b = 2^2 + 4(-2) = -4 < 0$ .

Thus, the matrix I created for this extension is  $\mathbf{A} = \begin{pmatrix} 2 & -2 \\ 1 & 0 \end{pmatrix}$ .

This means that my recursive sequence is defined as

$$\begin{pmatrix} a_n \\ a_{n-1} \end{pmatrix} = \begin{pmatrix} 2 & -2 \\ 1 & 0 \end{pmatrix} \cdot \begin{pmatrix} a_{n-1} \\ a_{n-2} \end{pmatrix}$$

When graphing this sequence, an interesting relationship is discovered:

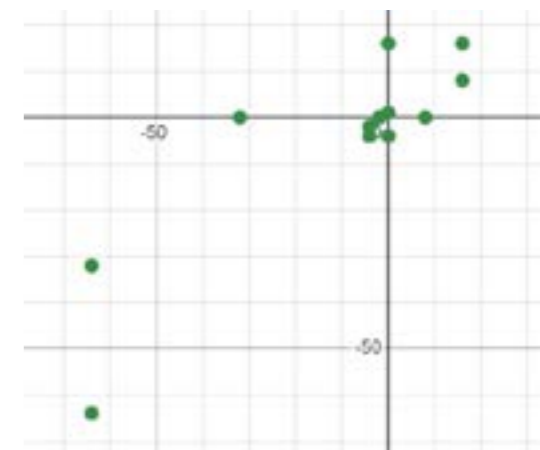


Figure 3: Complex eigenvalue based recursive sequence graphed on the x-y plane.

As opposed to a regular spiral, this spiral seems to be tilted, as if it's rotated about an ellipse. A derivation of the transformations that leads to this is the premise of my extension.

### Deriving the Transformations

In order to compute the transformations, the eigenvalues and eigenvectors would likely be necessary, so they should be calculated first.

For the eigenvalues, simply solve the characteristic polynomial we derived earlier of  $\lambda^2 - 2\lambda + 2 = 0$ , where  $\lambda = \frac{2 \pm \sqrt{-4}}{2} = 1 \pm i$ .

As the eigenvalues are conjugates, the eigenvectors will likely be too...let's compute the eigenvector when  $\lambda = 1 + i$ . The resulting matrix to row reduce is then:

$$\begin{pmatrix} 1-i & -2 & 0 \\ 1 & -1-i & 0 \end{pmatrix} \sim \begin{pmatrix} 1 & -1-i & 0 \\ 0 & 0 & 0 \end{pmatrix}, \text{ so my}$$

eigenvector is  $\begin{pmatrix} 1+i \\ 1 \end{pmatrix}$

Now, as is similar to separating the basis of a solution set, we can separate the real and imaginary parts of the eigenvector to form a matrix whose columns represent the eigenvector:

$$\mathbf{P} = \begin{pmatrix} 1 & 1 \\ 1 & 0 \end{pmatrix}, \text{ as the first column are the real components and the second are the imaginary components.}$$

Now, using diagonalization, we can trivially find the transformation matrix with  $\mathbf{P}^{-1} \cdot \mathbf{A} \cdot \mathbf{P} = \begin{pmatrix} 1 & 1 \\ -1 & 1 \end{pmatrix}$ , by matrix multiplication.

Now, in the spiral we saw earlier, it's intuitive that the transformations taking place for each iteration is a rotation and scalar (that's how the spiral shape forms). This can also be verified by looking at the form of our transformation matrix.

The generic form of a scalar matrix is  $\begin{pmatrix} r & 0 \\ 0 & r \end{pmatrix}$ , while the generic form of a rotation matrix is  $\begin{pmatrix} \cos(\theta) & -\sin(\theta) \\ \sin(\theta) & \cos(\theta) \end{pmatrix}$

Multiplying these matrices yields:  $\begin{pmatrix} r \cos(\theta) & -r \sin(\theta) \\ r \sin(\theta) & r \cos(\theta) \end{pmatrix}$ , which is in the same form as the transformation matrix we got as the top-left and bottom-right term are the same, while the top-right and bottom-left term are negative inverses of each other.

The scalar should simply be the magnitude of the eigenvalue,  $\lambda = i + i$ , which gives  $\sqrt{1^2 + 1^2} = \sqrt{2}$

We then get,  $\begin{pmatrix} 1 & 1 \\ -1 & 1 \end{pmatrix} = \begin{pmatrix} \sqrt{2} \cos(\theta) & -\sqrt{2} \sin(\theta) \\ \sqrt{2} \sin(\theta) & \sqrt{2} \cos(\theta) \end{pmatrix}$  As  $\cos(\theta) = \frac{1}{\sqrt{2}}$ ,  $\theta = \frac{\pi}{4}$ , which means that the spiral shown scales the points by  $\sqrt{2}$  and rotates them by 45 degrees.

What I could deduce about the reasoning for the tilt is that the transformation matrix we got will simply graph the straight spiral, but because we separated the eigenvector into the real and imaginary components, multiplying by matrix  $\mathbf{A}$  transforms it in the basis of the real and imaginary components  $\begin{pmatrix} 1 \\ 1 \end{pmatrix}$  and  $\begin{pmatrix} 1 \\ 0 \end{pmatrix}$ , respectively.

Therefore, for any sequence with complex eigenvalues, the spiral transformations can be derived in this method.

### 3 Conclusion

Here, we initially investigated fibonacci sequences to see how eigenvalues and eigenvectors can reveal new insights about them. Then, we extended that knowledge to trying to understand how recursive sequences with complex eigenvalues work; eventually forming spirals and computing the transformations which define them. This is really just the brink of the surface when it comes to exploring complex eigenvalues and eigenvectors, as the only patterns we deduced are those of the transformations, whereas one can also investigate the limits, the slope, and several other characteristics of any spiral. A good supplement may also be exploring if the spirals differ when the starting matrix doesn't define a recursive sequence.

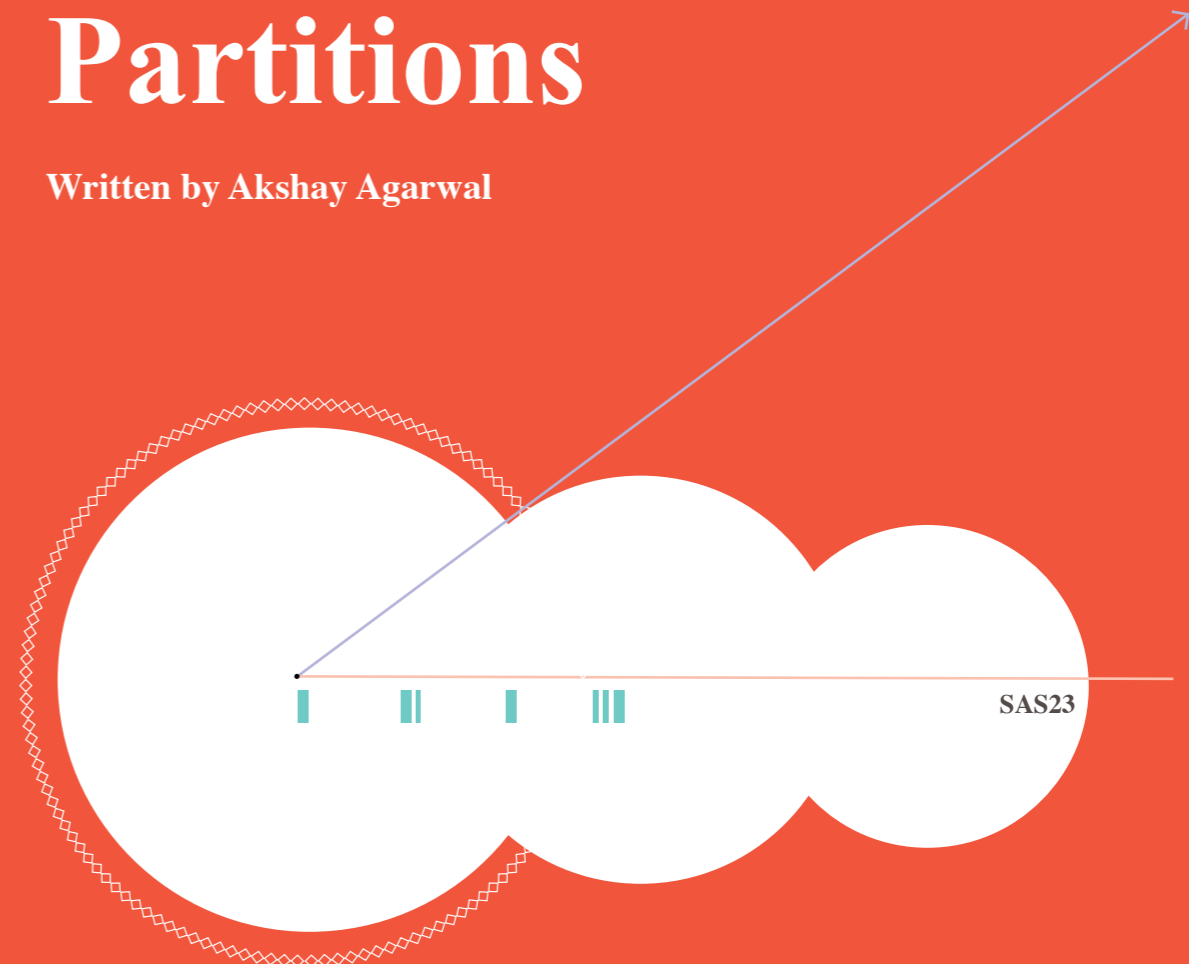
### References

Aron. (n.d.). reference — p5.js. P5js.org. Retrieved April 6, 2023, from <https://p5js.org/reference/group-IO>  
Fibonacci Numbers, T. (n.d.). Fibonacci numbers from eigenvectors and eigenvalues. Retrieved April 6, 2023, from

<https://www.d.umn.edu/~mhamp-ton/m3280f12/FibonacciNumbers.pdf>  
Ph.D, A. C. (2021, August 18). The Linear Algebra View of the Fibonacci Sequence. Medium.  
<https://medium.com/@andrew.chamberlain/the-linear-algebra-view-of-the-fibonacci-sequence-4e81f78935a3>

# 03 An Introduction to Combinatorial Partitions

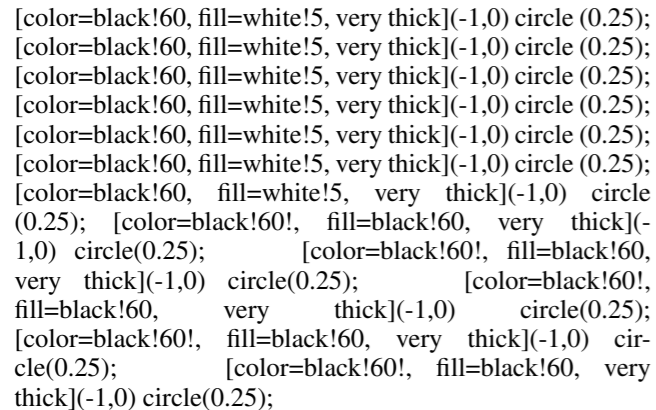
Written by Akshay Agarwal



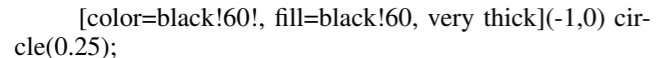
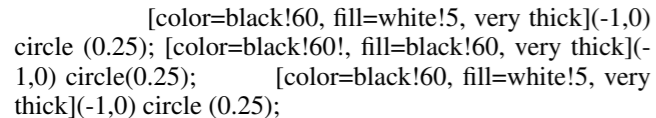
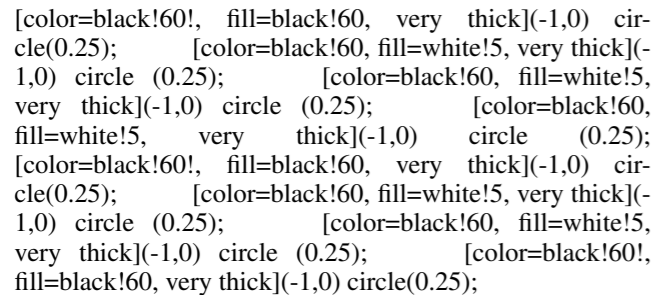




filled circles, as shown below.

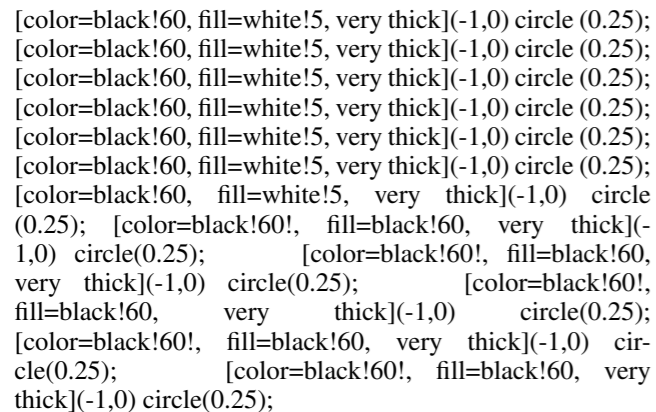


Let's try to simulate one of the configurations using this picture.



In this configuration, the filled in markers separated the candies into 0-3-2-0-1-0. Therefore, with this method, we will be able to count everything, including 0's. So we now know the correct solution 2.

**Solution 2:** Let us first draw out our filled circles and regular circles.



As we saw above, we just need to find the number of ways we can arrange the filled circles. As there are 11 total positions and 5 filled circles, the total number of ways is  $\binom{11}{5}$

=  $\boxed{462}$ . And 462 is indeed the correct answer.

### Deriving the Formulas

Now that we have a decent understanding of what stars and bars is and how to visualize it, let us try to use these techniques to generalize a formula.

We are going to derive two formulas pertaining to stars and bars. The first directly follows from example 1.0.1. If we consider  $n$  to be the number of candies and  $r$  to be the number of students Dr. Evil has to distribute them to, we had to arrange  $r - 1$  filled balls (as it takes  $r - 1$  bars to make  $r$  partitions), in a group of  $n + r - 1$  balls, leading to the formula:

**Theorem 1.2.2** If we need to split  $n$  identical items to  $k$  distinguishable groups, where each group can have 0 or more items, the total number of ways to distribute it is  $\binom{n+k-1}{k-1}$ .

Following from that, what if we modified the initial question slightly, such that now, each student must receive at least 1 candy.

**Example 1.2.1** Dr. Evil has to distribute 6 identical candies to 3 students, such that each student has at least one candy. How many ways are there to do this?

It may be intuitive that now, we don't have to worry about multiple sticks overlapping on a 0 spot, meaning we just have to arrange  $r - 1$  bars in  $n - 1$  spots, simply leading to the formula:

**Theorem 1.2.1** If we have to split  $n$  identical items into  $k$  distinguishable groups, where every group has at least one item, the number of ways to do so is  $\binom{n-1}{k-1}$ .

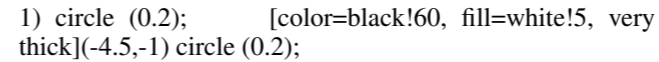
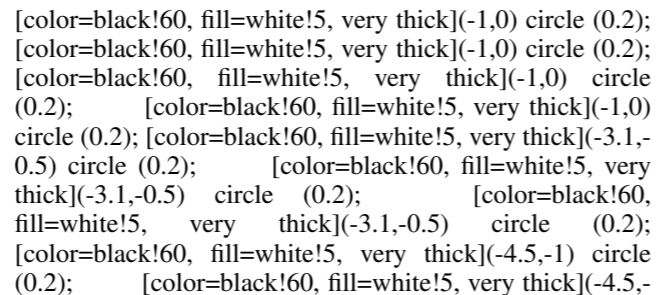
This is essentially what stars and bars is. In the next section, we'll look at the concept of partitions recursively, which sometimes overlaps with stars and bars problems.

## 3 Partitions Recursively

This section will be targeting case 2, where we're dealing with identical balls and identical boxes. As we can no longer use the Stars and Bars method, a recursive concept will be presented. As usual, we begin with a problem:

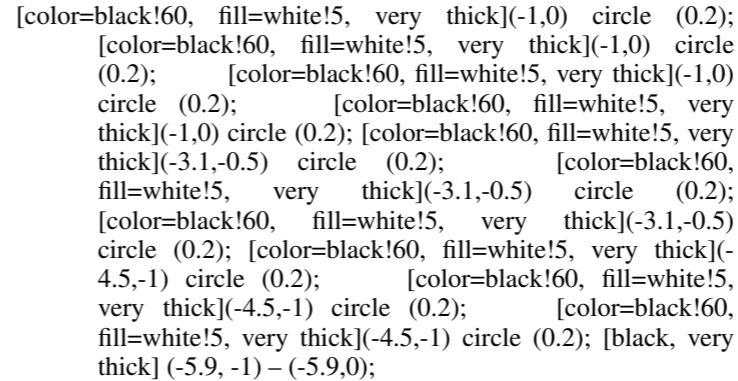
**Example 1.3.1** How many ways can 3 positive numbers sum to 10 if the order of the addends doesn't matter? By order of the addends doesn't matter, it means  $3 + 3 + 4$  is the same as  $4 + 3 + 3$ .

We'll start by drawing our example in the problem  $4 + 3 + 3$  into a diagram.



Thinking about this diagram recursively means to reduce the diagram to a simpler one which we also have control over. Here, this looks like creating a **one-to-one correspondence**, a term which means to make a change to the scenario, while keeping the answer constant.

We'll draw a line through the diagram, which signals removing the circles the line intersects.

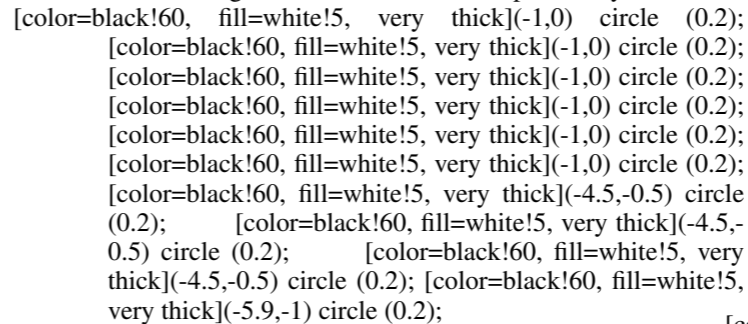


Let's think about what we can do with this. If we find the number of ways three numbers  $x_1 + x_2 + x_3 = 10$ , and if we let  $x'_i = x_i + 1$ , then the number of solutions to  $x'_1 + x'_2 + x'_3 = 7$ , is the same as the number of solutions to the prior equation. This is because every solution to  $x'_1 + x'_2 + x'_3 = 7$  is just a solution to  $x_1 + x_2 + x_3 = 10$  if you add 1 to each of the addends.

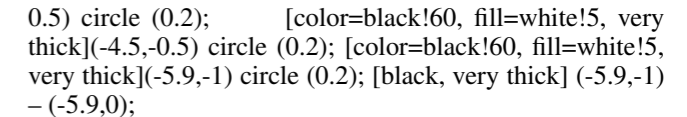
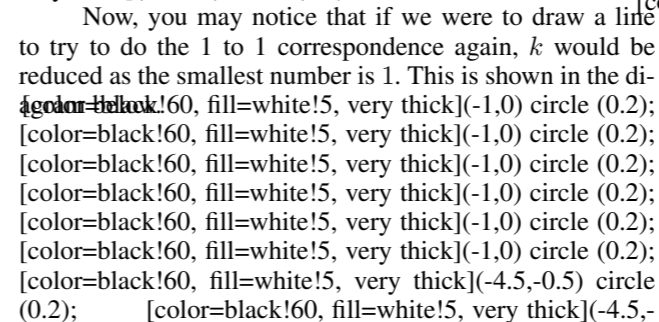
So we've reduced the number 10 to a much simpler number without changing the actual scenario.

If we let  $p(n, k) =$  the number of ways  $k$  positive numbers can sum to  $n$ , we unfortunately cannot generalize the above to say  $p(n, k) = p(n - k, k)$ ...this can be seen by drawing the Young Diagram with a different configuration.

This time, let us draw the Young Diagram with a different configuration that sums to 10. Specifically,  $6 + 3 + 1$ .

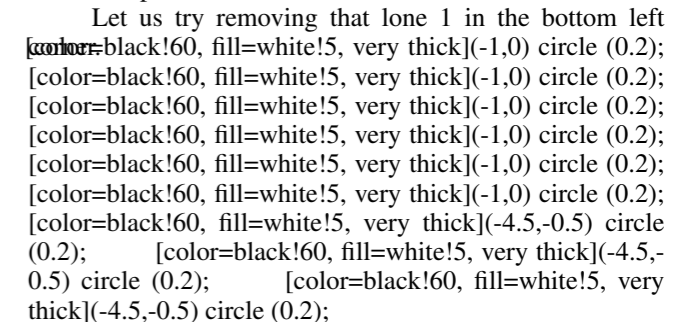


Now, you may notice that if we were to draw a line to try to do the 1 to 1 correspondence again,  $k$  would be reduced as the smallest number is 1. This is shown in the diagram below.



Therefore, we we wouldn't be able to subtract another 3 from  $n$  as that guarantees that each partition is at least 2. Therefore, we can try and cover the cases where a partition is 1 in a separate case.

Let us try removing that lone 1 in the bottom left ~~corner~~.



Now, we have a situation where we have two numbers sum to 9. As this is the case where at least one of the numbers is 1, we can just put a 1 as the third number. Therefore, this derivation works!

Putting it in the  $p(n, k)$  notation we used before, we get this case is  $p(n - 1, k - 1)$  as we're losing one group and one number. We can put this together with our  $p(n - k, k)$ , to develop our first formula.

**Theorem 1.3.1** Given  $p(n, k)$  is the number of ways  $k$  positive numbers can sum up to  $n$ , where the order doesn't matter,  $p(n, k) = p(n - k, k) + p(n - 1, k - 1)$ .

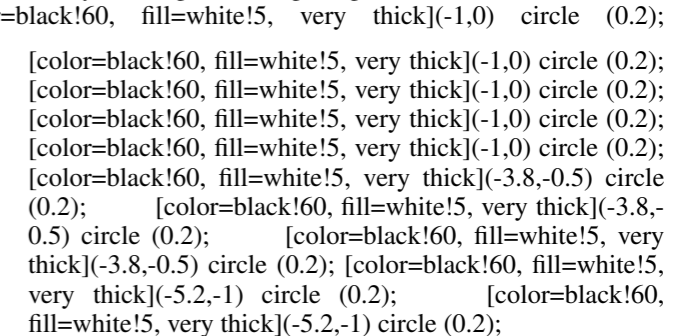
Using this, let's solve example 1.3.1.

**Solution 2:** In this problem, we want to find  $p(10, 3)$ . Using what we learned previously,  $p(10, 3) = p(7, 3) + p(9, 2) = p(4, 3) + p(6, 2) + p(9, 2)$ .  $p(4, 3) = 1$ , as the only way is  $1 + 1 + 2$ .  $p(6, 2) = 3$ , as the only ways are  $5 + 1, 4 + 2$ , and  $3 + 3$ .  $p(9, 2) = 4$ , as the only ways are  $8 + 1, 7 + 2, 6 + 3, 5 + 4$ . Summing these values up, we get  $4 + 3 + 1 = \boxed{8}$ .

But now, what if we change one word in the problem statement?

**Example 1.3.2** How many ways can 3 positive **distinct** numbers sum to 10 if the order of the addends doesn't matter? By order of the addends doesn't matter, it means  $3 + 5 + 2$  is the same as  $5 + 3 + 2$ .

Our initial formula unfortunately accounts for all cases, not just distinct cases, meaning we'll have to derive something else. As should be expected by now, let's start out by drawing the Young Diagram for  $5 + 3 + 2$ .



Once again, we can make a 1 to 1 correspondence. If every number is distinct and if we subtract one from each of the numbers, then they'll stay distinct. Therefore, we can draw a line through the first column like we did when we were deriving the  $p(n, k)$  formula.

Let us say  $q(n, k)$  = the number of ways  $k$  distinct numbers can sum to  $n$ . With what we did above, we think  $q(n, k) = q(n - k, k)$ , as there are  $k$  fewer balls. We can now start answering the example!

As you're probably suspecting, we have to account for the case where one of the numbers is 1. As expected, we will draw our Young Diagram again, this time with  $6 + 3 + 1$ .

Our first instinct would be to do what we did with  $p(n, k)$  and remove that singular ball in the bottom left corner. Let's take it out from our diagram.

Although it seems like we can do our 1 to 1 correspondence with this case in this manner, we are actually over counting. That is because in any of the two remaining rows, there can be one ball. Then, when we add a third group of one ball, we'll have two groups of one ball, which means that they **aren't distinct**. Therefore, we have to think of something else to do.

To come up with a correspondence that actually satisfies the case with one group having a 1, we can try to remove the entire column just like we did with the 1st case.

This actually works! Because we are going to add 1 to each of the first two rows, neither of them could be 1. So, we are sure they're distinct! Using our  $q(n, k)$  notation, this yields us  $q(n - k, k - 1)$  as we are losing one group when we take out one column, and we have  $k$  less balls.

We can add this to our initial  $q(n - k, k)$  to obtain our second formula!

**Theorem 1.3.2** If  $q(n, k)$  is the number of ways  $k$  distinct positive numbers sum to  $n$ ,  $q(n, k) = q(n - k, k) + q(n - k, k - 1)$ .

With this in mind, the solution to the example is rudimentary:

**Solution to Example 1.3.2:** We need to find  $q(10, 3)$ . Using the formula we derived earlier,  $q(10, 3) = q(10 - 3, 3) + q(10 - 3, 3 - 1) = q(7, 3) + q(7, 2) = q(4, 3) + q(4, 2) + q(7, 2)$ .  $q(4, 3)$  is obviously 0.  $q(4, 2) = 1$ , as the only configuration that work are  $3 + 1$ .  $q(7, 2) = 3$ , as the configurations that work are  $6 + 1$ ,  $5 + 2$ , and  $4 + 3$ . Summing these values up,  $0 + 1 + 3 = 4$ .

As expected, we will be deriving our final formula using a problem as well.

**Example 1.3.3** How many ways are there for two or more positive integers to sum to 10, such that the order matters? (for example,  $6 + 3 + 1$  is different from  $1 + 3 + 6$ ).

Let us first draw 10 balls, each representing one, in a row.

I will be using two different symbols to represent different things:  $+$  to separate the addends and  $*$  to combine the balls within an addend.

The diagram below simulates how we're interpreting the symbols.

I will be using two different symbols to represent different things:  $+$  to separate the addends and  $*$  to combine the balls within an addend.

The diagram below simulates how we're interpreting the symbols.

The simulation above shows  $1 + 2$ , as the  $*$  combines 1 and 1.

The example above perhaps gives you an idea of what we can do to solve this problem. Between any two balls, we can either put a  $+$  or  $*$ , which means there are 2 choices for every gap. As there are  $10 - 1 = 9$  gaps, we have  $2^9$  possibilities. However, we cannot combine all of them as the question asks for at least two positive integers. Therefore, our answer is  $2^9 - 1 = 511$ . This is the solution to example 1.3.3!

Hopefully, you will be able to generalize this to  $n$  numbers to obtain our third and final formula.

**Theorem 1.3.3** If we want to find the number of ways two or more positive numbers sum to  $n$ , where the order matters, the number of ways is  $2^{n-1} - 1$ .

## 4 Conclusion

This paper is an introduction to the world of partitions and aims to provide the fundamental knowledge necessary for further exploration. The concepts and formulas presented here are derived using rudimentary logic and mathematics. Therefore, you are encouraged to extend the presented concepts to try deriving more formulas on your own, especially for the last two types of partitions.

## References

N/A

# 04 Calculating Implied Volatility using the Black-Scholes Model

Written by Benjamin Cheong

## Calculating Implied Volatility using the Black-Scholes Model (ATLA Project)

**Benjamin Cheong**

cheong43465@sas.edu.sg

**Teacher Reviewers:**

Mr. Zitur, Mr. Craig

### Abstract

Options traders often use the Black-Scholes model or some extension of it to estimate the value of options. The Black-Scholes model employs different mathematical concepts including partial differential equations, stochastic calculus, and probability theory to estimate the value of a European call option. Despite its limitations, the Black-Scholes model remains largely unrivaled in terms of mathematical models estimating the value of options.

In this paper, I will explain the intuition behind the Black-Scholes formula. In my extension, I will analyze the volatility of the SPDR S&P 500 ETF Trust (SPY), an ETF that closely represents the US equity market. I plan to calculate the historical volatility of SPY and compare it with the implied volatility of SPY at different exercise prices. Finally, I will highlight a few limitations of the model that may have affected my calculations relating to the implied volatility of SPY shares.

*Keywords:* Black-Scholes model, partial differential equations, stock market, total derivative, volatility

## 1 The Black-Scholes Model

### 1.1 History and Background

Developed in 1973 by Fischer Black, Myron Scholes, and Robert C. Merton, the Black-Scholes model was created to calculate the value of a European call option. The creation of the model led to a significant increase in options trading volume and earned Scholes and Merton the Nobel Prize in Economics. To understand the Black-Scholes model, it is first important to understand what European options are. Options are financial derivatives that allow someone to buy or sell shares at a predetermined price on a specific date. European options differ from American options in the way that traders of European options are only allowed to exercise their options on the option expiry date while traders of American options can exercise their options anytime before the expiry date, therefore simplifying the mathematics required to estimate a value for European call options. Here is an example of a European call option to provide the reader with a better understanding of it:

*Let's say Bob buys a European call option from Dan for \$10. The call option states that in two days, Bob has the option to buy one Nestle share from Dan for \$200. Two days later, one Nestle share now costs \$300. Bob exercises his*

*option, buys one Nestle share from Dan for \$200, and sells that share for \$300, making a \$90 profit since he had to pay Dan \$10 in the beginning.*

The Black-Scholes model, if employed correctly, helps a trader accurately value options, enabling the trader to spot arbitrage opportunities in the market to generate profit.

### 1.2 The Model

The Black-Scholes Model can be broken down as follows:

$$C = N(d_1)S_t - N(d_2)Ke^{-rt}$$

where  $d_1 = \frac{\ln \frac{S_t}{K} + (r + \frac{\sigma^2}{2})t}{\sigma\sqrt{t}}$

and  $d_2 = \frac{\ln \frac{S_t}{K} + (r - \frac{\sigma^2}{2})t}{\sigma\sqrt{t}}$

$C$  = call option value

$S$  = share price of underlying stock

$K$  = exercise price

$r$  = risk-free interest rate

$N(d)$  = cumulative distribution function for normal distribution

$t$  = time to expiration of option

$\sigma$  = volatility/standard deviation of lognormal function

In layman's terms, a call option is valued by deducting the share price ( $S$ ) by the discounted present value ( $e^{-rt}$ ) of the exercise price ( $K$ ), both of which are weighted by a probability factor  $N(d_1)$  and  $N(d_2)$  respectively. We can illustrate this more clearly at call option maturity when the value of the call option is essentially the share price minus the exercise price.

$N(d_1)$  and  $N(d_2)$  are more difficult to understand but intuitively  $N(d_1)$  is the risk-adjusted probability that the option will not expire in-the-money while  $N(d_2)$  is the risk-adjusted probability that the option will expire in-the-money.

### 1.3 Present Value Adjustment to Call Option Price

We need to discount the exercise price to calculate the present value of the exercise price. Since the option exercise is at a future date, we need to take into account the value of

the option now versus the value at the time of expiration. We can use the formula for continuous compounding interest,  $e^{-rt}$ , where  $r$  is the risk-free interest rate and  $t$  is the time to maturity to discount the call option exercise price.

$$\text{NPV of call option price} = Ke^{-rt}$$

### 1.4 Highlights of Mathematical Derivation

The mathematical derivation of the Black-Scholes model is very complex, combining different branches of calculus including partial differential equations, stochastic calculus, martingales, and Itô's lemma. We will examine some of the concepts used in the derivation of the Black-Scholes model below.

The Black-Scholes model assumes that share prices follow a geometric Brownian motion with mean growth rate  $\mu$ , volatility  $\sigma$  and  $W$  is a Wiener process or Brownian motion. Brownian motion is a random process and is widely used to model percentage changes in share prices.

$$\frac{dS}{S} = \mu dt + \sigma dW$$

We apply a branch of calculus called Itô's lemma to calculate the payoff of an option  $V$  as follows:

$$dV = (\mu S - \frac{\partial V}{\partial S} + \frac{\partial V}{\partial t} + \frac{\sigma^2 S^2}{2} \frac{\partial^2 V}{\partial S^2} dt + \sigma S \frac{\partial V}{\partial S} dW)$$

\*Note that  $\partial f / \partial x$  represents the partial derivative of  $f$  with respect to  $x$ .

By using a concept called delta-hedge portfolio, we effectively short one option and long shares. This allows us to effectively remove  $dW$  from the equation, thus neutralizing the effect of the Brownian motion. As the portfolio is now fully-hedged, the appropriate return is the risk-free rate of interest  $r$ . This allows us to arrive at the Black-Scholes partial differential equation.

$$\frac{\partial V}{\partial t} + \frac{\sigma^2 S^2}{2} \frac{\partial^2 V}{\partial S^2} + rS \frac{\partial V}{\partial S} - rV = 0$$

### 1.5 $N(d_1)$ and $N(d_2)$

We will explain some key intuition behind  $N(d_1)$  and  $N(d_2)$ .

$$C = N(d_1)S_t - N(d_2)Ke^{-rt}$$

$$\text{where } d_1 = \frac{\ln \frac{S_t}{K} + (r + \frac{\sigma^2}{2})t}{\sigma \sqrt{t}}$$

$$\text{and } d_2 = \frac{\ln \frac{S_t}{K} + (r - \frac{\sigma^2}{2})t}{\sigma \sqrt{t}}$$

$N(d)$  is the cumulative distribution function (0% to 100%) which is used to calculate probabilities under a normal distribution function.  $N(d_2)$  can be thought of as a risk-adjusted probability that the future stock price will be above the exercise price at expiration.  $N(d_1)$  is thought of as the

risk-adjusted probability that the option will not be exercised. It is also the option delta or the sensitivity of the option price to changes in the share price of the underlying stock.

Greater volatility means that the call option has greater value. Greater volatility increases the value of  $d_1$  as the volatility in the numerator is squared over the volatility in the denominator. This leads to a higher probability produced by the normal distribution function and therefore a greater call option value. Greater volatility decreases the value of  $d_2$  as the volatility in the numerator is squared and negative over the volatility in the denominator. A lower  $d_2$  leads to a lower probability produced by the normal distribution function and a corresponding higher call option value.

Greater time to expiration means that the call option has greater value. Greater time to expiration affect  $d_1$  and  $d_2$  similarly. However, as the variable  $t$  increases, the function  $e^{-t}$  tends towards zero, decreasing the negative component of the equation, therefore leading to a greater call option value.

A higher share price over the exercise price will lead to a higher call option value. Similarly, a higher risk-free rate will result in a higher call option value.

## 2 Comparing Historical Calculated Volatility to Implied Volatility

I wanted to investigate how similar the historical calculated volatility was to the implied volatility of call options at different exercise prices of the SPY ETF in the month of September 2022 using the Black-Scholes model.

### 2.1 Calculation of Historical Volatility

The equation to calculate historical/annualized volatility is:

$$\text{HV} = \text{SD} \left( \sum_x = 1^d \ln \left( \frac{p_x}{p_{x-1}} \right) \right) \times \sqrt{d-1}$$

HV = historical volatility  
SD = standard distribution model  
 $d$  = number of days in the dataset  
 $P(d)$  = share price on that day  $d$

I am calculating the historical volatility of the S&P500 ETF index (SPY), a highly liquid and deeply-traded ETF, using the closing prices of the trading days of the last year-to-date. There were 252 trading days from the year-to-date of 21 May 2022. Historical volatility is considered as the standard deviation of the sum of the logarithmic returns. First, I used the equation  $\ln(p_x/p_{x-1})$  to determine the logarithmic returns for every day excluding the first day as there are no values for  $p_{x-1}$ . Next, I entered the result into the STDEV() standard deviation function in Google Sheets to calculate the standard deviation of all the logarithmic returns. Finally, I multiplied the historical volatility by the square root of the number of trading days in my dataset, since volatility is the square root of the variance, to calculate annualized volatility. My result of annualized volatility was 0.1784475146 or around 17.8448%.

(note that the date starts from the oldest to the newest)

Day Count	Date	Closing Price	Logarithmic returns
1	2021-05-21	414.940002	
2	2021-05-24	419.170013	0.01014266029
3	2021-05-25	418.23999	-0.002221190048
4	2021-05-26	419.070007	0.001982580585
5	2021-05-27	419.290009	0.0005248389734
6	2021-05-28	420.040009	0.00178714018
...	...	...	...
248	2022-05-16	400.089996	-0.004065819213
249	2022-05-17	408.320007	0.02036168606
250	2022-05-18	391.859985	-0.041146603
251	2022-05-19	389.459991	-0.006143453699
252	2022-05-20	389.630005	0.0004364425254
Annualized volatility			0.1784475146

\*Note that I only included the first ten days of my dataset

### 2.2 Calculation of Implied Volatility using Black-Scholes Model

Using the Black-Scholes model and the market call option value on Yahoo Finance, I estimated the variables of time to expiration of option and risk-free interest rate to reverse engineer the implied volatilities for the month of September 2022.

I estimated the time to expiration of the option by using the NETWORKDAYS() function in Google Sheets that computed the number of trading days between today's date, 21 May 2022, and the date that the options would expire, 30 September 2022. I divided that time by the total number of trading days in a year (253 days) to calculate the time to expiration in percentage form.

I estimated the risk-free interest rate for September 2022. I divided the number of trading days calculated above by 30 days, roughly the number of days in a month, to calculate the number of months until the option would expire, obtaining the result of 4.4 months. I estimated the risk-free interest rate by interpolating the 3-month and 6-month US treasury interest rates from the US Federal Reserve website of 1.03% and 1.51% respectively to calculate the US treasury interest rate in 4.4 months when the European call options would expire.

Calculating Risk-Free Rate	
3 month treasury rate (%)	1.03%
6 month treasury rate (%)	1.51%
Time to expiration (months)	4.57
Interpolated interest rate	1.28%

With all my values computed or given, I downloaded and used the GoalSeek function on Google Sheets which is similar to the .solve() function on the TI-Nspire calculator. I entered the values and began computing the implied volatilities—that is, the volatilities required to obtain the stated call option values. Note that I had to repeatedly change the exercise price as my research was with regards to the trends of volatility due to exercise price.

The detailed spreadsheet containing my calculations is in the Google Sheet link below:

<https://docs.google.com/spreadsheets/d/1.8CwUfFkIZNCd6nyynn6iug1TH0T3ISeTITq8oZuRI/edit#gid=0>

SPY Call Options expiring 30 Sep 2022

Reference date	20 May 22
Call option expiration date	30 Sep 22
Number of business days	%
S (share price of underlying stock)	389.63
K (exercise price)	440 ← enter exercise price
r (risk-free interest rate)	1.281%
t (time to option's expiration)	0.3810
σ (volatility)	18.90% ← Goal seek changes σ to find target option price
d1	-0.9417896729
d2	-1.058470044
N(d1)	0.1731501867
N(d2)	0.1449206003
C (call option value)	4.0190 ← Set goal seek to find target option price

### 2.3 Observations & Analysis of “Trends of Volatility due to Exercise Price” Graph

There are several significant takeaways from the “trends of volatility due to exercise price” graph.

SPY Call Options expiring 30 Sep 2022

Options	Exercise Price	Call Option Price	Using Goalseek	Volatility
SPY220930C0440000	390	38.22	25.04%	17.84%
SPY220930C0370000	370	31.3	25.02%	17.84%
SPY220930C0350000	350	28.57	23.88%	17.84%
SPY220930C0330000	330	23.88	23.84%	17.84%
SPY220930C0310000	310	17.98	23.61%	17.84%
SPY220930C0290000	290	10.86	18.12%	17.84%
SPY220930C0270000	270	9.53	20.80%	17.84%
SPY220930C0250000	250	8.4	18.87%	17.84%
SPY220930C0230000	230	6.31	18.90%	17.84%

The implied volatility stays above the annualized volatility for all the listed exercise prices. Implied volatility is based upon present volatility while annualized volatility is based upon the volatility of the past year-to-date. Therefore, this observation can be explained by the high volatility of the American market for the last three months after the Russian invasion of Ukraine in February. The lower annualized volatility is an average of a significantly larger dataset and therefore is less affected by the recent trend. In addition, the implied volatility at different exercise prices does not follow a clear trend throughout, though it seems to be largely decreasing after its initial maximum at around the \$390 exercise price.

Different exercise prices change the volatility. Based on further research from Investopedia, there is a concept called volatility skew where in-the-money options have higher implied volatility vs out-of-the-money call options. Although my graph looks a little skewed, I suspect that the deviation is from the current market volatility.

## 3 Limitations

### 3.1 American vs European Options

One limitation to my calculations of the implied volatility of the SPY index is that the S&P500 ETF index (SPY) is an American option, not a European option. This is significant because the mathematics behind the Black-Scholes model is geared towards the more straightforward European option.

While European options can only be exercised on the day of expiry, American options can be exercised on any day before the option expires. I researched American option pricing models and found that the Bjerksund-Stensland model is a model often used to price American options, but found that the math is too complex for this discussion.

### 3.2 Fat-tails

Another limitation is that the Black-Scholes model has a significant flaw that may have impacted our estimation. The Black-Scholes model assumes that the distribution of the option value is lognormal, but this is not necessarily true. The model fails to take into account the possibility of fat tails or kurtosis and Black Swans, a sudden largely unforeseen change in market conditions such as the 2007 financial crisis, meaning that a sudden change in how the option prices are distributed can have a drastic impact on the accuracy of the option pricing. This is extremely significant as it could cause the user of the Black-Scholes model to highly undervalue or overvalue certain options, causing the user significant financial loss.

### 3.3 Historical Volatility vs Current Volatility

Another limitation is that the annualized volatility that I calculated is evidently not a good predictor of the current implied volatility according to my graph. The reason behind the difference between the annualized and implied volatility can be attributed to the highly volatile market conditions that have been caused by the recent Federal Reserve interest rate hikes and the uncertainty over the Russia-Ukraine war. Since the implied volatility, which is based on the last few months, is greater than the annualized volatility, which is based on the last year-to-date, it is evident that annualized volatility cannot be relied upon in the increasingly-volatile market of today.

## 4 Conclusion

In conclusion, through my research, I found that the Black-Scholes model is primarily comprised of a present value adjustment equation taking into account the probabilities  $d_1$  and  $d_2$ , the probability that the option will not expire-in-the-money and the probability that the option will expire-in-the-money respectively, plotted over a normal distribution graph  $N(d)$ . Through my extension investigating the relationship between annualized volatility and implied volatility of the SPY ETF over the month of September 2022, I found that the implied volatility was significantly greater than the annualized volatility which can be attributed to the greater volatility in the past few months due to the uncertainty surrounding real-world events. Annualized volatility may not be a good predictor of current and future volatility.

Through my research of financial derivatives, I noticed that it is highly difficult to derive equations that adequately represent the uncertainty in financial markets. It is evident that even the Black-Scholes model, which won its creators the Nobel Prize in Economics, has several significant limitations. For example, the model relies on an assumption that option price is represented by lognormal distribution

and therefore does not account for the option price following other types of distribution models like fat-tail or kurtosis distribution.

### References

- "Deriving the Black-Scholes Equation" (QuantStart, n.d.). Retrieved from <https://www.quantstart.com/articles/Deriving-the-Black-Scholes-Equation/>.
- Hayes, A. (2022, April 3). "What Is the Black-Scholes Model?" Investopedia. <https://www.investopedia.com/terms/b/blackscholes.asp>.
- Hayes, A. (2022, February 8). "Volatility." Investopedia. <https://www.investopedia.com/terms/v/volatility.asp#toc-how-to-calculate-volatility>.
- "How to Calculate Historical Volatility in Excel" (Macroption, n.d.). Retrieved from <https://www.macroption.com/historical-volatility-excel/>.
- "Ito's Lemma" (QuantStart, n.d.). Retrieved from <https://www.quantstart.com/articles/Ito's-Lemma/>.
- Louis (2019, October 29). "The Black Scholes Model Explained" TradeOptionsWithMe. <https://tradeoptionswithme.com/black-scholes-explained/>.
- Nibley, B. (2021, June 21). "The Black-Scholes Model, Explained." SoFi. <https://www.sofi.com/learn/content/what-is-the-black-scholes-model/>.
- "Resource Center" (U.S. Department of the Treasury, n.d.). Retrieved from [https://home.treasury.gov/resource-center/data-chart-center/interest-rates/TextView?type=daily\\_treasury\\_yield\\_curve&#38;field\\_tdr\\_date\\_value\\_month=202205](https://home.treasury.gov/resource-center/data-chart-center/interest-rates/TextView?type=daily_treasury_yield_curve&#38;field_tdr_date_value_month=202205).
- Turner, E. (2010). "The Black-Scholes Model and Extensions." University of Chicago. <http://www.math.uchicago.edu/~may/VIGRE/VIGRE2010/REUPapers/Turner.pdf>.
- Veisdal, J. (2021, December 1). "The Black-Scholes Formula, Explained." Cantor's Paradise. <https://www.cantorsparadise.com/the-black-scholes-formula-explained-9e05b7865d8a>.

# 05 Countably and Uncountably Infinite Sets

Written by Benjamin Cheong

# Countably and Uncountably Infinite Sets

**Benjamin Cheong**

cheong43465@sas.edu.sg

## Abstract

Born in 1845, German mathematician Georg Cantor was a pioneer in developing set theory—in specific, infinite set theory. Infinite set theory is a branch of mathematics that focuses on studying the behavior of infinite collections of numbers. In this paper, we will establish that infinity is a concept and examine the conclusions Cantor drew regarding infinite sets, relating to countability and cardinality. Please note that this paper will not be describing proofs in a mathematically rigorous manner, but will rather be explaining in a more easy-to-understand manner.

*Keywords:* set theory, infinity, Cantor's diagonalization argument, cardinality, bijective, Cantor's theorem

## 1 Infinity is a Concept

Infinity only exists as a concept and has fundamental flaws when applied as a number. When we later delve into infinite sets, it is important to regard that infinity as a concept as well. First, let's prove infinity can't be a number.

Imagine a semi-circle with radius 1. The circumference of this semi-circle is  $\pi \cdot 1 = \pi$ .

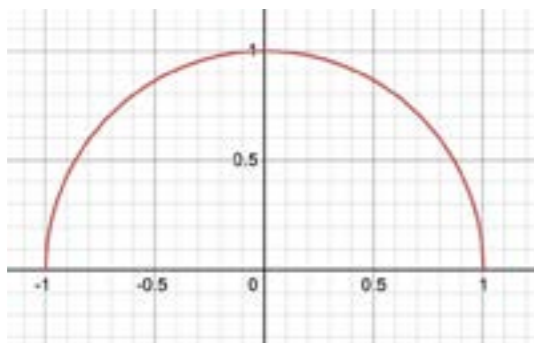


Figure 1: A single semicircle graphed on the  $x$ - $y$  plane

Now imagine two semi-circles with radius  $\frac{1}{2}$ . The total circumference of these two semi-circles is still  $\pi \cdot \frac{1}{2} + \pi \cdot \frac{1}{2} = \pi$ .

Copyright © 2023, Association for the Advancement of Artificial Intelligence (www.aaai.org). All rights reserved.

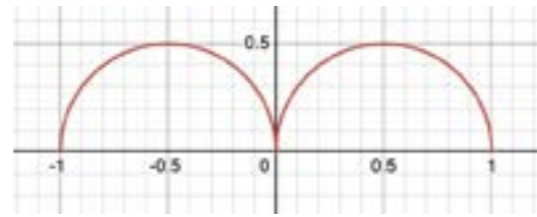


Figure 2: Two tangent semicircles with radius  $\frac{1}{2}$  lined up

Four semi-circles with radius  $\frac{1}{4}$ ? The total circumference will still be

$$\pi \cdot \frac{1}{4} + \pi \cdot \frac{1}{4} + \pi \cdot \frac{1}{4} + \pi \cdot \frac{1}{4} = \pi$$

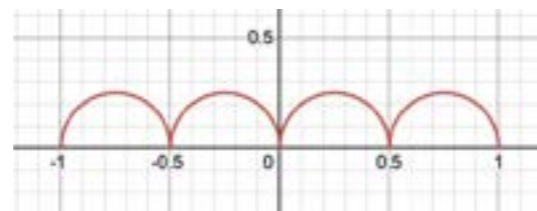


Figure 3: Four semicircles with radius  $\frac{1}{4}$

Eight semi-circles with radius  $\frac{1}{8}$ ? Sixteen semi-circles with radius  $\frac{1}{16}$ ? As the number of semi-circles increases, the total circumference remains the same at  $\pi$ . Yet, an infinite number of semi-circles each with an infinitely small radius would resemble a line instead. A line which is 2 units long.

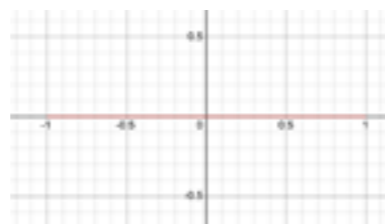


Figure 4: An 2 unit long line on the  $x - y$  plane

Therefore, when infinity is used as a number,  $\pi$  is equiv-

alent to 2. Since  $\pi$  cannot be equivalent to 2, therefore it follows that infinity cannot be used as a number. The limit as the number of semi-circles approaches infinity does approach 2, but, as we learn in calculus, the limit can often be different from the actual answer.

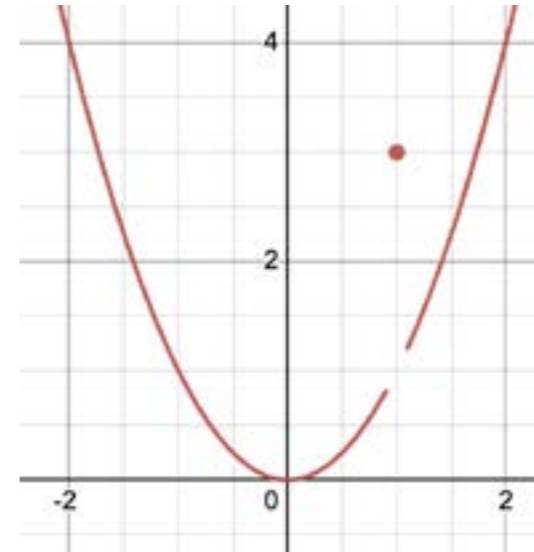


Figure 5: A graph of  $f(x) = x^2$ , for  $x \neq 3$

For example, in the above graph,  $f(x) = x^2$ , for  $x \neq 1$ , and  $f(x) = 3$  for  $x = 1$ . Therefore,  $\lim_{x \rightarrow 1} f(x) = 1$ , while  $f(1) = 3$ . Therefore, the limit is different from the actual answer when the graph has a jump or point discontinuity.

## 2 Countably and Uncountably Infinite Sets

To determine whether an infinite set is countable or uncountable, we can use bijection, a method developed by Cantor. A bijection is a one-to-one correspondence. If the infinite set can correspond one-to-one to the natural set, the infinite set is countable. If it cannot correspond one-to-one to the natural set, the infinite set is uncountable. Please note that the natural set of numbers is  $\{1, 2, 3, 4, 5, 6, 7, \dots\}$ . We will later show that any subset of a countably infinite set, such as the natural set, and an uncountably infinite set is also countably infinite and uncountably infinite, respectively. Here, we will assess the countability of a few infinite sets and explain our reasoning.

### 2.1 Countability of Even Integer Set

Does the even integer set correspond one-to-one to the natural set? Let's see.

Even Integers	2	4	6	8
Natural Numbers	1	2	3	4

Yes, it does! Every natural number corresponds to exactly one number in the even integer set.

### 2.2 Countability of Integer Set

Does the integer set correspond one-to-one to the natural set? Let's see.

Integers	0	1	-1	2
Natural Numbers	1	2	3	4

Yes, it does! To correspond every integer to a natural number, we have to start with zero and then go to the positive and negative of each following integer. By working to both positive and negative infinity, we can correspond every natural number to exactly one number in the integer set.

### 2.3 Countability of the Positive Rational Numbers Set

Does the positive rational number set correspond one-to-one to the natural set? Let's see.

Rational Number	1	2	$\frac{1}{3}$	$\frac{1}{2}$
Natural Numbers	1	2	3	4

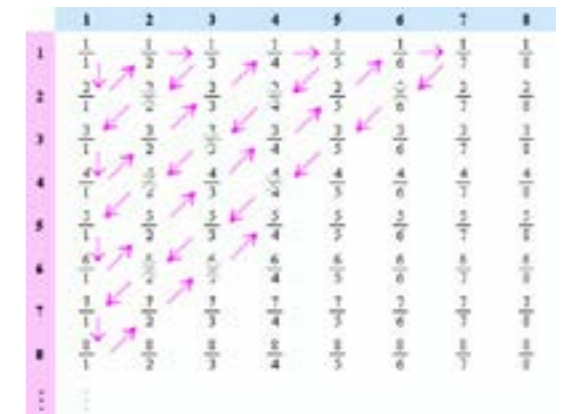


Figure 6: All rational numbers as fractions

Yes, it does! Since all rational numbers can be represented as a fraction, we can correspond every number in the positive rational number set to a number in the natural set by employing a diagonal approach shown above. The blue and pink numbers represent the denominator and numerator of the number respectively. All repeated numbers (e.g.  $\frac{1}{1}$ ,  $\frac{2}{2}$ ,  $\frac{3}{3}$ ) are skipped. No other approach would work as we cannot go to infinity and come back (e.g.  $1, \frac{1}{2}, \frac{1}{3}, \frac{1}{4}, 2, \frac{2}{3}, \frac{2}{5}, \dots$ ). Please also note that by proving the countability of the positive rational numbers set, we can easily prove the countability of the rational numbers set as a whole by adding zero in front and adding a negative number after each positive number—similar to what we did for the integer number set. All subsets of countably infinite sets must be countably infinite themselves because they are either finite or are made up of all the numbers in an already proven set and therefore share the same characteristics.

### 2.4 Countability of Real Number Set

Does the real number set correspond one-to-one to the natural set? Let's think about it.

No, it doesn't. There is no way to establish one-to-one correspondence between the real number set and the natural set. Although it may initially seem like the infinity between a real number set from  $[0, 1]$  should be the same infinity in a positive integer set, this conclusion fails to consider infinitely repeating numbers like  $\frac{1}{3}$ . The number  $\frac{1}{3}$  in the real number set is not represented in the positive integer set as it requires infinite decimals that do not exist in integers. A clearer proof that the real number set is uncountable can be shown by Cantor's diagonal argument. Cantor's diagonal argument proves that a real number set from  $[0, 1]$  is uncountable, therefore proving that all real number sets are uncountable. Using proof by contradiction, first assume that the infinite real number set is countable.

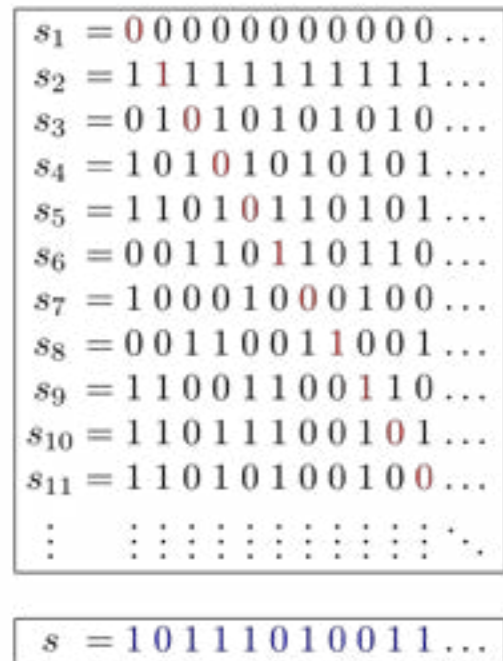


Figure 7: Diagram showing Cantor's diagonal argument

Since we assume the infinite real number set is countable, all real numbers should exist within the infinite real number set. The picture above is an infinite list of infinite digits. Look at the red-highlighted numbers and then look at the blue-highlighted numbers at the bottom. If the red-highlighted number is 1, the blue-highlighted number in its column becomes 0. If the red-highlighted number is 0, the blue-highlighted number in its column becomes 1. The blue-highlighted numbers at the bottom are different from any number in the infinite list. They are different from the number in the first row by the number in the first column, different from the number in the second row by the number in the second column, different from the number in the third row by the number in the third column, and so on. Therefore, the blue-highlighted numbers at the bottom are different from all the numbers in the infinite list and yet should exist as a number in the infinite list. Such a contradiction proves that

the real numbers are indeed uncountable.

Please note that the change from 0 to 1 is completely arbitrary. As long as you are somehow changing each of the red-highlighted numbers, you can prove Cantor's diagonal argument.

### 2.5 Countability of Irrational Number Set

Does the irrational number set correspond one-to-one to the natural set? Let's see.

No, it doesn't. Since the irrational number set is infinite, we can prove that it is uncountable using the same logic behind Cantor's diagonalization argument. Please note that we cannot state that the irrational number set is uncountable because it is a subset of the real number set. Otherwise, we would be able to state a finite, definitely countable set would be uncountable. Instead, we can state that the real number set is uncountable because the irrational number set is as well. For uncountable sets, the subset determines the overall set's countability, not the other way around.

## 3 Cardinality of Infinite Sets

The cardinality is the size of a set. Here, we will be determining the cardinality of the infinite sets previously discussed.

### 3.1 Cardinality Definitions

**Definition 1:** A has the same cardinality as B if there is a bijective function between the two.

**Definition 2:** A has cardinality less than B if there is an injective function from A to B but no bijective function. Note that injective functions are one-to-one functions where B may have more points that are not mapped by A.

Please also note that a bijective function is a function that is both injective and surjective. Surjective functions are one-to-one functions where A may have more points that are not mapped by B.

#### Definition 1 - Cardinality of Countably Infinite Sets:

Two sets have the same cardinality if there is a bijection between the two. Since countably infinite sets must have a bijection or one-to-one correspondence to the natural set to be countable, it follows that all countably infinite sets have the same cardinality as the natural set and each other.

#### Definition 2 - Cardinality of Uncountably Infinite Sets:

The cardinality of uncountably infinite sets is much more interesting. Countably infinite sets have cardinality less than uncountably infinite sets. There is an injective function from the natural set to the real number set because the natural set is a subset in the real number set. The real number set has integers, of which the positive belong to the natural set, and decimals. There is no bijective function from one to the other set because the natural set is countable and the real number set is uncountable.

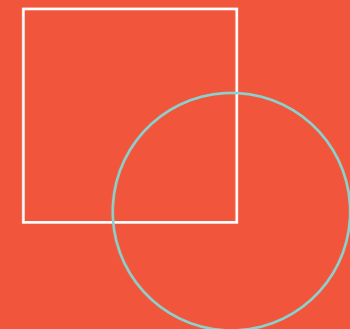
## 4 Conclusion

In conclusion, this paper has provided a clear introduction to countably and uncountably infinite sets. We began by ex-

plaining why infinity only exists as a concept and not a number. Next, we explained how one might determine whether infinite sets are countable or uncountable using bijection, a method devised by Georg Cantor. Finally, we examined the cardinality of countably and uncountably infinite sets.

## References

N/A.





# 06 Introduction to Chaos Theory: History Examples, Applications

Written by Sunghan Billy Park

## Introduction to Chaos Theory: History Examples, Applications

Sunghan (Billy) Park

park44253@sas.edu.sg

Teacher Reviewer:  
Ms. Poluan

### Abstract

Chaos theory is a branch of mathematics that deals with the study of dynamic systems and their seemingly random behavior. In this research paper, we aim to provide a comprehensive overview of chaos theory, covering its key concepts and examples, as well as its applications in various fields. We begin by discussing the history and development of chaos theory, including the pioneering work of figures such as Henri Poincaré and Edward Lorenz. We then delve into some examples of chaos theory, such as the double pendulum and Newton's three-body problem. Finally, we explore some of the real-world applications of chaos theory, including its use in predicting weather patterns and understanding biological systems. Overall, this research paper aims to provide a comprehensive and accessible introduction to chaos theory for students and researchers interested in this fascinating and important field.

*Keywords:* Butterfly effect, Double pendulum, Newton's three-body problem

### 1 Introduction and History

Chaos theory is defined as the branch of mathematics that deals with complex systems whose behavior is highly sensitive to slight changes in initial conditions, so that small alterations can give rise to strikingly great consequences. Chaos theory has its roots in the work of Henri Poincaré, a French mathematician who studied the stability of the solar system in the late 19th century. Pondering upon Newton's three-body problem, Poincaré discovered that the orbits of celestial bodies were not as predictable as previously thought, and that small variations in initial conditions could lead to significant differences in the long-term behavior of the system.

However, it was not until the 1960s that chaos theory was fully developed and recognized as a distinct field of mathematics. The development of chaos theory can be attributed to Edward Lorenz, a mathematician and meteorologist at the Massachusetts Institute of Technology. Lorenz was studying the behavior of weather patterns using computer simulations, when in 1961 he inadvertently discovered an interesting phenomenon. He was running simulations of twelve weather variables using a computer model, but to save time, he started halfway through a previous simulation. To his surprise, he found that the results were completely different. He

then realized that the numbers he used this time were truncated to three decimal places, while the previous simulation used six. This small, seemingly insignificant difference was amplified, resulting in a completely different outcome. This phenomenon, coined the "butterfly effect" by Lorenz (based on the metaphor that a butterfly flapping its wings in Brazil could cause a tornado in Texas), became the cornerstone of chaos theory.

## 2 Examples

### 2.1 The Double Pendulum

One of the most notable examples of chaos theory in action is the double pendulum. The name is rather self-explanatory; it is essentially two pendulums connected to each other which can be spun along an axis. The double pendulum is quite unique, solely because of its high sensitivity to initial conditions—a common trend within chaos theory.

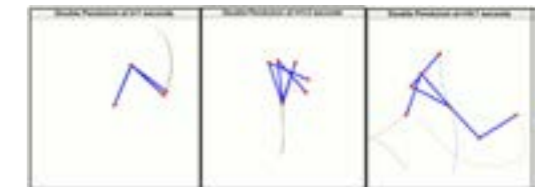


Figure 2.1.1: A simulation of three double pendulums dropping at the same time, with slightly different initial conditions. (Source: Wikimedia Commons)

As seen above, dropping the pendulum from 100.00 degrees, 100.01 degrees, and 99.9 degrees would look similar at first, but their paths would diverge drastically over time. In addition to this, the slight differences of air pressure, gravity, temperature, and other miniscule differences would also have an impact; in fact, it is said the double pendulum is so sensitive that the gravitational attraction of a nearby human could affect its course.

### 2.2 Newton's Three-Body Problem

Another well-known example of Newton's three-body problem in orbital mechanics. The discovery of this hypothetical problem dates back to 1687, where namesake as-

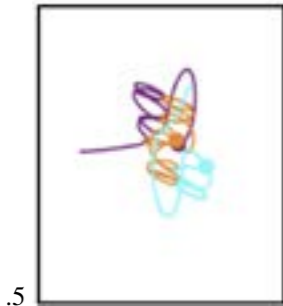


Figure 2.2.1: A subfigure

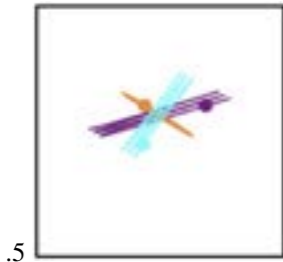


Figure 2.2.2: A subfigure

### 3 Applications

The applications of chaos theory are not limited to rather mundane scenarios of pendulums or butterflies; rather, these applications are far-reaching and play a part in meteorology, biology, social science, and even business.

As mentioned before with Lorenz, chaos theory is also used in predicting weather conditions, where observations that are self-similar in regions help reduce the uncertainty posed by the initial weather conditions, thereby reducing errors. This is why we can predict the weather many days in advance with confidence—a huge improvement from before.

In biology, chaos theory has played a part in population dynamics, which involves understanding how populations of organisms change over time. This can include factors such as birth and death rates, migration, and other influences. Chaos theory has been used to model the dynamics of populations of animals, plants, and other organisms, and has helped to explain how small changes in initial conditions can lead to large changes in population size over time. In fact, chaos theory has even been applied by biologists to understand and explain the spread of the COVID-19 virus.

Chaos theory has even been applied to concepts in the social sciences ranging from politics to psychology. Specifically, for politics, chaos theory has been used to study the factors that contribute to political instability, such as economic crises, social unrest, and changes in leadership. Researchers have used chaotic models to identify the conditions that are most likely to lead to regime change and to predict the likelihood of such changes occurring in different countries. For psychology, it has been used to study the factors that influence decision-making in social groups, such as the role of leadership and group dynamics. For example, researchers have used chaotic models to study how group size and composition can impact decision-making and to identify the conditions that are most likely to lead to group consensus. Chaos theory has also been applied in mental health: it is used to study the dynamics of mental health disorders, such as depression and bipolar disorder. Researchers have used chaotic models to develop predictions about the likelihood of relapse in patients and to identify the factors that contribute to the emergence of these disorders.

Finally, in terms of business and the stock market, chaos theory can explain to investors why healthy financial markets can suffer crashes and shocks. By using chaotic dynamics, investors can analyze the movements of prices and identify patterns that may not be immediately apparent.

### 4 Conclusion

In conclusion, chaos theory is a fascinating and complex field of study that has revolutionized our understanding of the world around us. First discovered by meteorologist Edward Lorenz, it deals with the behavior of dynamic systems that are highly sensitive to initial conditions, often referred to as the butterfly effect. Some examples of chaos theory include the double pendulum, Newton's three-body problem, and even time travel, while the real-world applications of chaos theory include predicting weather patterns, under-

standing biological systems, and modeling stock markets. Overall, chaos theory offers a new perspective on understanding complex systems and phenomena that were previously thought to be unpredictable. It has transformed our understanding of the world around us and continues to be a valuable tool in a various fields.



### References

- Butterflies, Tornadoes, and Time Travel*. American Physical Society.(2004). Retrieved January 8, 2023, from <https://www.aps.org/publications/apsnews/200406/butterfly-effect.cfm>
- Halton, C. (2023, January 2). *Chaos theory definition*. Investopedia. Retrieved January 8, 2023, from <https://www.investopedia.com/terms/c/chaostheory.asp#:text=Chaos%20Theory%20in%20the%20Stock%20Market.-Chaos%20theory%20is&text=Proponents%20of%20chaos%20theory%20believe,true%20health%20of%20the%20market>.
- Mangiarotti et al. (2020). Chaos theory applied to the outbreak of COVID-19: an ancillary approach to decision making in pandemic context. *Epidemiology and Infection*, 148. <https://doi.org/10.1017/s0950268820000990>
- Oestreicher, C. (2022). *A history of chaos theory*. Taylor & Francis. Retrieved January 8, 2023, from [doi.org/10.31887/DCNS.2007.9.3/coestreicher](https://doi.org/10.31887/DCNS.2007.9.3/coestreicher)
- Wikimedia Foundation. (2022, December 31). *Three-body problem*. Wikipedia. Retrieved January 8, 2023, from [https://en.wikipedia.org/wiki/Three-body\\_problem](https://en.wikipedia.org/wiki/Three-body_problem)
- Wikimedia Foundation. (2022, November 14). *Double pendulum*. Wikipedia. Retrieved January 8, 2023, from [https://en.wikipedia.org/wiki/Double\\_pendulum](https://en.wikipedia.org/wiki/Double_pendulum)

tronomer Issac Newton questioned whether long-term stability is possible—particularly the system comprising the Earth, the Sun, and the Moon—in his book *Principia Mathematica*.

The problem consists of three celestial objects moving around each other, and the goal is to find a closed-form solution to predict the course of these three objects. However, the smallest discrepancies, such as a slight difference of distance, can lead to chaos and randomness. Interestingly, there are a few special-case solutions to the three-body problem, such as the figure-eight solution (where the three bodies orbit each other in a figure-eight) or the elastic solution (where the three bodies orbit each other elastically).

Finally, a more theoretical but interesting example of chaos theory lies in the realm of a popular concept fantasized for centuries: time travel. Theoretically, if one were able to travel back in time and make a small alteration, it could result in significant changes in the future. For instance, imagine going back in time and striking up a conversation with a passerby. This person was on their way to a diner across the street, and this short conversation causes a delay of ten seconds. Because of this delay, as the person is crossing the street, he is hit by a car that would have missed him if it wasn't for the delay caused by the conversation. This person turns out to be Robert Oppenheimer, the man who would later go on to create the atomic bomb during World War II. As a result, the United States falls behind while the Axis develops their own atomic bomb and defeats the Allies. In this example, a seemingly insignificant conversation has drastically changed the course of history. However, one does not have to worry about this as time travel is not a reality... yet.

# 07 Investigating the Theoretical and Practical Applications of Fractals

Written by Doy yun, Munira Takalkar

## Investigating the Theoretical and Practical Applications of Fractals

Doy Yun Munira Takalkar

yun45629@sas.edu.sg, takalkar42662@sas.edu.sg

Teacher Reviewer:

Ms. Poluan

### Abstract

Fractals are fascinating geometrical figures that appear intricate and complex, but are actually made up of small repeating patterns. They can be found in various natural and man-made structures, such as snowflakes, coastlines, and African designs. This paper explores the different dimensions that distinguish fractals, highlights some notable mathematical examples, and showcases the practical applications of fractals in our world. By compiling various articles on the uses of fractals, it is evident that they have enormous potential for improving our understanding of patterns and providing more efficient ways of studying them. Fractals are a vast and exciting field that is yet to be fully explored, and their applications are endless. By delving into the world of fractals, we can gain a new appreciation for the beauty and complexity of our natural world, and perhaps even discover new ways of solving practical problems.

*Keywords:* fractals, Hausdorff dimension, Minkowski-Bouligand dimension, Mandelbrot set, Newton's fractal

## 1 Introduction

### 1.1 Background and Purpose of Research

This paper investigates both the theoretical and practical applications of fractals, providing an accessible understanding of seemingly abstract and infinite concepts. Conceptualized by the father of fractal geometry, Benoit Mandelbrot, with the intention of modeling nature, fractals are utilized to reflect a myriad of natural and chaotic processes, ranging from galaxy formation to cancer growth at a cellular level.

To model these natural phenomena, the idea of fractals as self-similar geometric figures emerged, signifying that each component regardless of magnitude has the same statistical properties as the whole. Such figures provide a basis to model the complexity, yet regularity, of certain forms of variety. Fractal geometry captures the jagged nature of figures, and as one zooms into a fractal, it appears to smooth out. As parts of this paper delve into abstract and theoretical ideas, it is essentially to keep the initial intent of fractals in mind: to model reality. Thus, the needless idealization of perfectly self-similar figures contradicts fractal geometry just as much as the diametric opposition of perfectly smooth figures.

## 2 Fractal Dimension

One of the key characteristics of a fractal is its possession of a fractal dimension exceeding its integer topological dimension (Albertovich & Aleksandrovna). Integer dimensions can be observed with two-dimensional and three-dimensional figures; however, while fractional dimensions align with similar concepts, they differ from standard dimensions present in Euclidean geometry (Ross).

### 2.1 Hausdorff Dimension

Fractals found in mathematics can be expressed in both algebraic and geometric manners. The most common mathematical definition, and the defining factor of a fractal, is the presence of self-similarity in a pattern (Ross). Self-similarity is not the only classification of a fractal, however. Self-similar fractals are repeated internally, meaning that when the pattern is enlarged, the same image is created at a smaller scale. Essentially, such figures are made up of smaller versions of themselves (Bishop).

The scale of this repetition, called fractal dimension, falls along the same scale as traditional dimensions within Euclidean space (Albertovich & Aleksandrovna). In geometry, a line is considered one-dimensional, a square is two-dimensional, and a cube is three-dimensional. When each of these is separated to produce self-similar objects, the scale at which the length, area, or volume – which can be referred to as magnitude – decreases is  $\frac{1}{2}$ ,  $\frac{1}{4}$ , and  $\frac{1}{8}$ , respectively, while the scale factor of a side length remains  $\frac{1}{2}$ . The dimension of these geometrical figures can therefore be thought of as any given power required to raise the scale factor of a side length such that it is equal to the scaled magnitude. Setting the magnitude at  $M$  and scale factor at  $s$ , the relation can be defined as  $M = s^D$ , with  $D$  defined as the figure's Hausdorff dimension (Albertovich & Aleksandrovna). Given  $M$  and  $s$ ,  $D$  can easily be found through the equation  $D = \log_s M = \frac{\log M}{\log s}$ .

Returning to the initial examples using standard geometrical figures present in Euclidean space, in the line's case, when scaled by a factor of  $\frac{1}{2}$ , the magnitude becomes  $\frac{1}{2}$  of the original, resulting in a dimension of 1, as  $\frac{1}{2} = (\frac{1}{2})^1$ . Looking at the square, when the length is scaled by the same factor of  $\frac{1}{2}$ , the magnitude is  $\frac{1}{4}$  of the initial figure's, resulting in a dimension of 2, as  $\frac{1}{4} = (\frac{1}{2})^2$ . This relation remains constant across figures of varying dimensions (Ross).

This evolved definition of dimension can be extended to fractal figures. Taking the Sierpinski triangle for instance, the scale of self-similarity is  $\frac{1}{3}$  of the original size, meaning that when a side length is scaled by  $\frac{1}{2}$ , the magnitude is scaled by  $\frac{1}{3}$ , forming the equation  $\frac{1}{3} = (\frac{1}{2})^D$ , where  $D$  equals approximately 1.585 (Bishop). In layman's terms, the Hausdorff dimension of a figure is essentially a measure of irregularity, with an increased dimension indicating increased roughness. As the fractal increases in complexity, the dimension heightens.

### 3 Correlation Dimension

Beneficial to the measuring of roughness in a data set is an understanding of the set's density, accomplished through the calculation of its correlation dimension, whereby balls of radius  $\varepsilon$  are placed centered at a point  $x$  of a point cloud and  $N_x(\varepsilon)$  represents the number of points within the ball (Ross). The radius is then varied, with  $N_x(\varepsilon) \propto \varepsilon^d$ , and the average value of  $N_x(\varepsilon)$  is found over various points to find  $C(\varepsilon)$ , which is also proportional to  $\varepsilon^d$ . To estimate  $d$  graphically, the graph of  $\ln(C)$  and  $\ln(\varepsilon)$  is plotted, and the slope of the curve is taken as the dimension (Bishop). This excludes the leftmost and rightmost sides of the curve, as these flatten due to being too small to reach other points and engulfing the entire set, respectively.

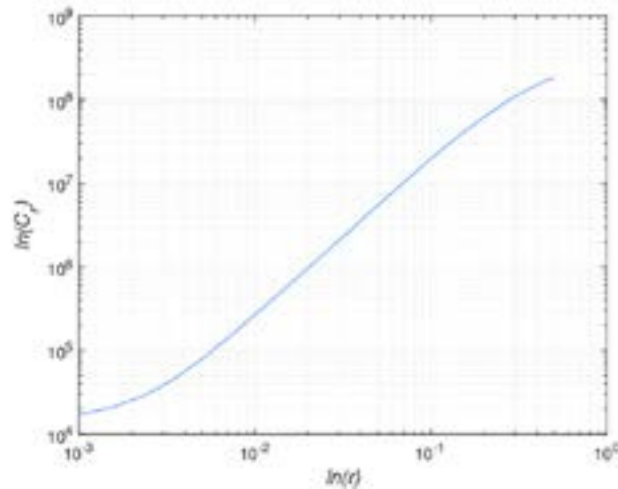


Figure 1: A sample curved produced by graphing  $\ln(C)$  against  $\ln(\varepsilon)$

(Arshad et al., 2021)

#### 3.1 Minkowski–Bouligand Dimension

While computing a figure's fractal dimension using Hausdorff dimension may be direct regarding simple or self-similar shapes, as Euclidean objects become more complex, it becomes more effectual to find their Minkowski–Bouligand dimension, a subset of fractal dimension. Minkowski–Bouligand dimension, additionally known as box-counting dimension, is a manner of determining the

fractal dimension of a set  $S$  in a metric space  $(X, d)$  (Albertovich & Aleksandrovna). This dimension is in many cases equivalent to a figure's Hausdorff dimension, though in certain sets the Minkowski dimension exceeds the Hausdorff dimension, such as in the set of rational points between  $[0, 1]$ , where they are 1 and 0, respectively. However, it consistently differs from a figure's correlation dimension, as it does not take into account the density of a set (Bishop).

In order to compute this dimensional value, boxes of side length are created along the set, with  $N(\varepsilon)$  representing the total boxes that come in contact with the data. Given a curve of length  $L$ , it can be found that  $N(\varepsilon) \propto \frac{L}{\varepsilon}$  (ross). Continuing, given a plane of area  $A$ ,  $N(\varepsilon) \propto \frac{A}{\varepsilon^2}$ , and given a three-dimensional data set of volume  $V$ ,  $N(\varepsilon) \propto \frac{V}{\varepsilon^3}$ . It can therefore be concluded that  $N(\varepsilon) \propto \frac{1}{\varepsilon^d}$ . In order to achieve the most accurate dimension,  $\varepsilon$  must be reduced, producing the equation  $d = \lim_{\varepsilon \rightarrow 0} \frac{\ln N(\varepsilon)}{\ln(\frac{1}{\varepsilon})}$  (if the limit exists). However, this definition begins to deteriorate when figures such as the Sierpinski triangle come into play, considering the consensus on its area is murky at best (Ross). In such instances,  $\log N(\varepsilon)$  is plotted against  $\log \frac{1}{\varepsilon}$ , with its slope taken as the dimension.

#### 3.2 Coastline Applications

Grown to become almost synonymous with fractal dimensions, the coastline paradox presents the question of how to calculate information regarding a coastline, considering it does not have a clearly defined length, resulting from ridges and inconsistencies that only compound as the field of view narrows (Bishop). Coastline lengths vary greatly, therefore, based on the scale of measurement, eventually approaching infinity. Taking into account a coastline's shape – neither truly self-similar, nor a primitive shape – the Minkowski–Bouligand dimension is the most effective dimension to determine a coastline's fractal dimension.

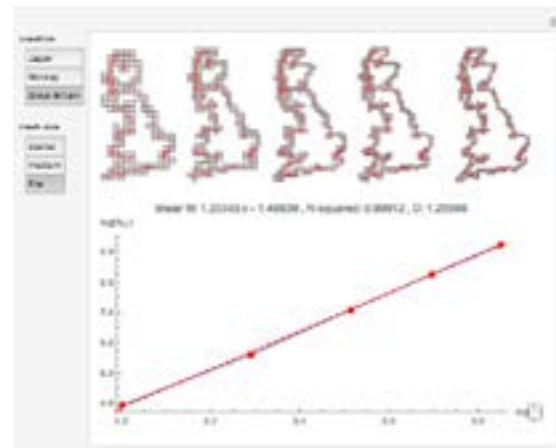


Figure 2: An estimation of the coastline of Britain's fractal dimension (Mahieu, 2014)

Through the slope of the line of best fit, it is apparent that the coastline of Britain's fractal dimension is approximately

1.25, acting as a quantitative index of the complexity of the region's coastline, comparable to others.

## 4 Mathematical Examples of Fractals

Fractals are what are known to be never-ending patterns, being infinitely complex and jagged. Though self-similarity isn't necessarily a requisite for fractals, due to the iterative nature of fractal creation, self-similarity in mathematical examples is widespread.

### 4.1 Dragon Curve

Dragon curves are defined as any member of a family of self-similar fractals, approximated by a recursive system of alternating directions, resulting in a fractal resembling the shape of the mythical creature. First investigated by NASA physicists John Heighway, Bruce Banks, and William Harter, the Heighway dragon curve is arguably the most prominent dragon curve (Albertovich & Aleksandrovna). Starting from a single line, the curve is constructed by an iterative process of the line splitting into two perpendicular smaller lines and forming an isosceles triangle with the original line. With each iteration, the direction of the split alternated between right and left, creating the curve. Another method in constructing this shape is to pick a pivot point, either on the far left or right, copy the original figure, and rotate it 90 degrees, alternating right and left. After undergoing just several iterations, the dragon curve is formed. As this particular fractal requires a recursive sequence of constant copying and pasting, it is considered to be a self-similar shape, with fractal dimension, or the dimensional value for self-similarity, being around 1.5236.

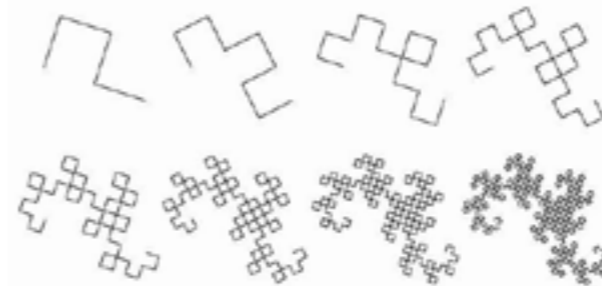


Figure 3: A model on how iterations create the dragon curve (Mahieu, 2014)

Several lesser-known versions of the dragon curve are also present, such as the twin dragon, terdragon, and golden dragon. The twin dragon, simply put, is two Heighway dragons placed back to back, with one of the dragons rotated 180 degrees. The terdragon is a more elaborate version of the Heighway dragon; as opposed to bisecting the initial line to form 90-degree angles, the terdragon trisects and forms 120-degree angles, resembling a sideways Z. The dimension for self-similarity is less than that of the Heighway dragon, approximately at 1.26186 (Ross).

The Golden Dragon fractal is one that is closely related to that of the Golden Ratio, first discovered by Leonardo

Davinci. The fractal dimension of this fractal is the golden ratio, or 1.618033. As seen by the comparison, the fractal dimension of the golden dragon fractal is more similar to that of the Heighway dragon than the Terdragon, thus, the shape of the golden dragon is also more alike to the Heighway dragon. However, instead of utilizing a perfectly perpendicular bisecting iterative sequence, the construction of the golden dragon relies predominantly on the side lengths of the two line segments (Albertovich & Aleksandrovna). The ratio between the two side lengths is  $r$ , with  $r$  being defined as  $(1/\Phi)^{(1/\Phi)}$ . With each iteration, the sides split into even more intricate segments, alternating right and left, maintaining the same ratio. The resultant dragon figure is a beautiful curve of intricate detail.

Though the dragon curves themselves do not have much use in the development of our knowledge in any field, it demonstrates the idea of how a simple code, under many iterations, can become complex and large.

### 4.2 Julia Set

Discovered by the renowned French mathematician, Gaston Julia, the Julia set is one of the most crucial examples of a mathematical fractal when it comes to the field of complex dynamics (Bishop). The Julia set, along with the Fatou set, are complementary sets defined by unique functions, with a set point and constant to produce a fractal. Fatou sets and Julia sets are similar in their iteration processes; however, the Fatou set consists of numerical values that behave similarly even when undergoing multiple iterations, whereas the Julia set consists of numerical values that behave chaotically when changed, even in the slightest quantity. Julia sets can be created using a variety of formulas, though the most widely known is the quadratic function defined by  $w = z^2 + C$ . The most significant factor in each set's difference are the initial values of  $Z$  and  $C$ , as the iteration process remains constant (Albertovich & Aleksandrovna). Both the values of  $Z$  and  $C$  are complex numbers, consisting of a real and imaginary part, thus resulting in the set's position on the complex plane as opposed to the standard Cartesian plane.

Though the value of  $Z$  consistently represents the point of interest, and the value of  $C$  represents as a constant, the multitude of combinations of these values allows for an infinite number of Julia sets. In each Julia set, the "fate" of each complex number  $Z$  is evaluated (Bishop). In other words, whether, as it is integrated, the number converges or diverges. The resultant is a myriad of different shapes, each visually represented by black areas and varied colors. The black regions indicate points where the numbers converge or stay between a bounded region as they undergo iterations. The colored regions, on the other hand, represent the complex numbers of  $Z$  that diverge, with the chromaticity indicating the speed at which the number tends toward infinity (Ross).

### 4.3 The Mandelbrot Set

Stemming from the revelation of Julia sets, the Mandelbrot set was created by Benoit Mandelbrot, utilizing the

same quadratic function,  $w = z^2 + C$ . As opposed to the Julia sets, however, the Mandelbrot set only has a singular variability factor,  $C$ , and always sets the initial value of  $Z$  to zero (ross). Due to this, the resultant is a singular image, which can be interpreted as a visual representation of all the quadratic functioned Julia sets.

It was discovered that for any Julia set, the point  $(0,0)$  on the complex plane determines the fate of the set, if the point is connected, or shaded black, then the entire set is connected; however, if the point is disconnected, or colored, then the entire set is infinitely disconnected (Albertovich & Aleksandrovna). Due to this, by compiling the origins of each Julia set at the origin point, the resultant image of the Mandelbrot set visually represents the behavior of all the complex  $C$  values in the Julia set, each point representing a unique Julia set (Bishop). If a Julia set with a pair of specific values for their variables doesn't diverge to infinity when iterated, the corresponding point is shaded black. Conversely, if, under iteration, the Julia set escapes to infinity, the point is colored, with the different hues representing the rate at which the complex  $C$ -values diverge to infinity.

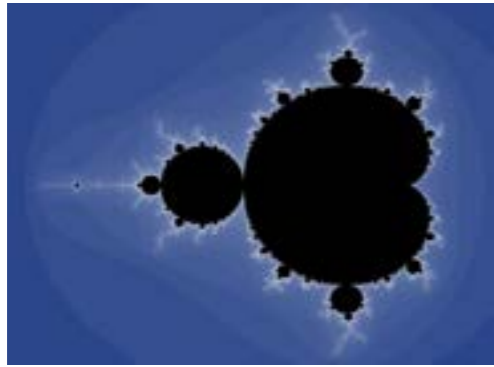


Figure 4: The Mandelbrot Set (*The Mandelbrot Set*, n.d.)

The outline of the Mandelbrot set consists of a main cardioid shape, and a smaller circular shape with converging black regions on either side. These two figures are within the x-value boundaries of -2 and 0.25, of which there are  $C$ -values to which the Julia set is connected. The cardioid shape represents the values of an attractive fixing point of the Julia sets, of which are between the bounds of -0.75 to 0.25 (Ross). The circular shape represents the values of behaving in a different manner and is situated within -1.25 and -0.75. The other values are unable to escape toward infinity, despite constant iterations; however, they do not fall into either criterion of behavior.

The Mandelbrot set itself poses several interesting phenomena, including many of the Julia sets themselves being embedded into the mapping of the Mandelbrot set. Infinitely many Julia sets of a variety of shapes and sizes can be found within all areas of the Mandelbrot set. Furthermore, a significantly scaled-down figure of the Mandelbrot set can be found centered around each of the respective Julia sets (Bishop). Taking the role of one of the more celebrated mathematical fractals, the Mandelbrot set is an excellent example of the idea of a complex structure being produced

simply utilizing elementary rules.

#### 4.4 Newton Fractals

Newton fractals are fractals that have been made using the generalized form of Newton's iteration. Contrary to belief, Isaac Newton was not the creator of this particular fractal series, and on the contrary, wasn't aware of its existence. Newton's iteration is undoubtedly a concept that is well-known in the calculus community, using derivatives to obtain a close approximation of the root(s) of a function. The iteration, also known as the Newton-Raphson method, is usually in the general form of  $x(n+1) = x(n) - [f(x)/f'(x)]$ , utilizing tangent lines slopes as a way to approximate (Albertovich & Aleksandrovna). Picking a starting point close to that of the approximation value leads to almost a sudden convergence to the root(s); however, when the starting approximation is inaccurate and has a high error bound, an interesting phenomenon occurs. In the context of calculus, the initial approximate value is typically picked within the realms of real numbers, but for Newton's fractals, this bound is expanded to imaginary numbers, and mainly employs complex numbers.

Newton's Fractals are a special case of Julia sets, with intricate details arising from simple functions due to the repetition of interactive sequences. The outcome of Newton's fractals is highly dependent on the starting point and can differ greatly from one another, despite the starting point yielding such a minuscule change (Bishop). Similar to the Mandelbrot set, Newton's fractals are set in the complex plane and can be represented as a map of all the possible starting values of the approximation. Undergoing multiple iterations, whichever root value each point ends up with is the color that is assigned, and when the point is placed back into its original position, Newton's fractal is formed (Ross). The fractal shape can change dramatically based on the initial function conditions, and the number of iterations undergone can enlarge the details within each fractal.

#### 4.5 The Fibonacci Sequence

An additional mathematical example of a fractal is the Fibonacci sequence, the less renowned counterpart of the golden ratio. This particular fractal, however, is unlike that of the previously explored fractals in this paper and can be classified as an arithmetic fractal rather than a geometric fractal. Named after Leonardo da Vinci's pen name, Fibonacci, the Fibonacci Sequence is a unique pattern of which is defined by the recursive rules of  $x_n = x_{n-1} + x_{n-2}$ . Setting  $x_0$  at 0 and  $x_1$  at 1 allows for the sequence to emerge as the following: 0, 1, 1, 2, 3, 5, 8, 13, 21, 34....

The golden ratio emerges from these numbers; as the sequence continues on to infinity, the ratio between  $x_n$  and  $x_{n-1}$  becomes closer and closer to what we now define as the golden ratio, or about 1.618. Using this ratio, Da Vinci was able to figure out the  $n$ th term of the Fibonacci sequences, proven to be  $x_n = (\Phi^n - (1 - \Phi)^n) / \sqrt{5}$ . Within his exploration, however, Da Vinci found that squaring the numbers within the Fibonacci sequence allowed for a perfectly fitted arrangement of squares, which, when connected,

became a perfect spiral, translating into the basis of divine proportions – the golden spiral.

### 5 Application of Fractals

Though fractals were initially a more theoretical discovery, they have since been found applicable in various aspects of our lives, in both natural and industrial settings. With their initial findings, fractals have been proven true to be an incredibly valuable tool in synthesizing and analyzing patterns, even when it isn't blatantly obvious. Using this tool has allowed for various advancements in the field of biology, computer science, and medicine, and will continue to assist in making groundbreaking discoveries.

#### 5.1 Fractals in Nature

Fractals, despite their basis being mathematical, are present everywhere in nature. From the physical shape of natural figures, to the formation of their growing patterns, fractals are highly prevalent in analyzing nature's patterns.

The Fibonacci sequence, due to its recursive rule of having the sum of the two previous terms be the next, has the valuable characteristic of space efficiency—a tool that greatly assists in effectively utilizing the space provided (Albertovich & Aleksandrovna). Consequently, tree branches, lightning, waterfalls, and even organisms' reproduction patterns mimic the sequence of Fibonacci, allowing for expansion with efficient usage of space. Furthermore, on account of the golden ratio being a principle law pertaining to natural figures, the golden spiral can be found translated into nature, such as in the shapes of seashells or the galaxy itself.

The Julia sets embedded into the Mandelbrot set are also seen in various natural references. Due to its flexibility in its manipulation of shape and size, Julia sets of diverse formations can be applied to similar organisms to better tailor the exact details of each one (Bishop). The shape of octopus tentacles, ferns, and waves are all in accordance with a branch of Julia sets, whether that be the entirety of the Julia set, or just a portion.

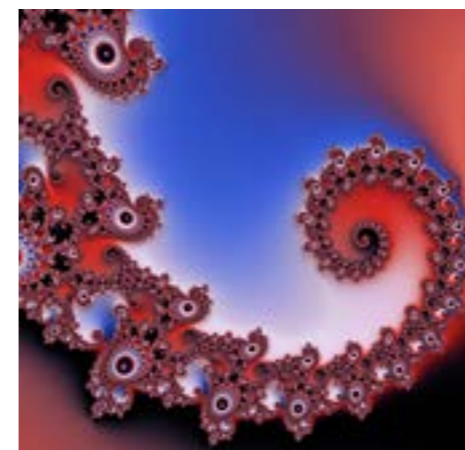


Figure 5: A Fractal Resembling an Octopus Tentacle (*Patenters - Industry IoT Consortium*, 2023)

In order to achieve the figure of an octopus tentacle or a wave, the entire Julia set would have to be used. However, in contrast, only a small portion of the Julia set would be used in mimicking the shape of a fern. The ability for nature to be described with a singular fractal opens up an array of possibilities in their application.

As fractals are highly relevant in nature, it is, in turn, highly relevant in modeling it with the assistance of modern technology. As aforementioned, fractals oftentimes resemble the shape of a natural figure, with their systemic but not perfectly symmetrical figure. As nature being imperfect has been an established fact, having a figure that can embed flaws into its design is highly useful in the field of computer science (Bishop). The iterative nature of fractals leading to more complex figures allows for code to be written in a much shorter amount of time, whilst simultaneously creating a more unique and accurate representation of nature as a result. Though the Mandelbrot set itself isn't found in natural applications, aspects of it have been applied in remodeling nature, coastlines, low-flying terrain navigation, area measurements, and even city planning (Ross). The assistance of fractals has likewise led to an improvement in the field of CGI, enabling graphic designers to create more realistic animations and models.

#### 5.2 Fractals in Medicine

Beyond seemingly abstract and disconnected applications, however, breakthroughs in the field of medicine using fractals have veritable implications on human life and well-being. From the use of fractals in ECG analysis to determine blood vessel health, to the fractal-like nature of the lungs, similar to that of a tree, whose functions both constitute respiration (Albertovich & Aleksandrovna). Surface area is directly proportional to the efficiency of gas exchange, a process by which oxygen and carbon dioxide move by diffusion across a surface, and fractal branching is an effectual method to maximize surface area while concurrently minimizing space.

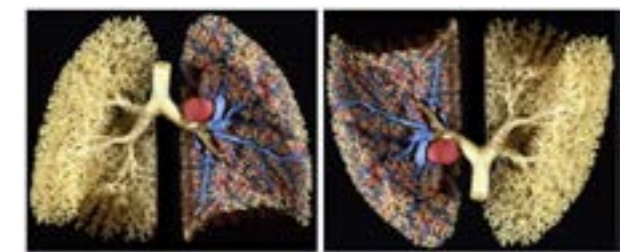


Figure 6: A comparison of the structure of human lungs and a tree. (Kelshiker, 2021)

Fractal patterns additionally have the potential to quantify the precise stage of deterioration of the retina during the clinical diagnosis of diabetic retinopathy, a complication of diabetes that damages the retina and affects 80 percent of all patients with diabetes for over ten years (Albertovich & Aleksandrovna). This quantification of deterioration opens pathways to evaluate the progress of treatment over time and

determine a reference value to act as an indicator of pathological cases, developing a non-invasive method of early detection of retinal vascular diseases. Diabetic retinopathy changes the structure of blood vessels, impacting the fractal dimension of the retina (Albertovich & Aleksandrovna). Apparent in Figure 4, when subjected to fractal analysis, pathological cases have a lower Minkowski-Bouligand dimension, as compared to a normal eye, aiding in the diagnosis of such a disease.

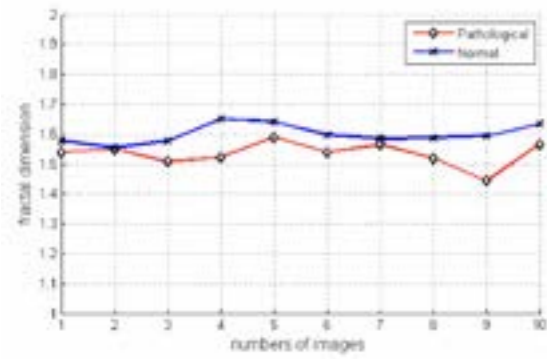


Figure 7: A comparison of the fractal dimension of blood vessels within normal eyes against that of patients with diabetic retinopathy. (Uahabi & Atounti, 2015)

## 6 Conclusion

The field of fractal geometry is a vast arena that has extensive potential in its applications in diverse disciplines. It will unquestionably contribute to a multitude of medicinal and technological advances, facilitating the rapid revolutionization of the world.

## References

- Albertovich, T. D. & Aleksandrovna, R. I. (2017, July 26). *The Fractal Analysis of the Images and Signals in Medical Diagnostics*. IntechOpen. <https://www.intechopen.com/chapters/55028>
- Arshad, M. H., Kassas, M., Hussein, A. E., Abido, M. A. (2021, January 4). *A Simple Technique for Studying Chaos Using Jerk Equation with Discrete Time Sine Map*. ResearchGate. [https://www.researchgate.net/publication/348243264\\_A\\_Simple\\_Technique\\_for\\_Studying\\_Chaos\\_Using\\_Jerk\\_Equation\\_with\\_Discrete\\_Time\\_Sine\\_Map](https://www.researchgate.net/publication/348243264_A_Simple_Technique_for_Studying_Chaos_Using_Jerk_Equation_with_Discrete_Time_Sine_Map)
- Bishop, C., Peres, Y. (2016). *Fractals in Probability and Analysis (Cambridge Studies in Advanced Mathematics)*. Cambridge: Cambridge University Press. doi:10.1017/9781316460238
- Kelshiker, A. (2021, March 16). *How Math Could Save Lives – Dartmouth Undergraduate Journal of Science*. <https://sites.dartmouth.edu/dujs/2021/03/16/ow-math-could-save-lives/>
- Mahieu, E. (2014, January). *Wolfram Demonstrations Project*. <https://demonstrations.wolfram.com/BoxCountingTheDimensionOfCoastlines/>
- Patterns - Industry IoT Consortium*. (2023, April 4). Industry IoT Consortium. <https://www.iiconsortium.org/patterns/>
- Ross, S. (2022). *Fractal Dimension - Box-Counting Correlation Dimension [Video]*. [https://www.youtube.com/watch?v=IfP4wAC4HtA&ab\\_channel=RossDynamicsLab](https://www.youtube.com/watch?v=IfP4wAC4HtA&ab_channel=RossDynamicsLab)
- The Mandelbrot Set*. (n.d.). <http://www.math.utah.edu/~alfeld/math/mandelbrot/mandelbrot.html>
- Uahabi, K. L., M. Atounti. (2015). *Applications of fractals in medicine*. Annals of the University of Craiova - Mathematics and Computer Science Series; <https://www.semanticscholar.org/paper/Applications-of-fractals-in-medicine-Uahabi-Atounti/ab3a0a5bde175e501896ffab1ac8319d111bc8bf>

# 08 Singular Value Decomposition and a Recommendation Algorithm

Written by Frank Xie

## Abstract

Given the dependence of most internet users on Google, Amazon, or other search and recommendation engines, it is important to recall the basis of many of these engines. This paper will reconstruct a rudimentary recommendation algorithm and present a potential use for it in the form of a book recommender using data from Kaggle. The main tool used in the algorithm is singular value decomposition, or SVD, and code was executed in Python.

**Keywords:** recommendation algorithm, Singular Value Decomposition (SVD), eigenvalues, diagonalization, Kaggle

# Singular Value Decomposition and a Recommendation Algorithm (ATLA Project)

Frank Xie

xie48478@sas.edu.sg

Teacher Reviewer:

Mr. Zitur

## 1 Introduction

As the digital world grows increasingly competitive, many online companies have raced to make their products and services more addictive, personal, and attractive than ever. As they cater to more people, however, it becomes next to impossible to use human time to customise or adjust to a significant degree - instead, algorithms are used. Among the most famous (or infamous) are the YouTube algorithm, Spotify's recommendations, and Amazon's "Customers who bought this item also bought..." One method used to make these algorithms is singular value decomposition, or SVD.

Singular value decomposition is an extremely useful technique in many areas of science, mathematics, and data analysis, and is an extended version of eigendecomposition, also known as diagonalisation. The reason that it is more powerful than diagonalisation is because it can factor all matrices, while diagonalisation can only be performed on certain (non-defective) matrices.

Before creating a SVD, the concept of singular values of an  $m \times n$  matrix  $\mathbf{A}$  should be considered first. These are the eigenvalues of  $\mathbf{A}^T\mathbf{A}$ , which must necessarily be  $n \times n$ , and there must exist an orthonormal basis for  $\mathbb{R}^n$  consisting of the eigenvectors of  $\mathbf{A}^T\mathbf{A}$ ,  $\mathbf{v}_1, \mathbf{v}_2, \dots, \mathbf{v}_n$  with associated nonnegative eigenvalues  $\lambda_1, \lambda_2, \dots, \lambda_n$ . With some renumbering, it is always possible to assume that the eigenvalues can be arranged in descending order such that

$$\lambda_1 \geq \lambda_2 \geq \dots \geq \lambda_n.$$

The square roots of each  $\lambda_n$  correspond to  $\sigma_1, \sigma_2, \dots, \sigma_n$  which are in descending order. These  $\sigma_n = \sqrt{\lambda_n}$  are the singular values of  $\mathbf{A}$ , and represent the lengths of the vectors  $\mathbf{A}\mathbf{v}_1, \mathbf{A}\mathbf{v}_2, \dots, \mathbf{A}\mathbf{v}_n$ , among other things. These values are key to creating a SVD.

The SVD can be stated as  $\mathbf{A} = \mathbf{U}\mathbf{\Sigma}\mathbf{V}^T$ , for any  $m \times n$  matrix  $\mathbf{A}$  with rank  $r$ , and  $\mathbf{\Sigma}$  a diagonal matrix of the form

$$\begin{pmatrix} \mathbf{D} & 0 & \dots & 0 \\ 0 & 0 & & \\ \vdots & & \ddots & \\ 0 & & & 0 \end{pmatrix}$$

and  $\mathbf{D}$  an  $r \times r$  matrix of the form

$$\begin{pmatrix} \sigma_1 & 0 & \dots & 0 \\ 0 & \sigma_2 & & \\ \vdots & & \ddots & \\ 0 & & & \sigma_r \end{pmatrix}$$

if  $\sigma_r$  is the least nonzero singular value of  $\mathbf{A}$ ; and where  $\mathbf{U}$  and  $\mathbf{V}$  are orthogonal matrices.

## 2 Construction of an SVD

The construction of a singular value decomposition can be split into 3 steps ("Linear Algebra and its Applications"). This example will show the decomposition of

$$\mathbf{A} = \begin{pmatrix} 3 & 2 & 2 \\ 2 & 3 & -2 \end{pmatrix}.$$

*Step 1.* Find an orthogonal diagonalisation of  $\mathbf{A}^T\mathbf{A}$ . This is often difficult with larger matrices (due to the difficulty in finding their eigenvalues), but for smaller matrices is doable. First, find the eigenvalues of  $\mathbf{A}^T\mathbf{A}$ , which in this case are 25, 9, and 0. Then, since  $\mathbf{A}^T\mathbf{A}$  is symmetric the eigenvectors must be orthogonal, so simply computing them is enough. We find the eigenvectors as unit vectors

$$\mathbf{v}_1 = \begin{pmatrix} 1/\sqrt{2} \\ 1/\sqrt{2} \\ 0 \end{pmatrix}, \quad \lambda = 25$$

$$\mathbf{v}_2 = \begin{pmatrix} 1/\sqrt{18} \\ -1/\sqrt{18} \\ 4/\sqrt{18} \end{pmatrix}, \quad \lambda = 9.$$

Then, finding a vector orthogonal to both vectors (i.e. noting that their dot product will equal 0) yields the final eigenvector

$$\mathbf{v}_3 = \begin{pmatrix} 2/3 \\ -2/3 \\ -1/3 \end{pmatrix}$$

*Step 2.* Set up  $\mathbf{\Sigma}$  and  $\mathbf{V}$ .  $\mathbf{V}$  is simply  $[\mathbf{v}_1 \ \mathbf{v}_2 \ \mathbf{v}_3]$ , for their corresponding eigenvalues in decreasing order. In the final SVD, the transpose,  $\mathbf{V}^T$  is used, which equals

$$\begin{pmatrix} 1/\sqrt{2} & 1/\sqrt{2} & 0 \\ 1/\sqrt{18} & -1/\sqrt{18} & 4/\sqrt{18} \\ 2/3 & -2/3 & -1/3 \end{pmatrix}.$$

Then, using the singular values (simply the square roots of the nonzero eigenvalues in order) 5 and 3,

$$\mathbf{\Sigma} = \begin{pmatrix} 5 & 0 & 0 \\ 0 & 3 & 0 \end{pmatrix}$$

Note the 0 column padding out the matrix into a  $2 \times 3$  matrix.

*Step 3.* Construct  $\mathbf{U}$ . Finally, using the formula  $\mathbf{u}_i = \frac{1}{\sigma_i} \mathbf{A}\mathbf{v}_i$ , so that  $\mathbf{U} = [\mathbf{u}_1 \ \mathbf{u}_2 \ \mathbf{u}_3]$ , we find

$$\mathbf{U} = \begin{pmatrix} 1/\sqrt{2} & 1/\sqrt{2} \\ 1/\sqrt{2} & -1/\sqrt{2} \end{pmatrix}$$

Then, the singular value decomposition of the matrix is

$$\mathbf{A} = \mathbf{U}\mathbf{\Sigma}\mathbf{V}^T = \begin{pmatrix} \frac{1}{\sqrt{2}} & \frac{1}{\sqrt{2}} \\ \frac{1}{\sqrt{2}} & -\frac{1}{\sqrt{2}} \end{pmatrix} \begin{pmatrix} 5 & 0 & 0 \\ 0 & 3 & 0 \end{pmatrix} \begin{pmatrix} \frac{1}{\sqrt{2}} & \frac{1}{\sqrt{2}} & 0 \\ \frac{1}{\sqrt{18}} & -\frac{1}{\sqrt{18}} & \frac{4}{\sqrt{18}} \\ \frac{2}{3} & -\frac{2}{3} & -\frac{1}{3} \end{pmatrix}.$$

This process can be cleverly modified to increase computation speed for computers, but this method will suffice for most human requirements.

## 3 Recommendation Algorithm

The code used here will be intentionally reductive, as programming a full implementation of all the steps involved in SVD is unnecessarily complex. For larger algorithms, some clever math and programming is required to reduce the processing power required, as the increase in processing power

would otherwise be roughly linear—not great for, say, 48 million data points. This implementation will be done in python.

The algorithm is in roughly three stages: preprocessing the data, performing singular value decomposition, and interpreting the output. The imported libraries are

```
1 import numpy as np
2 import pandas as pd
3 from scipy.linalg import svd
4 import matplotlib.pyplot as plt
5 from mpl_toolkits.mplot3d import Axes3D
6 import os
```

which are used to process and visualise the data. An extremely rigorously collected set of data on food preferences is used as an example dataset (where A = Apple, B = Banana, C = Curry, D = Durian, É = Éclair, and F = Fries; scores range from 0 to 10. Yes, I really asked people this. Yes, they were confused.):

	A	B	C	D	É	F
AM	4	10	10	6	3	7
BU	6	7	0	10	3	3
JL	7	10	10	5	3	10
JZ	6	7	4	3	6	7
HC	4	7	1	3	8	2
HY	3	6	10	5	7	6
RY	5	4	0	7	6	10
RP	6	9	0	4	1	6
JK	5	5	0	3	7	8
SB	2	8	10	4	9	7
ZK	5	1	10	1	10	10
WH	6	8	4	3	4	0
AL	0	0	10	0	10	10

### 3.1 Preprocessing the Data

This step either randomly generates or takes a .csv file and outputs a matrix that is users by items in size. This is necessary for the next steps, as the data that is given in the main method (see visualising the data) is unpacked into a list and needs to be a matrix.

```
1 def randmatrix(users, items): # creates
2     random matrix that is users x items
3     data = []
4     for i in range(users):
5         user = [np.random.randint(11)/10
6                 for _ in range(items)]
7         data.append(user)
8     mat = pd.DataFrame(data)
9     mat.index = ["User " + str(i) for i
10                 in range(users)]
11    mat.columns = ["Item " + str(i) for
12                  i in range(items)]
13    return mat
14
15 def matrix(users, values): # creates
16     predefined matrix (values) that is
17     users x items
18    data = []
19    for i in range(users):
20        user = [values[6*i + k] for k in
21                range(6)]
```

```

16 data.append(user)
17 mat = pd.DataFrame(data)
18 mat.index = ["User " + str(i + 1)
19 for i in range(users)]
20 mat.columns = ["Item " + str(i + 1)
21 for i in range(6)]
22 return mat

```

### 3.2 Processing the Data

This step simply performs SVD on the matrix  $A$  that is outputted from the previous step, returning the smallest possible  $U$ ,  $\Sigma$ , and  $V^T$ . While it is possible to program this decomposition myself, the library provided a significantly less computationally intensive algorithm. Usually, SVD is fairly difficult for a computer to process. This algorithm also reduces the dimensionality of  $U$  and  $V$  in order to keep the matrices as easy to visualise as possible. The columns that are kept ( $k$ ) correspond to the highest singular values.

```

1 def do_svd(mat, k=0, option=False): #
2     performs singular value decomposition
3     on matrix mat and returns sigma, u,
4     and vt
5     u, sigma, vt = svd(mat)
6     u = pd.DataFrame(u[:, :k])
7     vt = pd.DataFrame(vt[:, :k, :])
8     if option:
9         return sigma
10    else:
11        return u, vt

```

### 3.3 Interpreting the Output

The output is processed here. This method takes in an item and  $V^T$ , returning the most 'recommended' item based on the preferences of everyone in the dataset. This is computed by dotting each column of  $V^T$  with the item, and finding the item the least distance (which, by SVD, must be the most similar).

```

1 def recommend(item, vt, output_num=1): #
2     recommendation using dot product
3     distance
4     global rec
5     rec = []
6     for item in range(len(vt.columns)):
7         if item != item:
8             rec.append([item, np.dot(vt[
9 item], vt[item])])
10    final_rec = [i[0] for i in sorted(
11 rec, key=lambda x: x[1], reverse=True)
12 ]
13 return final_rec[:output_num]

```

### 3.4 Visualising the Data

Finally, the data is visualised. The method defined above simply plots the data using matplotlib, and the main method uses the above functions to extract data from the .csv and create a basic interface.

```

1 def plot_data(mat, data_type, camera=
2 None): # plots data using matplotlib
3 fig = plt.figure()
4 ax = fig.add_subplot(111, projection
5 ='3d')
6 if camera != None:

```

```

5 ax.view_init(elev=camera[0],
6 azim=camera[1])
7 for index, row in mat.iterrows():
8 ax.scatter(row[0], row[1], row
9 [2], alpha=0.8)
10 ax.text(row[0], row[1], row[2],
11 '{0} {1}'.format(data_type, index),
12 size=10)
13 plt.show()
14 // skip //
15 if __name__ == "__main__":
16 filename = os.getcwd()+"\\Downloads
17 \\"+"likesdata.txt"
18 a = matrix(12, list(np.array([[int
19 (i) for i in line.split(",")] for
20 line in open(filename, "r").readlines
21 (]]).reshape((-1)))) # this works
22 #a = randmatrix(20, 10)
23 u = do_svd(a, 3)[0]
24 vt = do_svd(a, 3)[1]
25
26 print(a)
27 n = int(input())
28 print("If you liked " + str(n) + ",
29 try " + str(recommend(n, VT, 2)))
30 print(rec)
31 plot_data(u, "User")
32 plot_data(vt.T, "Item")

```

The output of the program looks like this:

User	Item 1	Item 2	Item 3	Item 4	Item 5	Item 6
User 1	0	0	10	0	10	10
User 2	4	10	10	6	3	7
User 3	6	7	0	10	0	3
User 4	6	7	4	3	6	7
User 5	7	10	10	5	3	10
User 6	4	7	1	3	8	2
User 7	3	6	10	5	7	6
User 8	5	4	0	7	6	10
User 9	6	9	0	4	1	6
User 10	5	5	0	3	7	8
User 11	2	8	10	4	9	7
User 12	5	1	10	1	10	10

Figure 1: Printout of the data table

```

Recommend based on: 2
If you liked 2, try [1, 5]

```

Figure 2: The upper number is user-inputted; the algorithm returns that if a user liked curry (2) that they would most likely also like bananas (1) and fries (5)

## 4 Extension: Curing Ennui

I needed book recommendations, but interacting with people is cringe. So I used my algorithm to cure my book ennui.

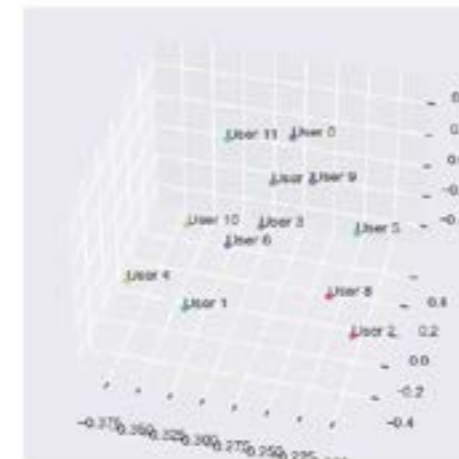


Figure 3: A graph is created that shows the propinquity (similarity) of each user - user 7 (RY) is very similar to user 9 (JK), as they are close to each other

### 4.1 How to Cure Ennui with Math

Having gone through the legwork of creating the algorithm, my extension is mostly in refining and applying the algorithm to something that will help me personally, and potentially others, with motivation. The first part of the extension is in finding the data, for which I turned to the scourge of Big Data - Kaggle. As much as I hate the modern invasion of privacy that the internet has provided, Alphabet's benevolence in providing this data is very helpful. The dataset I imported was Book Ratings: <https://www.kaggle.com/arashnic/book-recommendation-dataset?select=Ratings.csv>

### 4.2 Preprocessing

The book dataset was very large (340,556 unique users, each rating a large number of books), so efficiency was more important in analysing the dataset. The first task was to generate a matrix, with size users x books, which was done using the following code:

```

1 import os
2 import pandas
3 import numpy as np
4
5 df = pandas.read_csv(os.getcwd()+"\\"+
6 Ratings.csv")
7
8 books = df["ISBN"].unique()
9 books = books[:5000]
10 df_small = df.loc[df["ISBN"].isin(books)
11 ]
12 users = df_small["User-ID"].unique()
13 df = df_small.copy()
14
15 matrix = pandas.DataFrame(data=np.zeros(
16 dtype=np.uint8, shape=(len(users), len(
17 books))), index=users, columns=books)

```

```

16 for _, row in df.iterrows():
17     matrix.at[row["User-ID"], row["ISBN"]
18 ] = row["Book-Rating"]
19
20 matrix.to_csv(os.getcwd()+"\\"+matrix.
21 csv")
22 print(matrix)

```

which I ran separately from the main code, as this removes the necessity of generating the whole matrix every time this algorithm is run.

This preprocessing step also served to choose a sampling of the books - the first 5000 unique books by their ISBN, which was randomised. This was to reduce processing time, as the original algorithm I applied took extremely long to run, and would have generated a file that contained upwards of 400 GB of data.

### 4.3 Output

The output of the algorithm is similar to earlier. The matrix looks like this:



Figure 4: Output matrix

Most users fell along a particular line, but a few were outliers (they rated a lot of books!), and the most popular books also became outliers:

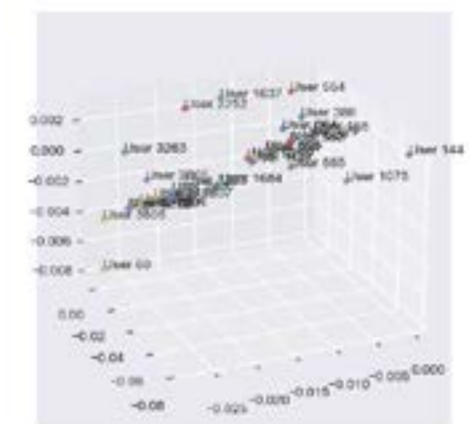


Figure 5: Graph of users



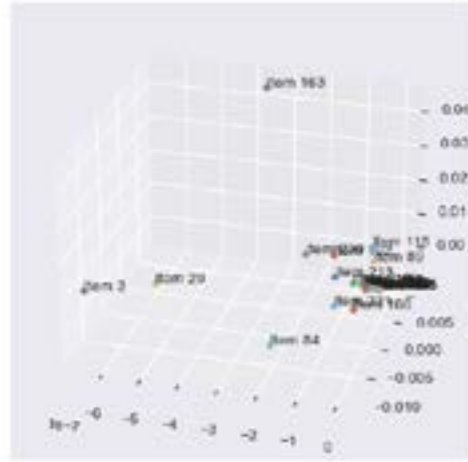


Figure 6: Graph of books

Note that the plots, for readability's sake, do not plot every single user or item. The most interesting part of the algorithm, for me, was getting the book recommendation, which was as follows:

```
Recommend based on: 160
If you liked 160, try [173, 9]
```

160 corresponded to *The Catcher in the Rye*, and 173 and 9 to *The Catcher in the Rye - Barron's Book Notes* and *The Adventures of Huckleberry Finn*, respectively. Conveniently, I haven't read *The Adventures of Huckleberry Finn* before, so I may very well read it now. Note that the algorithm is fairly efficient; even running with 16824500 datapoints ( $33649 \times 5000$ ), it only takes 10 minutes or so to run, after an update to the way the data is packed (as a matrix .csv, rather than a plain list).

## 5 Summary

This algorithm has been shown now to be useful enough in providing recommendations. The largest bottlenecks in performance come from the generation of the matrix and the matrix computations needed. Other implementations of this algorithm, or future uses of this implementation, should probably spend some time designing a more friendly GUI and optimising performance. Other datasets available online are also usable with this algorithm: <https://www.kaggle.com/shadey/spotify-2010-2019/data>, for example, which is a Spotify music preference dataset.

## References

Deep Dive into Netflix's Recommender System. (2021). Retrieved 25 January 2023, from <https://towardsdatascience.com/deep-dive-into-netflixs-recommender-system-341806ae3b48>  
 Understanding Singular Value Decomposition and its Application in Data Science. (2022). Retrieved 25 January

2023, from <https://towardsdatascience.com/understanding-singular-value-decomposition-and-its-application-in-data-science-388a54be95d>  
 Singular Value Decomposition (SVD) tutorial. (2023). Retrieved 25 January 2023, from [https://web.mit.edu/be.400/www/SVD/Singular\\_Value\\_Decomposition.htm](https://web.mit.edu/be.400/www/SVD/Singular_Value_Decomposition.htm)  
 Lay, Lay, Mcdonald (2015) *Linear Algebra and Its Applications*. Pearson.

# 09 Natural Eigenvectors in Higher Number Systems

Written by Gaurav Goel

# Natural Eigenvectors in Higher Number Systems

Gaurav Goel

goel47628@sas.edu.sg

Teacher Reviewer:

Mr. Craig

## Abstract

Linear algebra is generally introduced through working with the real number system in different dimensions ( $\mathbb{R}$ ,  $\mathbb{R}^2$ ,  $\mathbb{R}^3$ , and so on). However, there are a variety of alternative number systems that are fields, which embrace multidimensionality in a much more accessible and natural manner.

In this paper, I aim to investigate a few of these number systems, interpret them through linear algebra, and discover a higher number system which embraces eigenvalues in a natural way. Essentially, I will extend on my understanding of linear algebra and eigenvectors to interpret the behaviour of different number systems.

*Keywords:* eigenvalues, Clifford Algebra, multidimensionality, number systems

## 1 Exploration of Different Number Systems

There are a variety of different number systems that we can investigate. These include the rational numbers ( $\mathbb{Q}$ ), complex numbers ( $\mathbb{C}$ ), quaternions ( $\mathbb{H}$ ), finite fields ( $\mathbb{Z}_n$ ), and many more. However, the aim here is not to investigate an arbitrary number system. Rather, we want to investigate number systems that naturally incorporate elements and properties of linear algebra. This means that we want to find number systems that naturally combine scalar and vector properties. In fact, after some researching, there is indeed a class of number systems which do just this: Clifford Algebras.

A Clifford Algebra, denoted  $Cl_{a,b}(\mathbb{R})$ , is a class of algebras where any general element  $q = a + \vec{v}$ , where  $a$  is the scalar part and  $\vec{v}$  is the vector part. Adding two elements simply makes use of scalar and vector addition, but multiplying two elements gives us an interesting combination of scalar multiples, dot products, and cross products.

More generally speaking, if  $\vec{e}_1, \vec{e}_2, \vec{e}_3, \dots$  are orthogonal unit vectors, a Clifford Algebra element can be defined as:

$$q = a_0 + a_1\vec{e}_1 + a_2\vec{e}_2 + a_3\vec{e}_3 + \dots$$

In this case, the column vector representing our element  $q$  is:

$$\begin{pmatrix} a_0 \\ a_1 \\ a_2 \\ a_3 \\ \vdots \end{pmatrix}$$

And, since Clifford Algebras already define addition and multiplication between elements for us, we can directly take these definitions to linear algebra, by using vector addition and matrix multiplication. This gives us a number system framework that naturally incorporates vector and matrix properties.

Now that we have a basic understanding of how linear algebra can be applied to understand Clifford Algebras, we seek to understand how eigenvectors can be applied to these algebras. In particular, just as eigenvectors seek to understand how matrix multiplication and scalar multiplication act equivalently on a vector, in these Clifford Algebras, we want to discover whether or not element-wise multiplication and scalar multiplication act equivalently on elements.

We may begin by selecting a few basic Clifford Algebras and analyzing whether or not this is possible.

## 2 Complex Numbers

The most intuitive Clifford Algebra to begin with is  $Cl_{1,0}(\mathbb{R})$ , or the complex number system ( $\mathbb{C}$ ). This is because each  $z \in \mathbb{C}$  can be written in two components ( $a + bi$ ). In order to discover whether or not eigenvectors can be applied to complex numbers, we have to take two steps. First, we apply linear algebra to complex numbers. Second, we search for eigenvectors in this linear algebra representation of complex numbers.

### 2.1 Applying Linear Algebra to Complex Numbers

Applying linear algebra to complex numbers takes three steps. First, we need to represent each complex number as a vector in linear algebra. Second, we need to define addition in this algebra. Third, we need to define multiplication in this algebra.

First, it is not too hard to represent each complex number as a vector in linear algebra. To map  $\mathbb{C} \rightarrow \mathbb{R}^2$ , for each  $z \in \mathbb{C}$ , where  $z = a + bi$  (for  $a, b \in \mathbb{R}$ ), we have:

$$\mathbf{z} = \begin{pmatrix} a \\ b \end{pmatrix}$$

Then, for addition, given  $\mathbf{z}_1 = a_1 + b_1i$  and  $\mathbf{z}_2 = a_2 + b_2i$ , we know that  $\mathbf{z}_1 + \mathbf{z}_2 = (a_1 + a_2) + (b_1 + b_2)i$ . So, we have:

$$\begin{pmatrix} a_1 \\ b_1 \end{pmatrix} + \begin{pmatrix} a_2 \\ b_2 \end{pmatrix} = \begin{pmatrix} a_1 + a_2 \\ b_1 + b_2 \end{pmatrix}$$

This is just normal vector addition.

Finally, for multiplication, given  $\mathbf{z}_1 = a_1 + b_1i$  and  $\mathbf{z}_2 = a_2 + b_2i$ , we know that  $\mathbf{z}_1 \cdot \mathbf{z}_2 = (a_1a_2 - b_1b_2) + (a_1b_2 + a_2b_1)i$ . So, we have:

$$\begin{pmatrix} a_1 \\ b_1 \end{pmatrix} \cdot \begin{pmatrix} a_2 \\ b_2 \end{pmatrix} = \begin{pmatrix} a_1a_2 - b_1b_2 \\ a_1b_2 + a_2b_1 \end{pmatrix}$$

This is clearly not normal vector multiplication. Instead, we can give  $\mathbf{z}_2$  a multiplication matrix, say  $A_{\mathbf{z}_2}$ , such that  $\mathbf{z}_1 \cdot \mathbf{z}_2$  in the complex numbers equals  $A_{\mathbf{z}_2} \cdot \mathbf{z}_1$  in linear algebra.

In general, for  $\mathbf{z} = a + bi$ , say:

$$A_{\mathbf{z}} = \begin{pmatrix} a & -b \\ b & a \end{pmatrix}$$

Then, we have that  $\mathbf{z}_1 \cdot \mathbf{z}_2$  is:

$$\begin{pmatrix} a_2 & -b_2 \\ b_2 & a_2 \end{pmatrix} \begin{pmatrix} a_1 \\ b_1 \end{pmatrix} = \begin{pmatrix} a_1a_2 - b_1b_2 \\ a_1b_2 + a_2b_1 \end{pmatrix}$$

This checks out, so our new definition of multiplication holds.

### 2.2 Eigenvectors in the Complex Numbers

In order to find eigenvectors in the complex numbers, we ask: is it possible to find a set of complex numbers  $S$  such that for all  $z_1, z_2 \in S$ ,  $z_2 = \lambda_1 z_1$  and  $z_1 \cdot z_2 = \lambda_2 z_1$  (for  $\lambda_1, \lambda_2 \in \mathbb{R}$ )?

This can be verified in a few steps.

First, suppose we know  $z_0 = a_0 + b_0i \in S$ .

Then,  $z = a + bi \in S$  if and only if  $\mathbf{z} = \lambda_1 \mathbf{z}_0$  and  $\mathbf{z}_0 \cdot \mathbf{z} = \lambda_2 \mathbf{z}_0$ .

So, since  $\mathbf{z} = \lambda_1 \mathbf{z}_0$ :

$$\mathbf{z} = \lambda_1 \cdot \begin{pmatrix} a_0 \\ b_0 \end{pmatrix} = \begin{pmatrix} \lambda_1 a_0 \\ \lambda_1 b_0 \end{pmatrix}$$

This means:

$$\mathbf{z}_0 \cdot \mathbf{z} = \begin{pmatrix} a_0 \\ b_0 \end{pmatrix} \cdot \begin{pmatrix} \lambda_1 a_0 \\ \lambda_1 b_0 \end{pmatrix} = \begin{pmatrix} \lambda_1 a_0 & -\lambda_1 b_0 \\ \lambda_1 b_0 & \lambda_1 a_0 \end{pmatrix} \begin{pmatrix} a_0 \\ b_0 \end{pmatrix}$$

Since this is equal to  $\lambda_2 \mathbf{z}_0$ , we have:

$$\begin{pmatrix} \lambda_1 a_0 & -\lambda_1 b_0 \\ \lambda_1 b_0 & \lambda_1 a_0 \end{pmatrix} \begin{pmatrix} a_0 \\ b_0 \end{pmatrix} = \lambda_2 \begin{pmatrix} a_0 \\ b_0 \end{pmatrix}$$

With some manipulation, we get:

$$\begin{pmatrix} \lambda_1 a_0 - \lambda_2 & -\lambda_1 b_0 \\ \lambda_1 b_0 & \lambda_1 a_0 - \lambda_2 \end{pmatrix} \begin{pmatrix} a_0 \\ b_0 \end{pmatrix} = 0$$

Since the determinant of the left-hand matrix must be equal to 0, by the eigenvector characteristic equation, we get:

$$(\lambda_1 a_0 - \lambda_2)^2 + (\lambda_1 b_0)^2 = 0$$

However, this is only satisfied if both  $\lambda_1 a_0 - \lambda_2 = 0$  and  $\lambda_1 b_0 = 0$ . If  $\lambda_1 b_0 = 0$ , either  $\lambda_1 = 0$  or  $b_0 = 0$ , both of which are trivial solutions.

### 2.3 Summary for Complex Numbers

Unfortunately, these trivial solutions suggest to us that there exist no such eigenvectors and eigenvalues in the complex numbers. Intuitively though, this should make sense. When multiplying by a complex number, the result, for any other complex number, is a rotation and a dilation. This rotation sets it off the axis we would ideally want it to be on. Thus, we must look to different number systems for our solution.

## 3 Split-Complex Numbers

After recognizing that the previous issue lied within the sum of squares in the final characteristic equation, we may approach a different Clifford Algebra to overcome this issue, namely the split-complex number system ( $Cl_{0,1}(\mathbb{R})$ ), or  $\mathbb{R} \otimes \mathbb{R}$ . This number system works very similar to the complex numbers, except that  $i^2 = 1$  instead. In order to discover whether or not eigenvectors can be applied to split-complex numbers, we take the same two steps as last time. First, we apply linear algebra to this number system. Second, we search for eigenvectors in this linear algebra representation of split-complex numbers.

### 3.1 Applying Linear Algebra to Split-Complex Numbers

Once again, applying linear algebra to split-complex numbers takes three steps. First, we need to represent each  $\mathbf{z} \in Cl_{0,1}(\mathbb{R})$  as a vector in linear algebra. Second, we need to define addition in this algebra. Third, we need to define multiplication in this algebra.

First, just as before, it is not too hard to represent each  $\mathbf{z} \in Cl_{0,1}(\mathbb{R})$  as a vector in linear algebra. To map  $Cl_{0,1}(\mathbb{R}) \rightarrow \mathbb{R}^2$ , for each  $\mathbf{z} \in Cl_{0,1}(\mathbb{R})$ , where  $\mathbf{z} = a + bi$  (for  $a, b \in \mathbb{R}$ ), we have:

$$\mathbf{z} = \begin{pmatrix} a \\ b \end{pmatrix}$$

Then, for addition, given  $\mathbf{z}_1 = a_1 + b_1i$  and  $\mathbf{z}_2 = a_2 + b_2i$ , we know that  $\mathbf{z}_1 + \mathbf{z}_2 = (a_1 + a_2) + (b_1 + b_2)i$ . So, we have:

$$\begin{pmatrix} a_1 \\ b_1 \end{pmatrix} + \begin{pmatrix} a_2 \\ b_2 \end{pmatrix} = \begin{pmatrix} a_1 + a_2 \\ b_1 + b_2 \end{pmatrix}$$

This, once again, is just normal vector addition.

Finally, for multiplication, given  $\mathbf{z}_1 = a_1 + b_1i$  and  $\mathbf{z}_2 = a_2 + b_2i$ , we know that  $\mathbf{z}_1 \cdot \mathbf{z}_2 = (a_1a_2 + b_1b_2) + (a_1b_2 + a_2b_1)i$ . Note the difference here from last time. So, we have:

$$\begin{pmatrix} a_1 \\ b_1 \end{pmatrix} \cdot \begin{pmatrix} a_2 \\ b_2 \end{pmatrix} = \begin{pmatrix} a_1a_2 + b_1b_2 \\ a_1b_2 + a_2b_1 \end{pmatrix}$$

This is clearly not normal vector multiplication. Instead, we can give  $\mathbf{z}_2$  a multiplication matrix, say  $A_{\mathbf{z}_2}$ , such that  $\mathbf{z}_1 \cdot \mathbf{z}_2$  in the split-complex numbers equals  $A_{\mathbf{z}_2} \cdot \mathbf{z}_1$  in linear algebra.

In general, for  $\mathbf{z} = a + bi$ , say:

$$A_{\mathbf{z}} = \begin{pmatrix} a & b \\ b & a \end{pmatrix}$$

Then, we have that  $\mathbf{z}_1 \cdot \mathbf{z}_2$  is:

$$\begin{pmatrix} a_2 & b_2 \\ b_2 & a_2 \end{pmatrix} \begin{pmatrix} a_1 \\ b_1 \end{pmatrix} = \begin{pmatrix} a_1 a_2 + b_1 b_2 \\ a_1 b_2 + a_2 b_1 \end{pmatrix}$$

This checks out, so our new definition of multiplication holds.

### 3.2 Eigenvectors in the Split-Complex Numbers

In order to find eigenvectors in the split-complex numbers, we ask: is it possible to find a set  $S \subset \text{Cl}_{0,1}(\mathbb{R})$  such that for all  $\mathbf{z}_1, \mathbf{z}_2 \in S$ ,  $\mathbf{z}_2 = \lambda_1 \mathbf{z}_1$  and  $\mathbf{z}_1 \cdot \mathbf{z}_2 = \lambda_2 \mathbf{z}_1$  (for  $\lambda_1, \lambda_2 \in \mathbb{R}$ )?

This can be verified in a few steps.

First, suppose we know  $\mathbf{z}_0 = a_0 + b_0 i \in S$ .

Then,  $\mathbf{z} = a + bi \in S$  if and only if  $\mathbf{z} = \lambda_1 \mathbf{z}_0$  and  $\mathbf{z}_0 \cdot \mathbf{z} = \lambda_2 \mathbf{z}_0$ .

So, since  $\mathbf{z} = \lambda_1 \mathbf{z}_0$ :

$$\mathbf{z} = \lambda_1 \cdot \begin{pmatrix} a_0 \\ b_0 \end{pmatrix} = \begin{pmatrix} \lambda_1 a_0 \\ \lambda_1 b_0 \end{pmatrix}$$

This means:

$$\mathbf{z}_0 \cdot \mathbf{z} = \begin{pmatrix} a_0 \\ b_0 \end{pmatrix} \cdot \begin{pmatrix} \lambda_1 a_0 \\ \lambda_1 b_0 \end{pmatrix} = \begin{pmatrix} \lambda_1 a_0 & \lambda_1 b_0 \\ \lambda_1 b_0 & \lambda_1 a_0 \end{pmatrix} \begin{pmatrix} a_0 \\ b_0 \end{pmatrix}$$

Since this is equal to  $\lambda_2 \mathbf{z}_0$ , we have:

$$\begin{pmatrix} \lambda_1 a_0 & \lambda_1 b_0 \\ \lambda_1 b_0 & \lambda_1 a_0 \end{pmatrix} \begin{pmatrix} a_0 \\ b_0 \end{pmatrix} = \lambda_2 \begin{pmatrix} a_0 \\ b_0 \end{pmatrix}$$

With some manipulation, we get:

$$\begin{pmatrix} \lambda_1 a_0 - \lambda_2 & \lambda_1 b_0 \\ \lambda_1 b_0 & \lambda_1 a_0 - \lambda_2 \end{pmatrix} \begin{pmatrix} a_0 \\ b_0 \end{pmatrix} = 0$$

Since the determinant of the left-hand matrix must be equal to 0, by the eigenvector characteristic equation, we get:

$$(\lambda_1 a_0 - \lambda_2)^2 - (\lambda_1 b_0)^2 = 0$$

This means that  $\lambda_1 a_0 - \lambda_2 = \lambda_1 b_0$ , or that  $\lambda_2 = \lambda_1(a_0 - b_0)$ . Putting this back into our original matrix multiplication equation, we get:

$$\begin{pmatrix} \lambda_1 a_0 & \lambda_1 b_0 \\ \lambda_1 b_0 & \lambda_1 a_0 \end{pmatrix} \begin{pmatrix} a_0 \\ b_0 \end{pmatrix} = \lambda_1(a_0 - b_0) \begin{pmatrix} a_0 \\ b_0 \end{pmatrix}$$

With some manipulation, we have:

$$\begin{pmatrix} \lambda_1(a_0^2 + b_0^2) \\ \lambda_1(2a_0 b_0) \end{pmatrix} = \begin{pmatrix} \lambda_1(a_0^2 - a_0 b_0) \\ \lambda_1(a_0 b_0 - b_0^2) \end{pmatrix}$$

Breaking this into two parts, on the top we have:

$$\lambda_1(a_0^2 + b_0^2) = \lambda_1(a_0^2 - a_0 b_0) \implies b_0 = a_0$$

And, on the bottom we have:

$$\lambda_1(2a_0 b_0) = \lambda_1(a_0 b_0 - b_0^2) \implies a_0 = -b_0$$

This system of equations solves to  $a_0 = 0, b_0 = 0$ , which is, once again, trivial.

### 3.3 Summary for Split-Complex Numbers

Unfortunately, these trivial solutions also suggest to us that there exist no such eigenvectors and eigenvalues in the split-complex number system. While there is no intuitive explanation here, we must still look to different number systems for our solution.

## 4 $\text{Cl}_{1,1}(\mathbb{R})$

It seems so far that there is no Clifford Algebra which incorporates linear algebra and eigenvectors in a natural way. However, before generalizing our conclusions to the wider class of Clifford Algebras, it is worth considering an algebra with a larger column matrix. In particular, we will consider the Clifford Algebra  $\text{Cl}_{1,1}(\mathbb{R})$ . This number system can almost be considered as a combination of complex and split-complex numbers. Basically, in this system, we have two basis vectors  $i$  and  $j$ , such that  $i^2 = -1$  and  $j^2 = 1$ . This means that each  $\mathbf{z} \in \text{Cl}_{1,1}(\mathbb{R})$  can be expressed as  $\mathbf{z} = a + bi + cj + dij$ . In order to discover whether or not eigenvectors can be applied to  $\text{Cl}_{1,1}(\mathbb{R})$ , we take the same two steps as last time. First, we apply linear algebra to this number system. Second, we search for eigenvectors in this linear algebra representation of  $\text{Cl}_{1,1}(\mathbb{R})$ .

#### 4.1 Applying Linear Algebra to $\text{Cl}_{1,1}(\mathbb{R})$

Once again, applying linear algebra to  $\text{Cl}_{1,1}(\mathbb{R})$  takes three steps. First, we need to represent each  $\mathbf{z} \in \text{Cl}_{1,1}(\mathbb{R})$  as a vector in linear algebra. Second, we need to define addition in this algebra. Third, we need to define multiplication in this algebra.

First, just as before, it is not too hard to represent each  $\mathbf{z} \in \text{Cl}_{1,1}(\mathbb{R})$  as a vector in linear algebra. To map  $\text{Cl}_{1,1}(\mathbb{R}) \rightarrow \mathbb{R}^4$ , for each  $\mathbf{z} \in \text{Cl}_{1,1}(\mathbb{R})$ , where  $\mathbf{z} = a + bi + cj + dij$  (for  $a, b, c, d \in \mathbb{R}$ ), we have:

$$\mathbf{z} = \begin{pmatrix} a \\ b \\ c \\ d \end{pmatrix}$$

Then, for addition, given  $\mathbf{z}_1 = a_1 + b_1 i + c_1 j + d_1 ij$  and  $\mathbf{z}_2 = a_2 + b_2 i + c_2 j + d_2 ij$ , we know that  $\mathbf{z}_1 + \mathbf{z}_2 = (a_1 + a_2) + (b_1 + b_2)i + (c_1 + c_2)j + (d_1 + d_2)ij$ . So, we have:

$$\begin{pmatrix} a_1 \\ b_1 \\ c_1 \\ d_1 \end{pmatrix} + \begin{pmatrix} a_2 \\ b_2 \\ c_2 \\ d_2 \end{pmatrix} = \begin{pmatrix} a_1 + a_2 \\ b_1 + b_2 \\ c_1 + c_2 \\ d_1 + d_2 \end{pmatrix}$$

This, once again, is just normal vector addition.

Finally, for multiplication, given  $\mathbf{z}_1 = a_1 + b_1 i + c_1 j + d_1 ij$  and  $\mathbf{z}_2 = a_2 + b_2 i + c_2 j + d_2 ij$ , through expansion and distribution, we can find that  $\mathbf{z}_1 \cdot \mathbf{z}_2 = (a_1 a_2 - b_1 b_2 + c_1 c_2 + d_1 d_2) + (a_1 b_2 + b_1 a_2 - c_1 d_2 + d_1 c_2)i + (a_1 c_2 - b_1 d_2 + c_1 a_2 + d_1 b_2)j + (a_1 d_2 + b_1 c_2 - c_1 b_2 + d_1 a_2)ij$ . Note the difference here from last time. So, we have:

$$\begin{pmatrix} a_1 \\ b_1 \\ c_1 \\ d_1 \end{pmatrix} \cdot \begin{pmatrix} a_2 \\ b_2 \\ c_2 \\ d_2 \end{pmatrix} = \begin{pmatrix} a_1 a_2 - b_1 b_2 + c_1 c_2 + d_1 d_2 \\ a_1 b_2 + b_1 a_2 - c_1 d_2 + d_1 c_2 \\ a_1 c_2 - b_1 d_2 + c_1 a_2 + d_1 b_2 \\ a_1 d_2 + b_1 c_2 - c_1 b_2 + d_1 a_2 \end{pmatrix}$$

This is clearly not normal vector multiplication. Instead, we can give  $\mathbf{z}_2$  a multiplication matrix, say  $A(\mathbf{z}_2)$ , such that  $\mathbf{z}_1 \cdot \mathbf{z}_2$  in the split-complex numbers equals  $A(\mathbf{z}_2) \cdot \mathbf{z}_1$  in linear algebra.

In general, for  $\mathbf{z} = a + bi + cj + dij$ , say:

$$A_{\mathbf{z}} = \begin{pmatrix} a & -b & c & d \\ b & a & -d & c \\ c & -d & a & b \\ d & c & -b & a \end{pmatrix}$$

Then, we have that  $\mathbf{z}_1 \cdot \mathbf{z}_2$  is:

$$\begin{pmatrix} a_2 & -b_2 & c_2 & d_2 \\ b_2 & a_2 & -d_2 & c_2 \\ c_2 & -d_2 & a_2 & b_2 \\ d_2 & c_2 & -b_2 & a_2 \end{pmatrix} \begin{pmatrix} a_1 \\ b_1 \\ c_1 \\ d_1 \end{pmatrix} = \begin{pmatrix} a_1 a_2 - b_1 b_2 + c_1 c_2 + d_1 d_2 \\ a_1 b_2 + b_1 a_2 - c_1 d_2 + d_1 c_2 \\ a_1 c_2 - b_1 d_2 + c_1 a_2 + d_1 b_2 \\ a_1 d_2 + b_1 c_2 - c_1 b_2 + d_1 a_2 \end{pmatrix}$$

This checks out, so our new definition of multiplication holds.

#### 4.2 Eigenvectors in the $\text{Cl}_{1,1}(\mathbb{R})$

In order to find eigenvectors in  $\text{Cl}_{1,1}(\mathbb{R})$ , we ask: is it possible to find a set  $S \subset \text{Cl}_{1,1}(\mathbb{R})$  such that for all  $z_1, z_2 \in S$ ,  $z_2 = \lambda_1 z_1$  and  $z_1 \cdot z_2 = \lambda_2 z_1$  (for  $\lambda_1, \lambda_2 \in \mathbb{R}$ )?

This can be verified in a few steps.

First, suppose we know  $z_0 = a_0 + b_0 i + c_0 j + d_0 ij \in S$ .

Then,  $z = a + bi + cj + dij \in S$  if and only if  $z = \lambda_1 z_0$  and  $z_0 \cdot z = \lambda_2 z_0$ .

So, since  $z = \lambda_1 z_0$ :

$$z = \lambda_1 \cdot \begin{pmatrix} a_0 \\ b_0 \\ c_0 \\ d_0 \end{pmatrix} = \begin{pmatrix} \lambda_1 a_0 \\ \lambda_1 b_0 \\ \lambda_1 c_0 \\ \lambda_1 d_0 \end{pmatrix}$$

This means:

$$z_0 \cdot z = \begin{pmatrix} a_0 \\ b_0 \\ c_0 \\ d_0 \end{pmatrix} \cdot \begin{pmatrix} \lambda_1 a_0 \\ \lambda_1 b_0 \\ \lambda_1 c_0 \\ \lambda_1 d_0 \end{pmatrix}$$

$$= \begin{pmatrix} \lambda_1 a_0 & -\lambda_1 b_0 & \lambda_1 c_0 & \lambda_1 d_0 \\ \lambda_1 b_0 & \lambda_1 a_0 & -\lambda_1 d_0 & \lambda_1 c_0 \\ \lambda_1 c_0 & -\lambda_1 d_0 & \lambda_1 a_0 & \lambda_1 b_0 \\ \lambda_1 d_0 & \lambda_1 c_0 & -\lambda_1 b_0 & \lambda_1 a_0 \end{pmatrix} \begin{pmatrix} a_0 \\ b_0 \\ c_0 \\ d_0 \end{pmatrix}$$

Since this is equal to  $\lambda_2 z_0$ , we have:

$$\begin{pmatrix} \lambda_1 a_0 & -\lambda_1 b_0 & \lambda_1 c_0 & \lambda_1 d_0 \\ \lambda_1 b_0 & \lambda_1 a_0 & -\lambda_1 d_0 & \lambda_1 c_0 \\ \lambda_1 c_0 & -\lambda_1 d_0 & \lambda_1 a_0 & \lambda_1 b_0 \\ \lambda_1 d_0 & \lambda_1 c_0 & -\lambda_1 b_0 & \lambda_1 a_0 \end{pmatrix} \begin{pmatrix} a_0 \\ b_0 \\ c_0 \\ d_0 \end{pmatrix} = \lambda_2 \begin{pmatrix} a_0 \\ b_0 \\ c_0 \\ d_0 \end{pmatrix}$$

With some manipulation, we get:

$$\begin{pmatrix} \lambda_1 a_0 - \lambda_2 & -\lambda_1 b_0 & \lambda_1 c_0 & \lambda_1 d_0 \\ \lambda_1 b_0 & \lambda_1 a_0 - \lambda_2 & -\lambda_1 d_0 & \lambda_1 c_0 \\ \lambda_1 c_0 & -\lambda_1 d_0 & \lambda_1 a_0 - \lambda_2 & \lambda_1 b_0 \\ \lambda_1 d_0 & \lambda_1 c_0 & -\lambda_1 b_0 & \lambda_1 a_0 - \lambda_2 \end{pmatrix} \begin{pmatrix} a_0 \\ b_0 \\ c_0 \\ d_0 \end{pmatrix} = 0$$

Since the determinant of the left-hand matrix must be equal to 0, by the eigenvector characteristic equation, we get a very complicated equation. After simplifying and cancelling, we are left with:

$$\begin{aligned} & (\lambda_1 a_0 - \lambda_2)^4 - (\lambda_1 b_0)^4 + (\lambda_1 c_0)^4 + (\lambda_1 d_0)^4 + 2(\lambda_1 a_0 - \lambda_2)^2 \\ & (\lambda_1 b_0)^2 - 2(\lambda_1 a_0 - \lambda_2)^2 (\lambda_1 c_0)^2 - 2(\lambda_1 a_0 - \lambda_2)^2 (\lambda_1 d_0)^2 \\ & - 2(\lambda_1 b_0)^2 (\lambda_1 c_0)^2 - 2(\lambda_1 b_0)^2 (\lambda_1 d_0)^2 + 2(\lambda_1 c_0)^2 (\lambda_1 d_0)^2 \\ & = 0 \end{aligned}$$

Given that this equation is so complex, it is extremely hard to treat it similarly to our previous characteristic equations, which only had two terms. Rather, here we can search for nontrivial solutions that satisfy this equation.

For instance, consider:

$$z_0 = \begin{pmatrix} 0 \\ 1 \\ 1 \\ 0 \end{pmatrix}; z = \begin{pmatrix} 0 \\ 0 \\ 0 \\ 1 \end{pmatrix}$$

Then:

$$\begin{aligned} z_0 \cdot z &= \begin{pmatrix} 0 \\ 1 \\ 1 \\ 0 \end{pmatrix} \cdot \begin{pmatrix} 0 \\ 0 \\ 0 \\ 1 \end{pmatrix} = \begin{pmatrix} 0 & 0 & 0 & 1 \\ 0 & 0 & -1 & 0 \\ 0 & -1 & 0 & 0 \\ 1 & 0 & 0 & 0 \end{pmatrix} \begin{pmatrix} 0 \\ 1 \\ 1 \\ 0 \end{pmatrix} \\ &= \begin{pmatrix} 0 \\ -1 \\ -1 \\ 0 \end{pmatrix} = -1 \begin{pmatrix} 0 \\ 1 \\ 1 \\ 0 \end{pmatrix} \end{aligned}$$

As we can see, for these values, if  $\lambda = 1$ , the calculations check out.

After significantly more trial and error, we see that our potential nontrivial values of  $z_0$  and  $z$ , for arbitrary  $\lambda_1, \lambda_2 \in \mathbb{R}$  are limited to:

$$z_0 = \begin{pmatrix} 0 \\ \lambda_1 \\ \lambda_1 \\ 0 \end{pmatrix}; z = \begin{pmatrix} 0 \\ 0 \\ 0 \\ \lambda_2 \end{pmatrix}$$

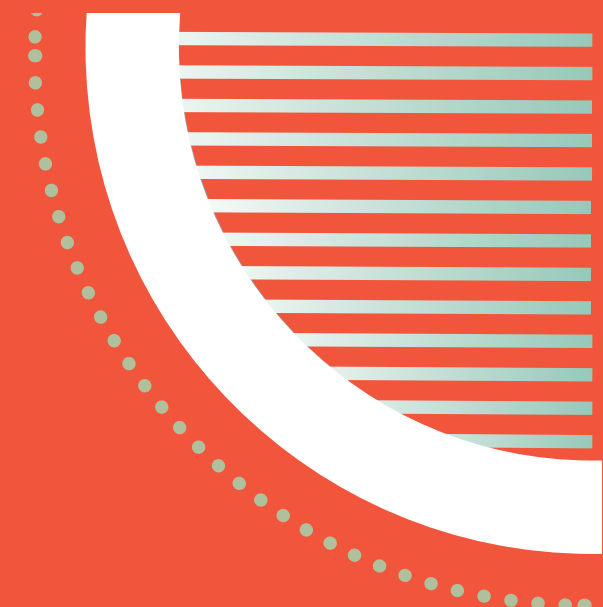
where:

$$z_0 \cdot z = -\lambda_1 \lambda_2 z_0$$

Unfortunately, although this is quite promising, since  $z_0$  and  $z$  are not scalar multiples, these specific elements do not fulfil our original expectations. However, these elements do have a name: pseudoscalars, which we will take a look at in our overall conclusion.

## 5 Conclusion

We have investigated a variety of number systems that embraced linear algebra in a more natural manner, by looking at number systems which naturally had column matrices and vector parts. While the goal was to find a linear group of numbers, through these investigations, we may conclude that no such group exists.



# 10 Evaluating Epidemiological Solutions through S-I-R Modeling

Written by Gaurav Goel

---

## Abstract

Through previous investigation, I have formed the opinion that even though linear algebra is a neat tool to conceptualize operations in higher math, the importance of linear algebra truly lies in its real-world computational application. As a result, for this project, I explored a topic with real-world implications.

In this paper, I aim to reanalyze the derivation of the SIR model through differential equations and linear algebra, and then my extension will be to adapt the SIR model to measure the impacts of epidemiological solutions such as vaccination and lockdown through the deaths sustained under different scenarios.

*Keywords:* SIR Model, pandemic, differential equations, epidemiology, computational modelling

# Evaluating Epidemiological Solutions through S-I-R Modeling

**Gaurav Goel**

goel47628@sas.edu.sg

**Teacher Reviewer:**

Mr. Craig

## 1 Exploration of the Basic SIR Model

The basic SIR model consists of three compartments: Susceptible, Infected, and Recovered. The flow of people in and out of these three compartments can be summarized by the diagram I have drawn below:

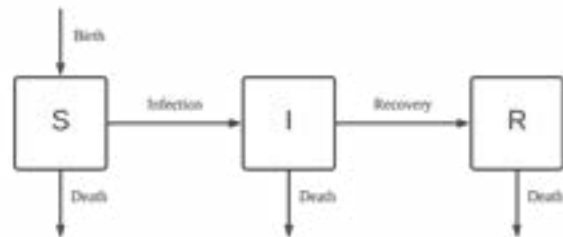


Figure 1: SIR model

Let's define some variables and then examine what each rate is.

First,  $S$ ,  $I$ , and  $R$  are the number of people in each of the respective compartments. Furthermore,  $S + I + R = N$ , which is the total population we are observing. Next, we need to define a birth/death rate. We will consider these equal, and use the variable  $\mu$  to signify the proportion of people that die over a period of time. Last, we use  $\gamma$  to represent

the recovery rate, or the proportion of infected individuals that recover over a period of time.

With this information, we can say that:

- the instantaneous birth rate is  $\mu N$
- the death rates out of each compartment are  $\mu S$ ,  $\mu I$ , and  $\mu R$  respectively
- the recovery rate is  $\gamma I$
- the infection rate is  $\beta SI$

At this point, our definitions raise the question: What is  $\beta$ ? This variable is slightly more complicated than the rest. In essence,  $\beta = kp$ , where  $k$  is the number of interactions a person makes with a certain population and  $p$  is the proportion that the average interaction between a susceptible individual and an infected individual spreads the infection.

Given the diagram, we can create a set of differential equations to model this idea.

$$\frac{dS}{dt} = \text{birth} - \text{death} - \text{infection} = \mu N - \mu S - \beta SI$$

$$\frac{dI}{dt} = \text{infection} - \text{death} - \text{recovery} = \beta SI - \mu I - \gamma I$$

$$\frac{dR}{dt} = \text{recovery} - \text{death} = \gamma I - \mu R$$

From here, there is a lot of additional theoretical analysis we could do.

For instance, we could derive the basic reproduction rate (the average number of individuals that each infected individual infects). In particular, we can ask ourselves: When are infections growing? We see that infections are growing when  $\frac{dI}{dt} > 0$ . This gives us:

$$\beta SI - \mu I - \gamma I > 0$$

$$\beta SI > \mu I + \gamma I$$

$$\frac{\beta SI}{\mu I + \gamma I} > 1$$

$$\frac{\beta S}{\mu + \gamma} > 1$$

In fact, this value,  $\frac{\beta S}{\mu + \gamma}$ , is the basic reproduction rate, or  $R_0$ . Conceptually, this can be explained by the idea that the

rate of infection is growing if each infected person is infecting more than one other individual, just as we see in our equation.

We could also analyze potential equilibrium states. In particular, we reach an equilibrium state when  $\frac{dI}{dt} = 0$ . This gives us:

$$\beta SI - \mu I - \gamma I = 0$$

$$(\beta S - \mu - \gamma)I = 0$$

This implies one of two things, First, when  $I = 0$ , there are no infections, which is known as the disease-free equilibrium, Second, when we have  $\beta S - \mu - \gamma$ , where there are still infections, we have what is known as an endemic equilibrium.

However, these same conclusions can be derived from observing a linear algebraic model of the SIR model.

## 2 Applying Linear Algebra to the SIR Model

In order to apply linear algebra to the SIR model, we must first discretize our differential equations. In other words, rather than taking instantaneous rates, we may look at the change in the SIR values over a small, macroscopic period of time, perhaps a week. Then, we get new equations, identical before, but using macroscopic rather than infinitesimal increments:

$$\frac{\Delta S}{\Delta t} = \text{birth} - \text{death} - \text{infection} = \mu N - \mu S - \beta SI$$

$$\frac{\Delta I}{\Delta t} = \text{infection} - \text{death} - \text{recovery} = \beta SI - \mu I - \gamma I$$

$$\frac{\Delta R}{\Delta t} = \text{recovery} - \text{death} = \gamma I - \mu R$$

Here, one approach would be to find the Jacobian matrix of the column vector of these differential equations, and then build the next generation matrix of these differential equations. However, as we will see later, that does not serve our purpose of looking at the overall model as a whole, and thus, we want a simpler linear algebraic model.

The simpler model is to create basic Markov Chain matrix, given the information we know about the changes in the respective values.

In particular, if we think of each value as its previous value plus the incremental change (e.g.  $S_{n+1} = S_n + \Delta S_n$ ), then we get the equations below.

$$S_{n+1} = S_n + (\mu N - \mu S - \beta SI)\Delta t$$

$$I_{n+1} = I_n + (\beta SI - \mu I - \gamma I)\Delta t$$

$$R_{n+1} = R_n + (\gamma I - \mu R)\Delta t$$

One edit we must make is to rewrite the  $S$  equation without the constant, giving us:

$$S_{n+1} = S_n + (\mu I + \mu R - \beta SI)\Delta t$$

If we consider each rate to be a macroscopic rate rather than an infinitesimal one, the  $\Delta t$  term vanishes. Thus, when represented as a matrix, we obtain the transition matrix:

$$\begin{pmatrix} 1 & \mu - \beta S & \mu \\ 0 & 1 + \beta S - \mu - \gamma & 0 \\ 0 & \gamma & 1 - \mu \end{pmatrix}$$

We must make one change here. In particular, we see that we cannot have the  $\beta S$  term inside our matrix, as  $S$  will continue to change. Thus, while this may increase error in our final model, simply for the sake of our calculations, we will approximate  $S$  to  $N$ . This gives us the final transition matrix of:

$$\begin{pmatrix} 1 & \mu - \beta N & \mu \\ 0 & 1 + \beta N - \mu - \gamma & 0 \\ 0 & \gamma & 1 - \mu \end{pmatrix}$$

Consider the initial state with a population of  $N = 1000$  and  $I_0 = 2$  infected people. Let us approximate values for the rest of the parameters (note that these values are exaggerated for the sake of the simulation). A proportion of approximately  $\mu = 0.01$  people are born and die each week. A proportion of  $\gamma = 0.08$  people will recover each week. And, we can assign  $k = 0.005$  and  $p = 0.05$ , giving us a value of  $\beta = 0.0025$ .

We now get an initial matrix of:

$$\begin{pmatrix} 998 \\ 2 \\ 0 \end{pmatrix}$$

We get a transition matrix of:

$$\begin{pmatrix} 1 & -2.49 & 0.01 \\ 0 & 3.41 & 0 \\ 0 & 0.08 & 0.99 \end{pmatrix}$$

After simulating this disease spread, we get these results (rounded to the nearest natural numbers):

yrs/wks	S	I	R
0/0	998	2	0
0.5/26	863	90	47
1/52	244	278	479
1.5/78	211	98	691
2/104	298	48	655
2.5/130	376	41	582
3/156	414	53	533
3.5/182	399	74	527
4/208	361	84	554
⋮	⋮	⋮	⋮
6/312	365	68	567
6.5/338	365	71	564

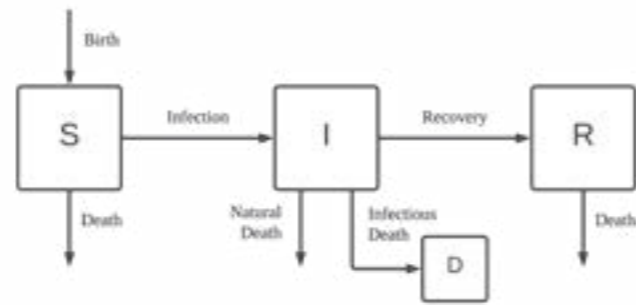


Figure 2: SIR model including infectious death

Furthermore, our new differential equations are as follows:

$$\frac{dS}{dt} = \text{birth} - \text{death} - \text{infection} = \mu N - \mu S - \beta SI$$

$$\begin{aligned} \frac{dI}{dt} &= \text{infection} - \text{death} - \text{infectious death} - \text{recovery} \\ &= \beta SI - \mu I - \alpha I - \gamma I \end{aligned}$$

$$\frac{dR}{dt} = \text{recovery} - \text{death} = \gamma I - \mu R$$

$$\frac{dD}{dt} = \text{infectious death} = \alpha I$$

Through the method we used before, we can take these differential equations into linear algebra once again. Our transition matrix is:

$$\begin{pmatrix} 1 & \mu - \beta N & \mu & 0 \\ 0 & 1 + \beta N - \mu - \alpha - \gamma & 0 & 0 \\ 0 & \gamma & 1 - \mu & 0 \\ 0 & \alpha & 0 & 1 \end{pmatrix}$$

Using the same values we had last time, but now including that  $\alpha = 0.015$ , we gain a new simulation.

Our initial matrix is once again:

$$\begin{pmatrix} 998 \\ 2 \\ 0 \\ 0 \end{pmatrix}$$

However, our transition matrix is now:

$$\begin{pmatrix} 1 & -2.49 & 0.01 & 0 \\ 0 & 3.395 & 0 & 0 \\ 0 & 0.08 & 0.99 & 0 \\ 0 & 0.015 & 0 & 1 \end{pmatrix}$$

With our new model, here are the results:

As we can see, the disease spread to around 65% of the population, and reached a steady state right around the sixth year.

Now, let's use this understanding to develop more sophisticated models.

### 3 The Infectious Death SIR Model

The first thing we will attempt to do is introduce the idea of death by infection. In this way, we can quantify exactly how large the mortality impact of the infection actually was. Using this, we can compare results across different treatments and solutions.

We introduce this idea by adding an extra compartment,  $D$ , for death by infection.

We can now define a few more variables.

We will call the proportion of infected individuals who die from the disease (not from natural causes)  $\alpha$ . This means that the rate of flow from  $I$  to  $D$  is  $\alpha I$ .

This is depicted in the diagram below:

yrs/wks	S	I	R	D
0/0	998	2	0	0
0.5/26	891	65	36	7
1/52	328	232	364	77
1.5/78	238	77	550	135
2/104	309	28	509	154
2.5/130	389	18	432	162
3/156	450	18	364	169
3.5/182	482	24	317	177
4/208	477	36	299	199
⋮	⋮	⋮	⋮	⋮
6/312	391	33	322	241
6.5/338	403	28	303	266

We can see how these results differed slightly from last time. With the incorporation of the infectious deaths compartment, we see a decrease in the number of infectious people and recovered people left over (probably because a lot of them died).

We will use this simulation as a control to measure against the solutions we propose.

### 4 The Lockdown SIR Model

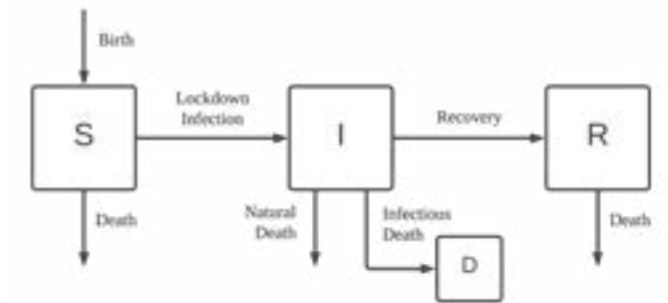
The first solution we can look at is putting citizens into lockdown. What effect does this solution have, and how should it impact our model. Well, in essence, lockdown does not help with anything, except for the fact that it decreases the number of interpersonal interactions in a country. In particular, this means that  $k$  will decrease. Say that the new value of  $k$  is  $kl$ , for some lockdown factor  $l$ . Then, for our new value of  $\beta$ ,  $klp = \beta l$ .

Our diagram is as follows:

And our differential equations:

$$\frac{dS}{dt} = \text{birth} - \text{death} - \text{infection} = \mu N - \mu S - \beta l SI$$

$$\begin{aligned} \frac{dI}{dt} &= \text{infection} - \text{death} - \text{infectious death} - \text{recovery} \\ &= \beta l SI - \mu I - \alpha I - \gamma I \end{aligned}$$



$$\frac{dR}{dt} = \text{recovery} - \text{death} = \gamma I - \mu R$$

$$\frac{dD}{dt} = \text{infectious death} = \alpha I$$

Once again, we create a transition Markov Matrix for these differential equations:

$$\begin{pmatrix} 1 & \mu - \beta l N & \mu & 0 \\ 0 & 1 + \beta l N - \mu - \alpha - \gamma & 0 & 0 \\ 0 & \gamma & 1 - \mu & 0 \\ 0 & \alpha & 0 & 1 \end{pmatrix}$$

This time, we fix  $l$  to be 0.6.

Our initial matrix is then:

$$\begin{pmatrix} 998 \\ 2 \\ 0 \\ 0 \end{pmatrix}$$

And our transition matrix is:

$$\begin{pmatrix} 1 & -1.49 & 0.01 & 0 \\ 0 & 2.395 & 0 & 0 \\ 0 & 0.08 & 0.99 & 0 \\ 0 & 0.015 & 0 & 1 \end{pmatrix}$$

Implementing lockdown gives us these results:

yrs/wks	S	I	R	D
0/0	998	2	0	0
0.5/26	985	6	7	2
1/52	950	18	26	6
1.5/78	869	41	73	17
2/104	745	63	155	37
2.5/130	640	61	237	62
3/156	595	43	278	83
3.5/182	596	28	279	97
4/208	616	20	258	106
⋮	⋮	⋮	⋮	⋮
6/312	705	11	157	127
6.5/338	715	12	142	131

In terms of our equations, there are a few implications. First, we use the variable  $\rho$  to represent the proportion of individuals who get vaccinated at birth. This gives us a rate of  $\mu(1 - \rho)N$  babies being born into the susceptible compartment and  $\mu\rho N$  babies being born into the recovered compartment.

Second, we use the variable  $\nu$  to represent the proportion of susceptible individuals who choose to get vaccinated during their lifetime. This gives us a rate of  $\nu S$  individuals flowing from the susceptible compartment to the recovered compartment.

Given these changes, here are our new differential equations:

$$\frac{dS}{dt} = \text{birth (w/out vaccine)} - \text{death} - \text{vaccination} - \text{infection} \\ = \mu(1 - \rho)N - \mu S - \nu S - \beta SI$$

$$\frac{dI}{dt} = \text{infection} - \text{death} - \text{infectious death} - \text{recovery} \\ = \beta SI - \mu I - \alpha I - \gamma I$$

$$\frac{dR}{dt} = \text{birth (w vaccine)} + \text{vaccination} + \text{recovery} - \text{death} \\ = \mu\rho N + \nu S + \gamma I - \mu R$$

$$\frac{dD}{dt} = \text{infectious death} = \alpha I$$

Our transitional Markov Matrix is:

$$\begin{pmatrix} 1 - \nu & \mu(1 - \rho) - \beta N & \mu(1 - \rho) & 0 \\ 0 & 1 + \beta N - \mu - \alpha - \gamma & 0 & 0 \\ \mu\rho + \nu & \mu\rho + \gamma & 1 + \mu\rho - \mu & 0 \\ 0 & \alpha & 0 & 1 \end{pmatrix}$$

Let's choose values for  $\rho$  and  $\nu$ . At birth, the vaccination rate can be  $\rho = 0.009$ . During a lifetime, the vaccination rate can be  $\nu = 0.01$ .

Our initial matrix is still:

$$\begin{pmatrix} 998 \\ 2 \\ 0 \\ 0 \end{pmatrix}$$

And our transition matrix is:

$$\begin{pmatrix} 0.93 & -2.4905 & 0.0095 & 0 \\ 0 & 3.395 & 0 & 0 \\ 0.0705 & 0.0805 & 0.9905 & 0 \\ 0 & 0.015 & 0 & 1 \end{pmatrix}$$

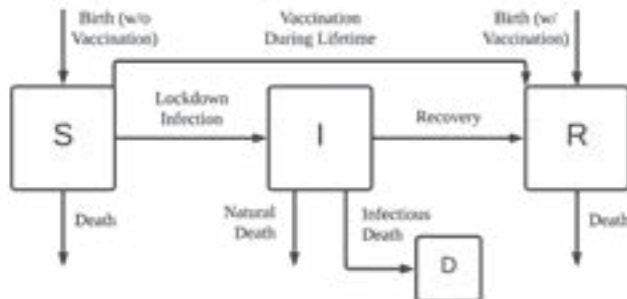
These vaccination statistics give us results of:

As we can see, even by just limiting interactions between people by 40%, lockdown is a solution that can literally halve the number of potential deaths.

## 5 The Vaccination SIR Model

The next solution we can look at is implementing vaccination. This can be implemented both at birth and during people's lifetimes, so we will assume both happen. In particular, this has two implications. One, some individuals are born directly into the recovered compartment as a result of being vaccinated from birth. Two, individuals who get vaccinated during their lifetimes skip over the infected stage and go directly from susceptible to recovered.

This can be seen in this diagram:



yrs/wks	S	I	R	D
0/0	998	2	0	0
0.5/26	744	37	237	5
1/52	422	109	473	36
1.5/78	290	64	623	71
2/104	300	27	640	88
2.5/130	338	14	616	96
3/156	373	9	591	100
3.5/182	400	7	572	103
4/208	420	7	561	106
⋮	⋮	⋮	⋮	⋮
6/312	445	11	564	119
6.5/338	443	13	572	123

$$\frac{dS}{dt} = \text{birth (w/out vaccine)} - \text{death} - \text{vaccination} - \text{infection} \\ = \mu(1 - \rho)N - \mu S - \nu S - \beta SI$$

$$\frac{dI}{dt} = \text{infection} - \text{death} - \text{infectious death} - \text{recovery} \\ = \beta SI - \mu I - \alpha I - \gamma I$$

$$\frac{dR}{dt} = \text{birth (w vaccine)} + \text{vaccination} + \text{recovery} - \text{death} \\ = \mu\rho N + \nu S + \gamma I - \mu R$$

$$\frac{dD}{dt} = \text{infectious death} = \alpha I$$

Our transitional Markov Matrix:

$$\begin{pmatrix} 1 - \nu & \mu(1 - \rho) - \beta N & \mu(1 - \rho) & 0 \\ 0 & 1 + \beta N - \mu - \alpha - \gamma & 0 & 0 \\ \mu\rho + \nu & \mu\rho + \gamma & 1 + \mu\rho - \mu & 0 \\ 0 & \alpha & 0 & 1 \end{pmatrix}$$

Our initial matrix:

$$\begin{pmatrix} 998 \\ 2 \\ 0 \\ 0 \end{pmatrix}$$

Our transition matrix:

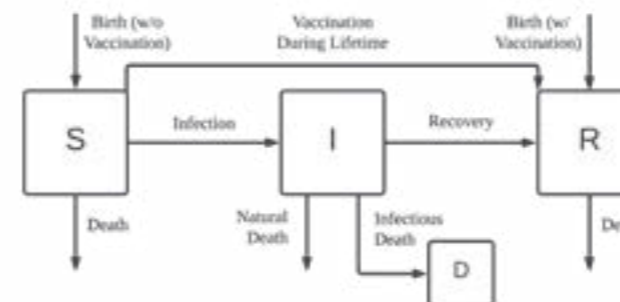
$$\begin{pmatrix} 0.93 & -1.4905 & 0.0095 & 0 \\ 0 & 2.395 & 0 & 0 \\ 0.0705 & 0.0805 & 0.9905 & 0 \\ 0 & 0.015 & 0 & 1 \end{pmatrix}$$

Finally, our results are:

As we can see once again, these levels of vaccination prove to be extremely effective in curbing the number of deaths. Even if only 0.9% of the population gets vaccinated each week, which means around 750 out of 1000 people over the course of 2.5 years, we can see massive benefits in terms of reducing the number of deaths sustained.

## 6 Combining the Two Solutions

Finally, we can combine the two solutions, as in the diagram below:



Our differential equations:

yrs/wks	S	I	R	D
0/0	998	2	0	0
0.5/26	798	4	220	1
1/52	681	5	354	3
1.5/78	613	4	438	5
2/104	576	3	491	6
2.5/130	558	2	523	7
3/156	551	1	545	8
3.5/182	550	0	560	8

4/208	553	0	572	8
⋮	⋮	⋮	⋮	⋮
6/312	577	0	607	8
6.5/338	584	0	615	8

Here, the combination of the two solutions proves to be far more effective than we could even imagine! This is because they both prevent the spread of the disease in different ways. Vaccination increases the number of individuals in the recovered compartment, while lockdown decreases the likelihood a susceptible individual will transition into the infected compartment. This model proves to be quite volatile, as the rate of infection is directly dependent on the number of infections present. Thus, by containing the number of infected individuals well from the beginning, we see massive benefits in the long-run.

### 7 Conclusion

To conclude, we first saw that we can adapt the SIR model in a variety of ways to mimic certain events and phenomena, and we were able to develop a variety of more complex models in order to analyze potential solutions to the spread of an infection or disease. Furthermore, we can see that using methods of lockdown and vaccination to contain the spread of disease are, in fact, extremely effective, especially when used in tandem.

I think perhaps the most important part of this project is the way that it can be translated into real-world applications, during pandemics and epidemics such as, say, COVID-19. Because of the adaptability of the SIR model, we can model the effect of solutions ranging far beyond just vaccination and lockdown. This means that this model can be an excellent predictor for world crises such as these diseases, and it amazes me just how much linear algebra and math can be applied to make an impact.

### Sources Used

Here are the range of sources I used in order to understand this topic:  
 Purdue University (Differential Equations and Linear Algebra)  
 Mathematical Association of America (The SIR Model for Spread of Disease)  
 Andrew Brouwer (Understanding the Basic Reproduction Number through Linear Algebra)  
 Wikipedia (Fundamental Matrix - Linear Differential Equations)



# 11 Finding an Alternate Model to Malthusian Population Growth Model

Written by Vyjayanti Vasudevan, Irene Choi, Morgan Ahn

## Finding an Alternate Model to Malthusian Population Growth Model

Vyjayanti Vasudevan Irene Choi Morgan Ahn

vasudevan773999@sas.edu.sg, choi790186@sas.edu.sg, ahn787838@sas.edu.sg

Teacher Reviewer:

Mr. Son

### Abstract

The Malthusian Population Growth Model has been used for decades to predict the outcome of a nation's living standards. However, many criticize this model, stating that it overlooks the major technological advancement today. In this paper, we will provide an introduction to the Malthusian Growth Model, its pros and cons, as well as an examination of alternate factors that should be considered when making predictions regarding population growth moving forward.

*Keywords:* Malthusian Checkpoints, population growth model, linear growth, analysis, predictions

### 1 Introduction

First observed by Thomas Robert Malthus in the first edition of his 1798 paper, the Malthusian growth model is one that has been trusted to demonstrate population stagnation for centuries. Malthus's publication 'An Essay on the Principle of Population' suggested that food production grows arithmetically while population numbers grow exponentially, stating that 'Malthusian Checkpoints' are necessary in order to maintain equilibrium between population growth and food production. Malthusian Checkpoints, as defined by Malthus's 1798 publication, categorize means of population regulation into two: one, positive checks, defined as checks that promote population regulation through reducing life expectancy, and two, preventative checks, defined as checks that lower the fertility rates of a population.

This paper aims to examine the Malthusian Growth Model and propose an alternative way to illustrate population management, accounting for other factors influencing population growth or stagnation. One common critique of the Malthusian Population Growth Model is that it does not account for modern sustained economic growth in the post-Industrial Revolution era.

### 2 Geometric and Linear Growth

The combined equation,  $F(0) + r_2t = P(0)e^{r_1t}$  (given the conditions  $P_0 = P(0)$  and  $F_0 = F(0)$  must be satisfied), is designed so that its cyclical pattern appropriately manages population size. ' $r_1$ ' represents the growth rate of the population density; ' $t$ ' represents the duration of time;  $P(0)$  represents the initial population density (in counts); ' $r_2$ ' represents the proportion of growth in food production;

$F(0)$  represents the initial amount of food production. We model this using logarithmic and linear growth, which the following equations display:  $P(t) = P(0)e^{r_1t}$  and  $F(t) = F(0) + r_2t$ .

The significance of the disparities in population growth versus that of consumer goods is that even throughout the same time period, the population will become large enough such that the resources available cannot maintain it. Malthus argued that the "Malthusian Catastrophe" would occur during the intersection of available resources and the population, stating that this was where further population growth would only result in the overexploitation of the economy.

### 3 Key Terminology

#### 3.1 Neo-Malthusianism

Neo-Malthusianism is a movement that embodied the panic of the British people following the Black Death in England. Many used Malthus's initial hypothesis to advocate in favor of their own policies. The main purpose of Neo-Malthusianism is to promote population planning; however, more modern versions of Neo-Malthusianism also discuss the use of modern contraceptives, straying from Malthus's initial commendation of abstinence. Such ideologies that poverty would only be worsened through charity and the increase in the reproduction of the lower class were also used to implement laws that decreased immigration quotas.

#### 3.2 Preventative Checks

Preventative checks include population management prior to the "Malthusian Catastrophe," where resources available are unable to satisfy population demand. Malthus promoted abstinence until marriage and laws that punished parents who had children they could not provide for (ie. schooling, food, and shelter).

#### 3.3 Positive Checks

Positive checks occur during the Malthusian crisis, or when nations have already reached excessive economic strain, ranging from famines to droughts and deathly wars which limit the life span of citizens. Malthus's argument was that as nations reach resource scarcity, the quality of their healthcare and other essential services decline. This in-

nately lowers the life expectancy of a population, resulting in population decline.

#### 4 Malthusian Model Application in the Real World

The Malthusian population growth model is based on the idea that population growth will outstrip food production, leading to a population crash. The model argues that population growth will increase at a geometric rate (i.e. 2, 4, 8, 16, etc.) while food production will only increase at an arithmetic rate (i.e. 2, 4, 6, 8, etc.). This will eventually lead to a population crash due to starvation and disease. The Malthusian model can be applied to other real-world contexts, including population studies, economic analysis, and environmental research.

One of the most common applications of the Malthusian model is studying population growth in developing countries. The model can be used to analyze the potential consequences of high population growth rates in these countries, such as food insecurity, poverty, and environmental degradation. For example, researchers have used the Malthusian model to study population growth in sub-Saharan Africa, where population growth rates have been among the highest in the world and food production has struggled to keep pace.

The Malthusian model is also relevant in economic analysis, which can be used to understand the relationship between population growth and economic development. For example, some economists have used the model to study how population growth affects economic growth and the distribution of wealth.

In addition, the Malthusian model has been applied in environmental research, particularly in the study of resource depletion. The model can be used to understand how population growth can strain water, land, and energy availability, contributing to environmental problems such as deforestation and pollution.

What's more, Malthus based his theory on observations of population growth in his time, particularly in Europe, where population growth had been increasing rapidly. The Malthusian model was modeled off of historical events marked by overpopulation, food scarcity, and a high death rate. The Black Death, which ravaged Europe in the 14th century, and The Great Famine in Ireland during the 19th century are examples of such events.

In summary, the Malthusian Population Growth Model highlights the potential consequences of unchecked population growth, and it is still a relevant topic in today's world. It has diverse applications in real-world contexts, such as population studies, economic analysis, and environmental research.

#### 5 Drawbacks of the Malthusian Population Growth Model based on Historical Evidence

The Malthusian population growth model has been used to explain population growth and its potential consequences

in various real-world situations. However, the model's predictions have not always come to pass, and there have been instances where the model has not been able to predict population growth accurately.

One example of a situation where the Malthusian model has been used to explain population growth is in sub-Saharan Africa. In many countries in this region, population growth has outpaced food production, leading to concerns about food security. This is consistent with the Malthusian model's prediction that population growth will outstrip food production, leading to a population crash.

Another example of a situation where the Malthusian model has been used to explain population growth is in the history of Europe. Some historians have argued that the Malthusian model can help explain the population crashes during the Black Death in the 14th century, and the Great Famine in Ireland in the 19th century. These historical events fit well with the Malthusian model's predictions of population crashes due to starvation and disease. However, there are also examples of situations where the Malthusian model cannot predict population growth accurately. One example is in developed countries such as Japan and Europe, where population growth has slowed or even decreased in recent years. This is inconsistent with the Malthusian model's prediction that population growth will continue to increase. Another example is the global population growth in recent decades, where the availability of birth control and other family planning has played a crucial role in curbing population growth. This has led to some countries experiencing below-replacement fertility rates, which is also inconsistent with the Malthusian model's prediction of population growth.

The Malthusian Population Growth Model has been used to explain population growth and its potential consequences in various real-world situations. Still, it is not a one-size-fits-all model, and there are examples where the model's predictions have yet to come to pass. The model's prediction that population growth will outstrip food production, leading to a population crash, has been seen in some developing countries and historical events. Also, it does not consider the availability of birth control and other forms of family planning. The model also does not consider the technological advancement in food production, which has allowed for a higher food supply.

#### 6 Alternate Models

Although the Malthusian theory of population suggests a method to analyze the relationship between population growth and food supplies, it still has some limitations in its applications. One of the main criticisms is that the theory does not reflect the technological advancements of current society. Since the theory roots in early Europe, where the food supply was unstable, it assumes food availability to be the most important factor in population growth. Malthus failed to predict the technological development that decreased food insecurity, reducing the correlation between food availability and population growth. To deal with the problems that arise from the Malthusian theory, two main theories of the population were developed.

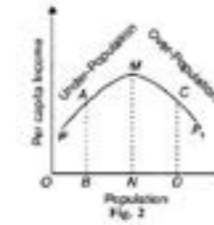


Figure 1: (Source: Top 3 Theories of Population, Kwatiah)

One of the two theories is called the optimum theory of population. The optimum population is the state in which given the resources available, produces maximum returns of income per head.

As shown by the graph, when the population reaches point  $M$ , the per capita income is maximized. Thus, according to the optimum theory of population, society will favor population increase or decrease based on the per capita income; thus, when the society is underpopulated the society will shift to increase its population and vice versa. Point  $M$  changes with the change of any of the following factors: natural resources, production techniques, stock of capital, habits of the people, the ratio of the working population, working hours of labor, and modes of business organizations. To numerically measure how much the current population deviates from the optimum population, in other words, Maladjustment, Dalton suggested the following formula:  $M = \frac{A-O}{O}$ , when  $M$  stands for maladjustment,  $A$  for the actual population, and  $O$  for the optimum population. When  $M$  is positive, the country can be assumed to be overpopulated and when  $M$  is negative, the country is understood as underpopulated. However, due to the current inability to precisely measure the optimum population, the equation is only used for academic purposes. The optimum theory of population has some superiorities over the Malthusian theorem. For example, while Malthus suggests a directly proportional relationship between food supply and population growth, Canaan, one of the founders of the optimum theory of population growth, related the problem of the population to both the industrial and agricultural output of the country. Moreover, since the optimum theory of population growth takes improvements in knowledge and other advancements into account while deciding the optimum population for the country, the optimum theory of population growth is known to be more practical and applicable in real life. Yet, there are still limitations to the theory. Since the optimum population ( $O$ ) is yet impossible to calculate, the mathematical model of population growth still remains vague. Although it may be one of the new theories for population growth with strong theoretical evidence, it still has some limitations to being practically applied.

The other theory explaining population growth is the theory of demographic transition. The theory of demographic transition is based on observed population changes in countries. According to the theory, although the exact numbers may differ based on how people distinguish phases, there are about 5 different stages of population change: high sta-



Figure 2: (Source: Top 3 Theories of Population, Kwatiah)

tionary stage, early expanding phase, late expanding phase, low stationary stage, and declining phase. During the high stationary stage, also known as the pre-transition stage, both the birth rate and the mortality rate remain high. As the stage represents the period before the industrial revolution, parents who needed more family members to support the work tended to have more children, while the high mortality rate due to poor health services kept the population growth low and stable. Next, during the early expanding phase, also known as the population explosion stage, the birth rate keeps on increasing while the death rate decreases. Due to an increased supply of food and improvement in sanitary conditions, death rates started to significantly fall while birth rates were still kept high due to a need for more workforces in the family. This stage is often shown in Least Developed Countries (LDCs). During the late expanding stage, both the birth rate and the death rate start to decrease. As economic conditions got better and the overall education level started to increase, people started to favor less on having a child and started spending more time on themselves. However, there is still a gap between the death rate and the birth rate during the third stage. Most of the developing countries are in the third phase. The low stationary stage is when the birth rates and death rates of countries are approximately the same. During this stage, the population steadily rises. Most of the developed countries are in this stage. During the declining phase, mortality rates start to exceed the birth rates of countries. Due to people's willingness to have a smaller family with fewer children, the elderly population increases while the younger population decreases. The information is also shown below.

#### 7 Analysis of Different Models

As this population growth theory is based on real-life evidence, it does not have a clear mathematical formula to follow. However, because it reflects how society has changed over time, it is one of the most well-accepted theories of population growth. In situations where mathematical calculations are required and exact numbers are asked, the Malthusian theory may be the best theory to follow. However, to see the real change in population over time in regard to birth and death rates, the demographic transition might be the best

theory to rely on.

## 8 Conclusion: The Future of Malthusian Theorem

With our ever-evolving world, we may never see a population growth model that perfectly reflects reality; however, the founding principles of all proposed theories link two main concepts together—supply and demand. Thomas Robert Malthus himself referenced the Malthusian checkpoint as occurring when the economic strain on the economy, caused by scarcity, will lead to starvation and war. Many believe his model still applies in the current day, using Japan as an example of a nation with more resources than people that demand it. However, we have also seen it fail under many circumstances. Whether it be in China with massive unemployment rates despite having more resources than necessary to maintain its population. Unevenly distributed wealth and unpredictability in the development of nations go completely unaccounted for by the Malthusian theorem. As a result, multiple criticisms of the model have been made in the current day. Rather than discard the model as a whole, scientists and politicians should come together in the future in order to enhance the capabilities of nations' in population management.



### References

- How Populations Grow: The Exponential and Logistic Equations — Learn Science at Scitable. (2023). Retrieved 29 January 2023, from <https://www.nature.com/scitable/knowledge/library/how-populations-grow-the-exponential-and-logistic-13240157/>
- Sachs, J. (2008). Are Malthus's Predicted 1798 Food Shortages Coming True? (Extended version). Retrieved 29 January 2023, from <https://www.scientificamerican.com/article/are-malthus-predicted-1798-food-shortages/>
- Thomas Malthus. (2023). Retrieved 29 January 2023, from <https://ucmp.berkeley.edu/history/malthus.html>
- Thomas Malthus — Biography, Theory, Overpopulation, Poverty, Facts. (2022). Retrieved 29 January 2023, from <https://www.britannica.com/biography/Thomas-Malthus>
- Top 3 Theories of Population (With Diagram). (2016). Retrieved 29 January 2023, from <https://www.economicdiscussion.net/theory-of-population/top-3-theories-of-population-with-diagram/18461>
- Who Is Thomas Malthus?. (2023). Retrieved 29 January 2023, from <https://www.investopedia.com/terms/t/thomas-malthus.asp>

# 12 Investigating Applications of Linear Algebra Concepts in Natural Language Processing

Written by Gyulim Jessica Kang

# Investigating Applications of Linear Algebra Concepts in Natural Language Processing (ATLA Project)

Gyulim Kang

kang782455@sas.edu.sg

Teacher Reviewer:

Mr. Zitur

## Abstract

Due to the rapid development of the Internet throughout the 21st century, researchers now have an abundance of information at their fingertips. This overflow of information has produced many positive consequences—such as providing researchers with more data to analyse, ensuring increased accuracy—but also presents several critical challenges, especially in the field of natural language processing (NLP). This branch of artificial intelligence centers around the structure of language, constructing rules to establish intelligent systems with the ability to extract meaning from speech and text. A crucial NLP technique widely used today is latent semantic analysis (LSA), which dissects the relationships between terms within a set of documents to produce common topics. LSA establishes these topics first by analysing word frequencies across different documents, then by performing singular value decomposition (SVD). SVD is a crucial step in LSA that performs dimensionality reduction upon the original matrix that depicts the frequency of each word in each document within the corpus. The foundation of SVD lies within concepts in linear algebra—the study of the properties of vector spaces and matrices—such as matrix factorization, eigenvalues, and eigenvectors. Linear algebra forms the basis of countless areas of computer science such as machine learning, image processing, natural language processing, and more. This study aims to investigate the applications of specific linear algebra concepts within LSA and their limitations. Finally, the study seeks to extend these applications to gain more insight into the performance of LSA in broader, real-life contexts such as within information retrieval through search engines.

**Keywords:** Natural Language Processing (NLP), Latent Semantic Analysis (LSA), Singular Value Decomposition (SVD), eigenvalues, eigenvectors

## 1 Introduction

### 1.1 Background and Purpose of Research

The purpose of this paper is to explore the implementations of linear algebra concepts within latent semantic analysis in different settings and analyze their limitations. The growing prevalence of the Internet has produced a rich and accessible source of data for research in unprecedented degrees. As a result, researchers in the field of natural language processing (NLP) are often able to compile a large collection of documents—sometimes hundreds of thousands—when investigating their research questions. However, it is often

the case that researchers are not able to individually understand and analyze each document due to the massive sample size. This challenge has led to the development of key machine learning techniques such as topic modeling that are able to extract topics from a set of documents and classify documents into clusters based on these topics.



Figure 1: A basic visual representation of topic modeling processes

The underlying principles of many topic modeling techniques such as latent semantic analysis are rooted in linear algebra. This paper will examine the step-by-step process of latent semantic analysis, analyze the extent of the use of certain linear algebra concepts, and finally, assess the limitations of latent semantic analysis. This paper assumes a familiarity with basic linear algebra.

## 2 Explanation of Latent Semantic Analysis Process

### 2.1 Basic Principles

Latent semantic analysis is largely founded upon two fundamental principles. The first is that the meaning of sentences, documents, and individual words is calculated mathematically. The “meaning” of a word is defined as its average frequency across all of the documents it occurs in, and the meaning of sentences and documents is defined the sum of the “meanings” of all of the words they contain. The second

principle states that within LSA, associations between different words and sentences are described implicitly (Foltz, 1996). This means that latent semantic analysis cannot identify specific topics but is able to organize documents into clusters containing the most relevance to a specific topic.



Figure 2: A diagram depicting the transition between a scattered collection of documents to organized document clusters.

### 2.2 Initial Steps

The first step when performing LSA is to construct a term-document frequency matrix. The rows are represented by each unique word, and the columns are represented by each document within the corpus. The entry at the intersection of row  $i$  and column  $j$  will be represented by the term frequency value of word  $i$  within document  $j$ . This frequency can be calculated in multiple ways, but the preferred method is to use Term Frequency-Inverse Document Frequency.

$$w_{i,j} = tf_{i,j} \times \log\left(\frac{N}{df_i}\right)$$

The equation above describes the method used in latent semantic analysis to calculate the Term Frequency-Inverse Document Frequency (TF-IDF) score, which is the product two statistics: term frequency and inverse document frequency.  $tf_{i,j}$  represents term frequency (TF) and  $\log\left(\frac{N}{df_i}\right)$  represents inverse document frequency (IDF).  $tf_{i,j}$  denotes the raw number of occurrences of word  $i$  in document  $j$ ,  $df_i$  denotes the number of documents containing word  $i$ , and  $N$  denotes the total number of documents within the dataset. Since the term frequency counts only the number of occurrences of a word within each document, the inverse document frequency was incorporated to offset the incorrect emphasis that may be placed on common words such as “a,” “an,” “the,” “she,” and “they” without giving sufficient weight to more meaningful words. This is because higher frequency does not always warrant higher significance (Kaur & Kaur, 2021).

The inverse document frequency is obtained by taking the logarithm of the result when dividing the total number of documents by the number of documents containing the term. It is important to note that this quotient ( $N/df_i$ ) will always be greater than or equal to 1; as a result, the IDF and TF-IDF score will approach 0 as the term appears in more documents and the quotient approaches 1.

Overall, the TF-IDF score places weights on words based on their rarity, ensuring that more significance is placed upon the words that occur frequently within a document but infrequently across the corpus, or the entire set of documents. A high TF-IDF score is achieved if the term appears frequently in a specific document but less frequently across the whole collection of documents.

### 2.3 Singular Value Decomposition

The next step of LSA involves reducing the dimensions of the term-document frequency matrix. This is an important step of the process because large, complex data sets often contain higher dimensions that are more difficult for the computer to process and interpret (“Singular value decomposition”, 2017). SVD is a process that can optimize the amount of information preserved within the matrix while still lowering the dimension to enable faster and more accurate analysis. The decomposition can be expressed in the form  $\mathbf{A} = \mathbf{U}\mathbf{\Sigma}\mathbf{V}^T$ , where  $\mathbf{U}$  and  $\mathbf{V}$  are orthogonal matrices and  $\mathbf{\Sigma}$  is a diagonal matrix.

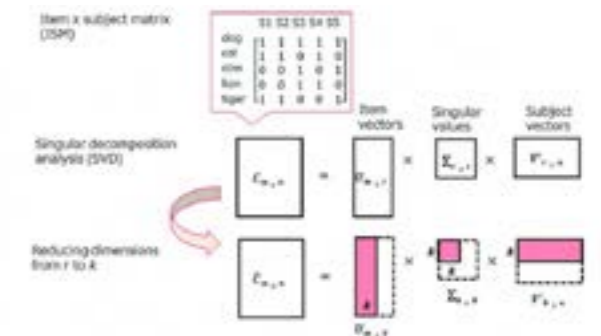


Figure 3: A representation of the process of SVD leading up to dimensionality reduction

$\mathbf{U}$  and  $\mathbf{V}$  represent rotations and  $\mathbf{\Sigma}$  represents a dilation in each coordinate direction. Rotations and dilations are examples of linear transformations and are utilized in SVD to reconfigure the dimensions of the original term-document frequency matrix. By the definition of an orthogonal matrix,  $\mathbf{U}^T = \mathbf{U}^{-1}$  (the inverse of  $\mathbf{U}$ ) and  $\mathbf{V}^T = \mathbf{V}^{-1}$ . SVD is a crucial step within the process of topic modelling because large, complex data sets often contain higher dimensions, making them sparse; they are also noisy, meaning that they contain many low-frequency words. These characteristics make it more difficult for the computer to process and interpret the documents to produce a common set of topics and document clusters. SVD optimizes the preservation of valuable information while reducing dimensions for faster, more accurate analysis (Kherwa & Bansal, 2017). We are able to find matrix  $\mathbf{U}$  by finding the diagonalizations of  $\mathbf{A}^T \mathbf{A}$ :

$$\begin{aligned} \mathbf{A}\mathbf{A}^T &= (\mathbf{U}\mathbf{\Sigma}\mathbf{V}^T)(\mathbf{U}\mathbf{\Sigma}\mathbf{V}^T)^T \\ &= (\mathbf{U}\mathbf{\Sigma}\mathbf{V}^T)(\mathbf{V}\mathbf{\Sigma}^T\mathbf{U}^T) \\ &= \mathbf{U}(\mathbf{\Sigma}\mathbf{\Sigma}^T)\mathbf{U}^T \\ &= \mathbf{U}(\mathbf{\Sigma}^2)\mathbf{U}^{-1} \end{aligned}$$

$$\begin{pmatrix} 0.65520174 & -0.75545396 \\ 0.75545396 & 0.65520174 \end{pmatrix}$$

The diagonal entries of  $\mathbf{\Sigma}$  will be equivalent to the square roots of the two positive eigenvalues (which were 5(3+) and 5(3-)) in descending order:

$$\begin{pmatrix} 5.39834564 & 0 \\ 0 & 0.92620968 \end{pmatrix}$$

Finally, we find  $\mathbf{V}$  using the fact that  $\mathbf{V} = \mathbf{A}^{-1}\mathbf{U}\mathbf{\Sigma}$ , then normalize:

$$\begin{pmatrix} 0.92388 & 0.382683 \\ 0.382683 & -0.92388 \end{pmatrix}$$

Now that we have all three matrices— $\mathbf{U}$ ,  $\mathbf{V}$ , and  $\mathbf{\Sigma}$ —we will be able to construct our SVD factorization ( $\mathbf{U}\mathbf{\Sigma}\mathbf{V}^T$ ) of matrix  $\mathbf{A}$ :

$$\begin{pmatrix} 0.65520174 & -0.75545396 \\ 0.75545396 & 0.65520174 \end{pmatrix} \begin{pmatrix} 5.39834564 & 0 \\ 0 & 0.92620968 \end{pmatrix} \begin{pmatrix} 0.92388 & 0.382683 \\ 0.382683 & -0.92388 \end{pmatrix}$$

### 3 Application of LSA

#### 3.1 Walkthrough

To apply these concepts in a real-life, a dataset on Kaggle was chosen that contained information about various news articles across a range of media outlets—including the New York Times, CNN, and more—from the years 2016 to 2017. The features of the dataset included the ID, title, publication, author, date, year, month, URL, and full text of each article.

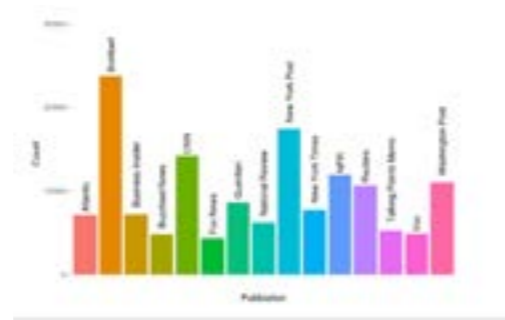


Figure 4: Publications represented within dataset

For the analysis, the main focus was on the “title” and “content” columns, as these were the columns that contained information most relevant to the topics covered within the article. Before constructing the word frequency matrix, the dataset was pre-processed to remove extraneous information such as punctuation, numbers, or articles (eg. ‘a’) that do not contribute meaning to the article’s content and risk hindering accuracy of analysis.

First, the eigenvalues must be derived using the following equation:  $\det(\mathbf{A} - \lambda\mathbf{I}) = 0$ . After finding the corresponding eigenvectors, they must be organized in descending order. The columns of  $\mathbf{U}$  will be the eigenvectors of  $\mathbf{A}$ . The eigenvectors must also be normalized, meaning that each term in the vector should be divided by the vector’s magnitude to scale it to an eigenvector that has a unit length of 1. Next, we can find  $\mathbf{\Sigma}$ : the diagonal entries are equivalent to the positive square root of the eigenvalues organized in descending order.

Finally,  $\mathbf{V}$  can be found using the following equation:

$$\begin{aligned} \mathbf{A} &= \mathbf{U}\mathbf{\Sigma}\mathbf{V}^T \\ \rightarrow \mathbf{A}\mathbf{V} &= \mathbf{U}\mathbf{\Sigma}\mathbf{V}^T\mathbf{V} \\ \rightarrow \mathbf{A}\mathbf{V} &= \mathbf{U} \\ \rightarrow \mathbf{V} &= \mathbf{A}^{-1}\mathbf{U}\mathbf{\Sigma} \end{aligned}$$

The vectors of  $\mathbf{V}$  must also be normalized. Let’s say we have the following matrix:

$$\mathbf{A} = \begin{pmatrix} 3 & 2 \\ 4 & 1 \end{pmatrix}$$

The first step would be to find the diagonalizations of  $\mathbf{A}\mathbf{A}^T$  and  $\mathbf{A}^T\mathbf{A}$  to find matrices  $\mathbf{U}$  and  $\mathbf{V}$ , respectively.

$$\mathbf{A} \cdot \mathbf{A}^T = \begin{pmatrix} 25 & 10 \\ 10 & 5 \end{pmatrix}$$

$$\mathbf{A}^T \cdot \mathbf{A} = \begin{pmatrix} 13 & 14 \\ 14 & 7 \end{pmatrix}$$

The characteristic polynomial of  $\mathbf{A}\mathbf{A}^T$  is the following:

$$\begin{aligned} (13 - \lambda)(17 - \lambda) - 14 \times 14 &= 0 \\ 221 - 30\lambda + \lambda^2 - 196 &= 0 \\ \lambda^2 - 30\lambda + 25 &= 0 \end{aligned}$$

Using the quadratic formula, we can deduce that the eigenvalues of  $\mathbf{A}\mathbf{A}^T$  are 5(3+22) and 5(3-22). The corresponding eigenvectors are the following:

$$\begin{pmatrix} -1 + 5\sqrt{2} \\ 7 \end{pmatrix} \begin{pmatrix} -1 - 5\sqrt{2} \\ 7 \end{pmatrix}$$

Arranging the eigenvalues in descending order, we arrive at the following matrix for  $\mathbf{U}$  (this is before normalizing):

$$\begin{pmatrix} -1 + 5\sqrt{2} & -1 - 5\sqrt{2} \\ 7 & 7 \end{pmatrix}$$

After normalizing, we get the following final matrix for  $\mathbf{U}$ :



Figure 5: Dataset representation within Jupyter notebook

```
1 stop_words = set(stopwords.words('
  english'))
2 newHeadlines = []
3
4 for x in headlines:
5     x = x.lower()
6     x = x.replace(" ", "")
7     x = x.replace(".", "")
8     for character in string.punctuation:
9         x = x.replace(character, '')
10    x = x.replace("the new york times",
11    '')
12    x = ''.join(c for c in x if not c.
13    isdigit())
14    x = x.strip()
15    newHeadlines.append(x)
```

Afterward, the next step was to construct the term frequency matrix and perform the SVD factorization, respectively. This was achieved by using the built-in functions of the Scikit Learn library, a Python library that contains many useful machine learning tools such as dimensionality reduction, regression, and more.

```
1 tfidfvectorizer = TfidfVectorizer(
  analyzer='word', stop_words='english'
  )
2 tfidf_wm = tfidfvectorizer.fit_transform
  (df['New Headlines'])
3 tfidfvectorizer1 = TfidfVectorizer(
  analyzer='word', stop_words='english'
  )
4 tfidf_wm1 = tfidfvectorizer1.
  fit_transform(df['New Content'])
5 svd = TruncatedSVD(n_components=100)
6 lsa = svd.fit_transform(tfidf_wm)
```

After constructing the term-document matrices, we can observe the features—the unique words that comprise the rows of the matrices. The features can be derived using the code below.

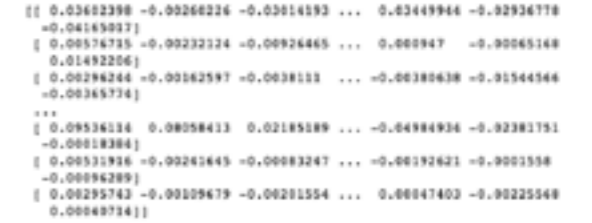


Figure 6: Constructing the term-document frequency matrix containing the TF-IDF scores for each term within the Title and Content columns

```
1 dictionary = tfidfvectorizer.
  get_feature_names()
2 print(dictionary)
```

### 3.2 Results

Afterward, document clusters were identified by implementing additional code. Before observing the clusters, the silhouette scores of the clusters were reviewed to confirm how effectively the document clusters were created. Viewing the silhouette scores enables us to assess the performance of the LSA model on the dataset and determine whether specific conditions (such as those in pre-processing) must be adjusted to obtain the desired degree of accuracy.

```
1 s_list = []
2
3 for clus in tqdm(range(2,21)):
4
5     km = KMeans(n_clusters=clus, n_init
6     =50, max_iter=1000) # Instantiate
7     KMeans clustering
8
9     km.fit(lsa) # Run KMeans clustering
10
11     s = silhouette_score(lsa, km.labels_
12     )
13     s_list.append(s)
14
15 plt.plot(range(2,21), s_list)
16 plt.show()
```

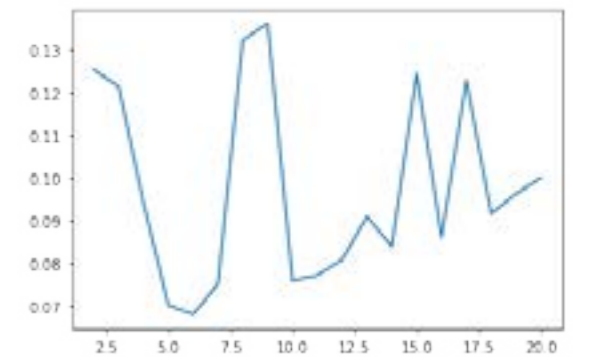


Figure 7: Silhouette score plot

This plot shows that most of the silhouette scores are on the higher end of the scale, suggesting that most of the

clusters are linearly separable or there is little to moderate amount of overlaps among them. To verify this result, a T-distributed Stochastic Neighbor Embedding (TSNE) scatterplot was created. A TSNE scatterplot enables us to view higher-dimensional data in a low dimensional space—in this case, two-dimensional since the plot contains two axes—while preserving the overall structure. This means that similar points that are close to each other in the higher-dimensional space will also be close together in the TSNE scatterplot.

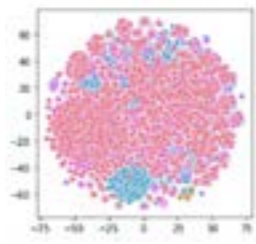


Figure 8: TSNE scatterplot

Although most of the clusters are represented with the color pink, making the distinctions between clusters a bit difficult to discern, it can be seen that most of the clusters are organized in an orderly manner of circular shapes rather than being spread out. Figure 9, which depicts LSA performed upon a very small set of documents (therefore direct topic assignment was possible), illustrates this difference; it can be observed that while the documents pertaining to the green, purple, blue, and red topics are clustered in a relatively orderly way, the documents pertaining to the orange topic are very spread out. This explains the reason why the majority of the silhouette scores for this dataset are on the lower end of the scale.

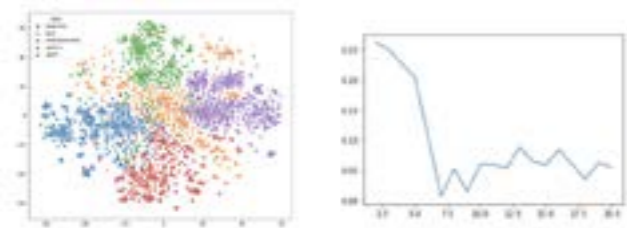


Figure 9: Sample TSNE plot with low silhouette score

### 3.3 Limitations of LSA

A key limitation of LSA is that it does not determine specific topics from a set of documents as it is an unsupervised algorithm. As a result, it is mainly utilized to cluster similar documents together. Additional topic modeling techniques that are newer to the field of NLP such as BERTopic leverages TF-IDF to create easily interpretable topics and keywords within each topic description. The BERTopic technique was utilized to conduct a more in-depth analysis of the

dataset and verify the accuracy of the visualizations created above (Appendix).

## 4 Extension

### 4.1 Walkthrough

In order to extend this application and investigate a common real-life use of LSA—information retrieval through search engines—a search engine was created based on the same dataset. LSA is an ideal technique to utilize for creating search engines as it does not rely on keyword searches, meaning that only results containing the literal keywords inputted into the search engine will appear, but rather on semantic searches. This allows the search engine to return relevant results without necessarily containing the exact words inputted.

Using the term-document matrix for the ‘content’ column that was created previously in the Application section, a word cloud was constructed to observe the words that occurred the most often.



Figure 10: Word Cloud

To begin creating the search engine, a function called `search_results` was constructed. This function involved using the term-document matrices containing each term’s TF-IDF score for each document to compile a list of the articles that contained words with the highest similarity to those within the search query.

The Python library primarily used for this extension was Gensim, which contains numerous functions for document indexing, topic modeling, and similarity retrieval with large corpora. The `MatrixSimilarity` function seen below calculates the similarity of each feature—terms and documents—within the corpus against the other and stores this information in an index matrix; we will use this matrix later to compare the similarities of the words within our search query to these features.

```
1 from gensim.similarities import
  MatrixSimilarity
2 articleIndex = MatrixSimilarity(lsa1,
  num_features = lsa1.num_terms)
```

After writing the code that would analyse the terms within the search query and fetch the most relevant articles (by identifying the terms within the TF-IDF term-document matrix then using the results to investigate the similarities of the terms to other terms and documents through the index matrix), the search engine printed the list of the five most relevant articles along with the percentage of relevance using the similarity value from the index matrix.

## 4.2 Results

The following figure depicts a sample query and its search results from the search engine. Although some of the articles did not explicitly contain the words within the queries, these articles still came up as results because they contained the words most similar to the words in the query.



Figure 11: Search engine performance

Upon a further investigation into these results by reading the article content, it was observed that all of the articles were sufficiently relevant to the inputted search queries. To further test the performance of the search engine, however, it may be beneficial to input longer, more complex phrases (eg. “impact of controversial art on galleries nationwide”, “statistics of hate crimes”, etc.) to observe whether the results are relevant not only to the specific words within the query but the overall meaning of the query.

## 5 Conclusion

### 5.1 Summary

In summary, eigenvalues and eigenvectors have numerous applications within the field of Natural Language Processing that form the basis of LSA, a prominent topic modelling technique. Singular Value Decomposition is a key process based upon linear algebra concepts that is utilized within LSA to perform dimensionality. LSA has several important advantages and disadvantages. By analysing a reduced representation of the original term-document frequency matrix (through SVD) that preserves the correlation of terms between documents, LSA is able to ensure the accuracy of its analysis to some extent. However, some disadvantages are that LSA is not able to explicitly describe topics within the corpus and that its accuracy can diminish overtime as the size of the corpus increases. Some limitations of this investigation are that additional applications of linear algebra concepts in topic modelling such as Non-negative Matrix Factorization (NMF) were not covered in detail. The evaluation of the search engine results could also have been more comprehensive by investigating the search engine’s performance based on more diverse (eg. in length, complexity, and topic) search queries. The field of textual analysis is ever-evolving, and there are numerous complex and innovative methods regarding the automation of this analysis that can be explored. In future studies, I would like to dive further into NMF and experiment with using different search queries on search engines created using LSA to overcome the limitations within the investigation of the current study.

## References

Carlsson, Gunnar. “Topology and data.” *Bulletin of the American Mathematical Society* 46.2 (2009): 255-308.

Garin, A., & Tauzin, G. (2019, December). A topological reading” lesson: Classification of MNIST using TDA. In 2019 18th IEEE International Conference On Machine Learning And Applications (ICMLA) (pp. 1551-1556). IEEE.

Koplik, G. (2022, June 16). Persistent homology: A Non-Mathy Introduction with Examples. Medium. Retrieved July 5, 2022, from <https://towardsdatascience.com/persistent-homology-with-examples-1974d4b9c3d0>

Otter, Nina, et al. “A roadmap for the computation of persistent homology.” *EPJ Data Science* 6 (2017): 1-38.

Talebi, S. (2022, June 17). Persistent Homology. Medium. Retrieved July 6, 2022, from <https://medium.datadriveninvestor.com/persistent-homology-f22789d753c4>

Tauzin, Guillaume, et al. “giotto-tda: A Topological Data Analysis Toolkit for Machine Learning and Data Exploration.” *J. Mach. Learn. Res.* 22 (2021): 39-1.

Zomorodian, Afra, and Gunnar Carlsson. “Computing persistent homology.” *Discrete & Computational Geometry* 33.2 (2005): 249-274.

## 6 Appendix



Figure A1: Plot representing similarities between topics. It can be observed that the clusters of topics are well-organized, which aligns with the high silhouette scores that we arrived at previously using LSA. The bar chart below shows the most common topics and their keywords.



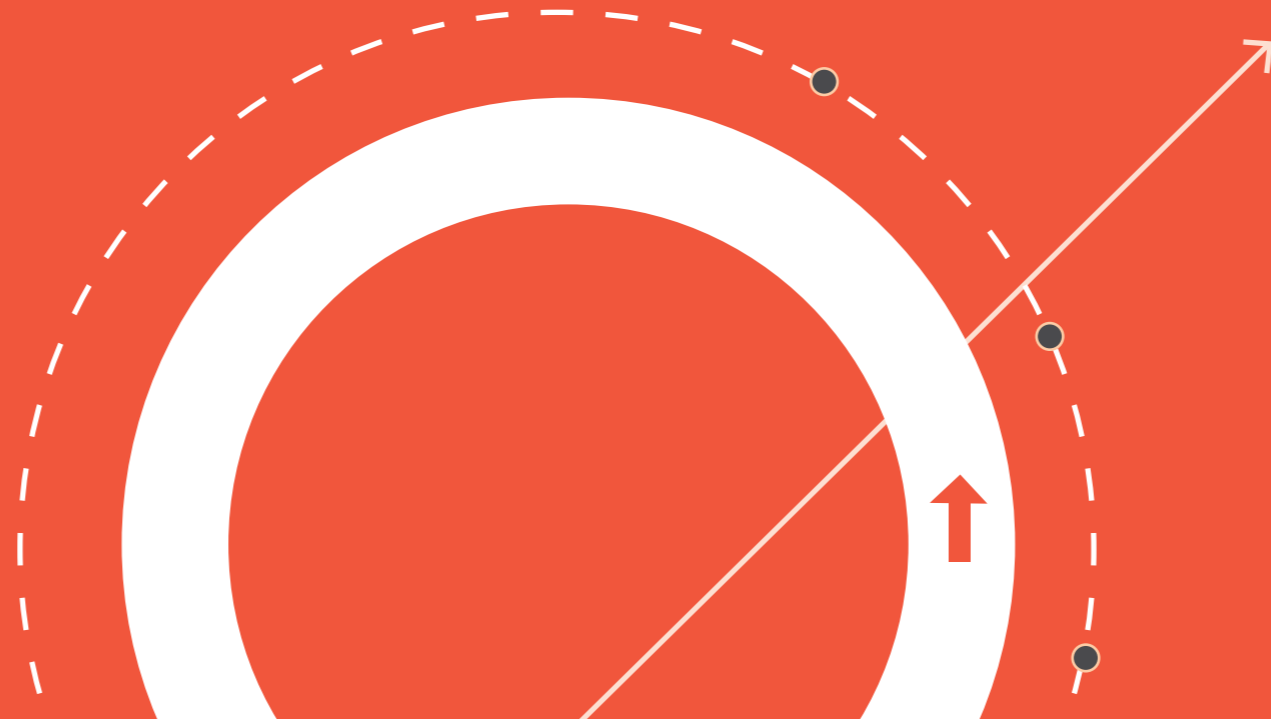
Figure A2: Common topics bar chart  
 For example, we can infer that Topic 0 is related to healthcare, Topic 2 is related to police and/or police violence, Topic 3 is related to firearms and firearm-related policies, and so on.



# 13

## Creating a Machine Learning Pipeline To Perform Topological Data Analysis

Written by Gyulim Jessica Kang



# Creating a Machine Learning Pipeline To Perform Topological Data Analysis

Gyulim Kang

kang782455@sas.edu.sg

Teacher Reviewer:

Mr. Son

## Abstract

In applied mathematics, topological data analysis (TDA) utilizes concepts from topology to extract qualitative features from data such as its shape. TDA has a variety of approaches to extract structure from unstructured data, or point clouds, and it is well-suited for high-dimensional and noisy data sets. Point clouds are a finite set of points within the data, and persistent homology is used to represent the data as a simplicial complex: a complex of simplexes, or triangles generalized in multidimensional spaces. The first step of TDA involves repeatedly using filtration on the point cloud to arrive at a filtered complex. Second, the key topological features of the filtered complex—the number of connected components and holes—are analyzed through persistent homology. Finally, the timeline of the birth and death of topological features throughout the process of filtration is displayed in a persistent diagram. The computation of persistent homology is a fast-evolving area with numerous intriguing challenges; new algorithms and software implementations in the field are being updated and released rapidly. Premised on the idea that the shape of data sets contains relevant information, TDA represents a promising bridge between topology and data science that warrants further exploration.

**Keywords:** Topological Data Analysis (TDA), point cloud, simplicial complex, Vietoris-Rips complex, persistent homology, persistence diagram, filtration, vectorization methods

## 1 Introduction

### 1.1 Background and Purpose of Research

This paper explores topological data analysis, an on-the-rise data science tool, and its applications in machine learning. The growing prevalence of the Internet has produced a rich and accessible source of data for research to unprecedented degrees. The application of persistent homology in data science provides a robust theoretical foundation for a mathematically rigorous analysis of shape within data (Carlsson, 2009). The shape of the data can be interpreted in several forms depending on the type of data. For example, let's say we have data consisting of a finite number of points scattered in the coordinate space; you naturally start thinking about how these points are roughly shaped or clustered. This is similar to how we look up at the stars in the night sky and see constellations in the shapes of polar bears



Figure 1: Geo-referenced point cloud of Red Rocks, Colorado

or scorpions. That is because it is one of our human tendencies to extract familiar, meaningful shapes from seemingly random and scattered data. Here is another example: if you have handwritten image data, you can envision characteristics such as how many holes there are in the numbers. TDA aims to encode the persistent homology of a dataset in an accessible visual representation called the persistent diagram. The principles of topological data analysis are rooted in persistent homology and the premise that the shape of a dataset contains relevant information. This paper will examine the framework of TDA, provide examples of TDA results on various datasets, and analyze its applications in machine learning along with its limitations.

## 2 Key Definitions

### 2.1 Point Clouds

Let's say our data is given as a finite set of points in Euclidean space  $\mathbb{R}^d$ . We call this set of points a point cloud. For example, a set containing each reflection of a laser pulse from a lidar forms a 3-dimensional point cloud with  $(x, y, z)$  coordinates. A set of points might appear to be randomly scattered on the surface, but there might be some hidden geometric, or topological patterns. Ultimately, TDA uses homology to answer meaningful questions such as 'How can we identify geometric features from data?' and 'How do we know that these geometric features are significant?'

### 2.2 Simplicial Complex

A simplex is the generalization of a triangle, the fundamental shape of geometry, in multidimensional spaces. For example, a 0-simplex is a point, a 1-simplex a line, a 2-simplex a triangle, a 3-simplex a tetrahedron, and so on (Koplik, 2022). Within TDA, we can use persistent homology

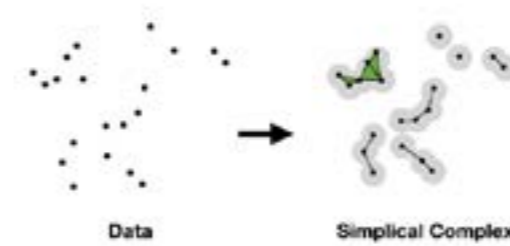


Figure 2: (Talebi, 2022)

to translate data into a collection of triangles: a simplicial complex. The formal definition of a simplicial complex is as follows, satisfying the two conditions below: Every face of a simplex from  $K$  is also in  $K$ . The non-empty intersection of any two simplices  $\epsilon_1, \epsilon_2$  in  $K$  is a face of both  $\epsilon_1$  and  $\epsilon_2$ .

When performing TDA, we use the following steps to transform the dataset into a simplicial complex. First, we plot our data in an  $N$ -dimensional space, with a dimension for each unique variable. Second, we choose a radius  $\epsilon$  and draw an  $N$ -dimensional ball of radius  $\epsilon$  around each data point in the point cloud. Third, if two balls overlap we connect the corresponding points with a line, or a 1-simplex. If three balls overlap, we fill in the area between them to form a triangle, or a 2-simplex. This continues in the same pattern for subsequent intersections and simplices. Through the simplicial complex, we can derive the homology group, composed of connected components, holes, and cavities.  $H_0$  commonly represents the group of connected components,  $H_1$  the group of holes, and  $H_2$  the group of cavities. A natural question arises: How are we supposed to know the best radius at the outset? This is where persistent homology comes in.

### 2.3 Vietoris-Rips Complex

The Vietoris-Rips Complex is a way of forming a topological space from distances in a set of points (Garin & Tauzin, 2019). In other words, we create a simplicial complex that can be defined from any distance  $\delta$  by forming a simplex for every finite set of points in the data that has a diameter at most  $\delta$ . Formally, we construct a Vietoris-Rips complex through the following process:

1. Draw a circle around each point with a radius of  $\epsilon$ .
2. If  $\epsilon$  is greater than the distance between points  $i$  and  $j$  in the point cloud, in other words, if the intersection of two circles includes both their centers, we connect the two center points with a line segment.
3. If three points form a triangle, we fill in the area to create a 2-simplex.

Below, we will create a plot of our own to analyze through TDA. First, we use Numpy array to generate 8 random points for our point cloud.

Looking at this chart, we can think about what geometric intuition we can gain from the collection of points. For example, it may appear that the four dots clustered at the top left of the plot are going to form a square. In this way,

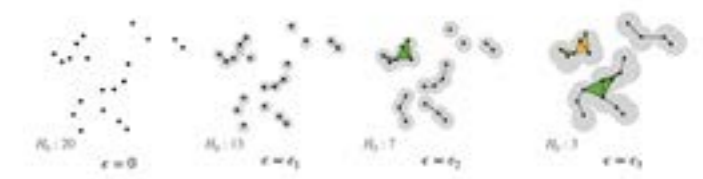


Figure 3: Evolving Complex



Figure 4: Randomly generated eight point plot

humans strive to extract familiar geometric shapes from random collections by connecting points that are close to each other. The approximation of topological space from the point cloud with this simple idea is called the Vietoris-Rips Complex.

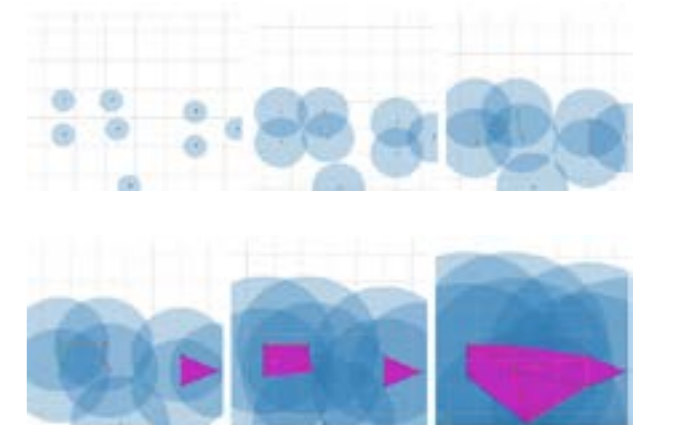


Figure 5: Transformation of the Vietoris Rips Complex

The screenshots above showcase the transformation of the simplicial complex as the epsilon value gets larger: overlap increases, and more connected components ( $H_0$ ) and holes ( $H_1$ ) are birthed in the complex. It can be observed from the diagrams that triangles and edges appear, merge, and disappear with the change of epsilon. Additionally, the total number of components decreases over time; if  $\epsilon$  is sufficiently large, there will only be one united connected component remaining in the simplex. In summary, the number of components and holes can be important indicators of key geo-



metric features, and we can obtain them by computing the homology of the complex.

By visualizing the complexes, we are able to gain geometric intuition. However, it is difficult to determine which epsilon value best represents the shape of data merely through observation. For every epsilon, we must be able to summarize how the number of components and holes are being changed. Persistent homology, an algebraic method for computing topological features in a space, allows us to do this (Otter et al., 2017). It is the concept of measuring which features are born and die from the complex as the epsilon value, or radius, changes. Persistent homology is the primary method used in TDA to study qualitative features of data that persist across multiple scales. It has many advantages as well; it is robust to perturbations of input data, independent of dimensions and coordinates, and provides a compact representation of the qualitative features of the input.

### 3 TDA Framework

#### 3.1 Filtration

The initial step of TDA is to repeatedly use filtration to arrive at a filtered complex. Filtration is defined as the process of adjusting the parameter of epsilon, or the radius, to assess changes in the dataset. Filtration has numerous applications in real life, including height filtration on images. Performing height filtration allows us to conduct image segmentation. For example, in the picture of wood cells below, we can use height filtration to extract the connected components (in this case, individual cells) from the image. Although imperfect, this algorithm has a high level of accuracy; this is impressive considering only a few parameters, such as the blur parameter, need to be adjusted.



Figure 6: Original Wood Cell Image



Figure 7: Blurred image with 1 dimension of color



Figure 8: Connected Components

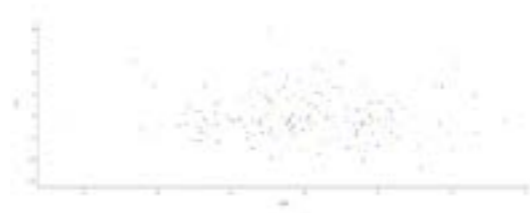


Figure 9: First Point Cloud

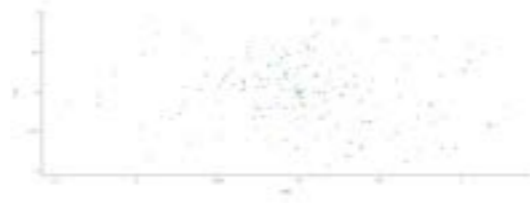


Figure 10: Second Point Cloud

#### 3.2 Persistence Diagram

A persistent diagram represents the birth and death of connected components and holes of a Vietoris-Rips complex throughout the change of epsilon. In order to construct the diagram, persistent homology tracks when two balls of radius epsilon, each centered around a point on the point cloud, intersect. A point is added to the diagram when the ball in one connected component first intersects a ball of another connected component, because the merging of two connected components signifies the death of one of them. The final remaining simplex dies at infinity. A point located near the diagonal means that this feature died almost immediately after it was born. In other words, this means that the further its persistence, the greater its persistence. High persistence features are generally thought to be statistically significant, while lower persistence features more representative of statistical noise.

Comparing Two Persistent Diagrams (bottleneck/Wasserstein distance) When comparing the persistent diagrams of two point clouds, we are able to utilize metrics such as the Wasserstein distance. The Wasserstein distance is a distance function between probability distributions on a particular metric space  $M$ . This metric compares the probability distributions of two different variables, where one variable is derived from the other by random or deterministic perturbations.

Now, we will try experimenting with using TDA and persistence diagrams to discriminate between two point clouds extracted from distributions that look similar to the naked eye but are, in reality, completely different.

The first point cloud consists of 200 points extracted from a Gaussian normal distribution. Therefore, statistically, the geometric information of this point cloud will be similar to the geometric information that a normal distribution surface would have.

The second point cloud consists of 200 points scattered by

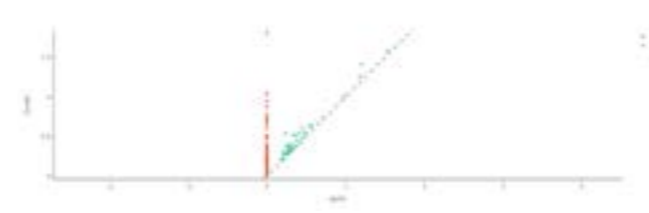


Figure 11: Persistent diagram of first point cloud

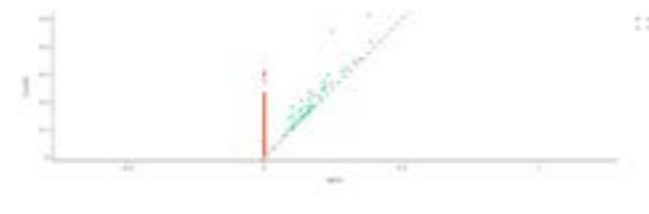


Figure 12: Persistent diagram of second point cloud

first randomly selecting 200 angles and applying constant noise to two adjacent circles. Although these point clouds were created differently, it's difficult to distinguish between the two point clouds to determine which was created through which distribution. Now we will see if we can observe a distinct pattern within their respective persistent diagrams. One difference that can be observed is that in the second persistent diagram, unlike the first, the persistence of the  $H_1$  group is especially strong.

Regarding the application of persistent diagrams in machine learning, however, persistent diagrams aren't suitable for use as input vectors because the number of points constituting the diagram will differ depending on the image. In other words, each data set will be represented as a vector of a different dimension. As a result, it is necessary to transform the persistent diagram into a vector of some fixed dimension by using vectorization methods such as HeatKernel.

#### 4 Sample Application in Machine Learning

Vectorization Methods (HeatKernel) One vectorization method often used in TDA is HeatKernel. Given a persistence diagram made up of the triples  $[b, d, q]$  representing birth-death-dimension, subdiagrams corresponding to various homology dimensions are taken into account individually and seen as sums of Dirac deltas. Then, a rectangular grid of locations uniformly sampled from suitable ranges of the filtering parameter is used to perform the convolution using a Gaussian kernel. The reflected pictures of the subdiagrams around the diagonal are processed in the same way, and the difference between the outputs of the two convolutions is computed. A (multi-channel) raster picture can be compared to the outcome. Machine Learning Pipeline MNIST: Binarization  $\rightarrow$  Filtration  $\rightarrow$  Persistent Diagram This pipeline uses a mix of various filtering, distance metrics (eg. Wasserstein, bottleneck), and vectorization methods including HeatKernel. This pipeline can be used to perform

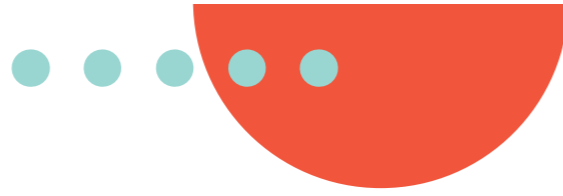
efficient machine learning and TDA analysis on the training data. What's noteworthy is that when we use this pipeline, we're no longer using any information from the image pixels themselves. Instead, we're only using the topological features of the image data seen from multiple perspectives.

### 5 Conclusion

In conclusion, persistent homology has many applications in data science. Persistent homology is the primary method used in TDA to study qualitative features of data that persist across multiple scales. It has a lot of advantages too; it's robust to perturbations of input data, independent of dimensions and coordinates, and provides a compact representation of the qualitative features of the input. For future work, I would like to dive deeper into the mathematical background of persistent homology along with the various applications of TDA in real life.

### References

- Carlsson, Gunnar. "Topology and data." *Bulletin of the American Mathematical Society* 46.2 (2009): 255-308.
- Garin, A., Tauzin, G. (2019, December). "A topological reading" lesson: Classification of MNIST using TDA. In 2019 18th IEEE International Conference On Machine Learning And Applications (ICMLA) (pp. 1551-1556). IEEE.
- Koplik, G. (2022, June 16). Persistent homology: A Non-Mathy Introduction with Examples. Medium. Retrieved July 5, 2022, from <https://towardsdatascience.com/persistent-homology-with-examples-1974d4b9c3d0>
- Otter, Nina, et al. "A roadmap for the computation of persistent homology." *EPJ Data Science* 6 (2017): 1-38.
- Talebi, S. (2022, June 17). Persistent Homology. Medium. Retrieved July 6, 2022, from <https://medium.datadriveninvestor.com/persistent-homology-f22789d753c4>
- Tauzin, Guillaume, et al. "giotto-tda: A Topological Data Analysis Toolkit for Machine Learning and Data Exploration." *J. Mach. Learn. Res.* 22 (2021): 39-1.
- Zomorodian, Afra, and Gunnar Carlsson. "Computing persistent homology." *Discrete Computational Geometry* 33.2 (2005): 249-274.



# 14 Evaluating Affirmative Action in School Choice: Comparing Mechanisms with Minority Reserves

Written by Gyulim Jessica Kang

## Evaluating Affirmative Action in School Choice: Comparing Mechanisms with Minority Reserves

Gyulim Kang

kang782455@sas.edu.sg

Teacher Reviewer:

Mr. Son

### Abstract

In the economic theory of two-sided many-to-one matching, a particular problem of interest is the mechanism of school assignment. Ever since the deferred acceptance algorithm was first proposed by Gale and Shapley (1962), there has been much research about mechanisms that optimally match students to schools in real-world situations. Pathak and Sönmez (2013) tried to incorporate truncated preferences into the existing matching framework, whereas Hafalir, Yenmez and Yildirim (2013) considered reserves for minority students. In this paper, we explore the relatively undeveloped area of truncated preferences in school matching with minority reserves. Specifically, we present a novel framework for mechanism analysis with minority reserves and compare mechanisms by their stability, Pareto optimality, and vulnerability to manipulation. Our results show that the old Chicago mechanism is at least as manipulable as any other stable mechanism and is strictly more manipulable than the serial-dictatorship mechanism.

*Keywords:* Gale-Shapley algorithm, market design, mechanism design, school choice, truncated preferences

### 1 Introduction

Given a set of men and women whose preferences are in the opposite gender, how should we form pairs such that no agent has the incentive to rematch? This question was originally proposed and answered by Gale and Shapley in 1962; since then, the solutions to the variants of the question have been applied to school choice, medical residency matching, and the assignment of cadets to military branches. Gale and Shapley tried to find a one-to-one stable matching (a set of pairings in which (1) all men and women find their partners acceptable and (2) no man/woman pair prefers each other to their assigned partners). By a process called the deferred acceptance algorithm, Gale and Shapley proved that a stable matching exists for any finite set of men and women and their preferences. The algorithm is described as follows:

- 1) Each man proposes to his most preferred woman. Each woman selects her most preferred man out of those who proposed to her and puts him on her waiting list; the rest are rejected.
- 2) Each man that was rejected proposes to his next preferred woman. Each woman selects her most preferred

man among those that proposed to her, including the man on the waiting list.

- 3) Repeat Step 2 until no men who are available to propose are left.

Gale and Shapley proved that the matching obtained at the termination of the algorithm is stable. For example, consider the following situation with 5 men and 4 women:

$$\begin{aligned} p(m_1) &= w_1, w_2, w_3, w_4, m_1 \\ p(m_2) &= w_4, w_2, w_3, w_1, m_2 \\ p(m_3) &= w_4, w_3, w_1, w_2, m_3 \\ p(m_4) &= w_1, w_4, w_3, w_2, m_4 \\ p(m_5) &= w_1, w_2, w_4, m_5, \square \end{aligned}$$

$P(m_i)$  denotes the preference relation of  $m_i$ ; for instance,  $m_5$  prefers  $w_1$  over  $w_2$ ,  $w_2$  over  $w_4$ , and  $w_4$  over staying single.  $m_5$  would rather stay single than be matched with  $w_3$  or  $w_5$ . Assume that the preferences of the women are as follows:

$$\begin{aligned} p(w_1) &= m_2, m_3, m_1, m_4, m_5, w_1 \\ p(w_2) &= m_3, m_1, m_2, m_4, m_5, w_2 \\ p(w_3) &= m_5, m_4, m_1, m_2, m_3, w_3 \\ p(w_4) &= m_1, m_4, m_5, m_2, m_3, w_4 \end{aligned}$$

If we apply the deferred acceptance algorithm to this specific example,

1.  $m_1$ ,  $m_4$ , and  $m_5$  propose to  $w_1$ , who only holds  $m_1$ ;  $m_2$  and  $m_3$  propose to  $w_4$ , who only holds  $m_2$ . This yields a tentative matching

$$\begin{pmatrix} w_1 & w_2 & w_3 & w_4 \\ m_1 & \square & \square & m_2 \end{pmatrix}$$

2.  $m_3$ ,  $m_4$ , and  $m_5$  propose to  $w_3$ ,  $w_4$ , and  $w_2$ , respectively;  $w_4$  rejects  $m_2$  and holds  $m_4$ . The tentative matching is thus revised to

$$\begin{pmatrix} w_1 & w_2 & w_3 & w_4 \\ m_1 & m_5 & m_3 & m_4 \end{pmatrix}$$

3.  $m_2$  proposes to  $w_2$ , who rejects  $m_5$  and holds  $m_2$ . The tentative matching is thus revised to

$$\begin{pmatrix} w_1 & w_2 & w_3 & w_4 \\ m_1 & m_2 & m_3 & m_4 \end{pmatrix}$$

4.  $m_5$  proposes to  $w_4$ , who rejects  $m_5$  and holds  $m_4$ , which stops the procedure and results in

$$\begin{pmatrix} w_1 & w_2 & w_3 & w_4 & (m_5) \\ m_1 & m_2 & m_3 & m_4 & (m_5) \end{pmatrix}$$

In addition, each man weakly prefers his match under the deferred acceptance algorithm compared to any other woman that he could have been matched to in another stable matching. Additional properties of the deferred acceptance algorithm include Pareto optimality, which describes the existence of a matching where there is no other matching that makes some agents better off without making anyone worse off, and manipulability, which is equivalent to an agent's ability to profit from a mechanism by misrepresenting his preferences.

### 1.1 Introduction to School Choice Context

An interesting application of the deferred acceptance algorithm is that many of its consequences can be extended to many-to-one matchings; examples include situations where an agent on one side is matched to more than one agent on the other side, such as the internship assignment problem or college admission problem.

Applications of matchings in school choice have been made to mimic real-life scenarios. Ehlers, Hafalir, Yenmez, and Yildirim studied controlled choice over public schools; Benabbou, Chakraborty, Ho, Sliwinski, and Zick investigated the impact of diversity constraints on public housing allocation. Pathak and Sönmez compared various mechanisms by their susceptibility to manipulation.

This paper is structured as follows. In Section 2, we will compare multiple matching algorithms that are known to record truncated preferences under diversity situations. More specifically, we will be discussing factors including stability, manipulability, and Pareto optimality for each mechanism.

## 2 General Framework

We first start with some traditional definitions often used in the market design theory of school choice.

1. a finite set of students  $A = a_1, \dots, a_n$ ;
2. a finite set of schools  $C = c_1, \dots, c_m$ ;
3. a capacity vector  $q = (q_{c_1}, \dots, q_{c_m})$ , where  $q_c$  is the capacity of school  $c \in C$  or the number of seats in  $c \in C$ ;
4. a students' preference profile  $P_A = (P_{a_1}, \dots, P_{a_n})$ , where  $P_A$  is the strict preference relation of student  $a \in A$  over  $C$ . In other words,  $c P_a c'$  means that student  $a$  strictly prefers school  $c$  to school  $c'$ ;

5. a schools' priority profile  $\succ_C = (\succ_{c_1}, \dots, \succ_{c_m})$ , where  $\succ_c$  is the strict priority ranking of school  $c \in C$  over  $A$ ;  $a \succ_c a'$  means that student  $a$  has higher priority than student  $a'$  to be enrolled at school  $c$ ;
6. a type space  $T = t_1, \dots, t_k$ ;
7. a type function  $\tau: S \rightarrow T$ , where  $\tau(a)$  is the type of student  $a$ ;
8. for each school  $c$ , the type specific constraint vector  $q_c^T = (q_c^{t_1}, \dots, q_c^{t_k})$  such that  $q_c^T \leq q_c$  for all  $t \in T$ .

### 3 School Choice Applications

To incorporate diversity quotas into school choice mechanisms, we start with some definitions.

1. For each school  $c_i$ ,  $Q_0(c_i)$  of the seats are determined by the students' composite scores, while  $Q_t(c_i)$  of the seats are set aside for students in each of the  $t$  types, with composite score determining relative priority among students in type  $t$ . Therefore,  $\sum_t Q_t(c_i) = q(c_i)$ .
2. The matching algorithm treats each selective enrollment high school as  $t + 1$  hypothetical schools: The set  $S_b$  of seats at each school  $b$  is partitioned into subsets  $S_{bt} = S_{0b} \cup S_{1b} \cup \dots \cup S_{tb}$ . The seats in  $S_{0b}$  are "open seats," for which students' priorities are determined entirely by composite scores. Seats in  $S_{ib}$  are "reserved" for students of type  $i$ —they give type  $i$  students priority over other students, and use composite scores to rank students within type  $i$ .
3. **The matching algorithm must convert students' true preferences  $P_i$  into strict preferences over the full set of hypothetical schools.**

The last definition is of particular interest, since we are given full autonomy over how we will set the preference of hypothetical schools over one another. To elaborate, take student  $a$  of type  $t$ . Will he prefer to be placed in the set  $S_{0b}$  or  $S_{ib}$  for school  $b$ ? Obviously, he is ineligible for a place in  $S_{ib}$  where  $i \neq t$  and  $i \neq 0$ , so that preference is trivial—just place  $S_{ib}$  such that a  $P_a S_{ib}$ . The preference between  $S_{0b}$  and  $S_{tb}$  is much less obvious; to solve this dilemma, we apply the Gale-Shapley algorithm for each case.

Assume we have students  $a_1, a_2, a_3, a_4$  and school  $S$  with preference  $a_1 > a_2 > a_3 > a_4$ . Students  $a_1$  and  $a_4$  are in type 1 and students  $a_2$  and  $a_3$  are in type 2.  $S$  has a quota of 3 and must take in at least one student from each type. In other words,  $|S_{0b}| = |S_{1b}| = |S_{2b}| = 1$ . If we assume  $S_{0b} P_a S_{tb}$  for each student  $a$  of type  $t$ , the Gale-

Shapley algorithm yields,  $\begin{pmatrix} S_0 & S_1 & S_2 \\ a_1 & a_2 & a_4 \end{pmatrix}$  which is unstable with a blocking pair of  $(a_3, S)$ . On the other hand, if  $S_{tb} P_a S_{0b}$ , the Gale-Shapley algorithm yields a stable matching of  $\begin{pmatrix} S_0 & S_1 & S_2 \\ a_3 & a_1 & a_2 \end{pmatrix}$ .

According to this observation, it only seems right that we adapt the assumption of  $S_{tb} P_a S_{0b}$ . Under this definition, we get the following result:

**Theorem 3.1.** *The matching obtained from the Gale-Shapley algorithm with minority reserves is stable.*

Proof) Assume there exists a school  $S$  and a student  $a$  in type  $i$  such that  $S P_a \mu(a)$ . At some point  $a$  applied to  $S_i$  and  $S_0$  and was rejected. Every student in  $S_0$  is ranked higher than student  $a$ . Additionally, every student in  $S_i$  is ranked higher than any student of type  $i$  in  $S_0$ . Therefore,  $(a, S)$  cannot form a blocking pair and the matching is stable. ■

We now wonder whether the qualities of the original Gale-Shapley algorithm will transfer to this framework.

**Theorem 3.2.** *The matching obtained from the Gale-Shapley algorithm with minority reserves is Pareto-efficient for students (student-optimal) out of all stable matchings.*

Proof) Because the Gale-Shapley algorithm is student-efficient, this matching is optimal for students out of all stable matchings. However, we must also observe whether the matching is Pareto efficient for all matchings. Consider the following example:

$$\begin{aligned} p(a_1) &= c_1, c_2, a_1 \\ p(a_2) &= c_2, c_1, a_2 \\ p(a_3) &= c_1, c_2, a_3 \\ p(c_1) &= a_2, a_3, a_1, c_1 \\ p(c_2) &= a_1, a_3, a_2, c_2 \end{aligned}$$

If we apply the Gale-Shapley algorithm where the student applies to the school, we get a stable matching  $\begin{pmatrix} c_1 & c_2 \\ a_2 & a_1 \end{pmatrix}$ . However, the Pareto optimal matching for students is  $\begin{pmatrix} c_1 & c_2 \\ a_1 & a_2 \end{pmatrix}$ , so the Gale-Shapley algorithm is not Pareto-efficient out of all mechanisms. ■

The Gale-Shapley algorithm is student-optimal out of all stable mechanisms but may not be Pareto efficient for the students. Another characteristic we must observe is the strategy-proofness (non-manipulability) of the Gale-Shapley mechanism.

**Theorem 3.3.** *The matching obtained from the Gale-Shapley algorithm with minority reserves is strategy-proof.*

Proof) Assume otherwise. Then, there will be a student-school matching that a student could misreport his preferences.

*Claim 1: The mechanism that yields the student-optimal stable matching (in terms of stated preferences) makes it a dominant strategy for each student to state his true preferences.*

Proof. Consider for contradiction that some nonempty subset  $A'$  of students misreport their preferences and are strictly better off under some matching  $\mu$ , which is stable for  $A'$ . This would imply that  $\mu(a) \succ_a G S_{min}(a)$  for every  $a \in A'$ .

1.  $\mu(A') \neq G S_{min}(A')$ . Choose  $c \in \mu(A') \setminus G S_{min}(A')$ , for example  $c = \mu(a')$ . Then,  $a'$  prefers  $c$  to  $G S_{min}(a')$ , so  $c$  prefers  $G S_{min}(c) = a$  to  $a'$ . But  $a$  is not in  $A'$  since  $c$  is not in  $\mu(A')$ , so  $a$  prefers  $c$  to  $\mu(m)$ . Thus  $(a, c)$  blocks  $\mu$ .
2.  $\mu(A') = G S_{min}(A') = C'$ . Let  $c$  be the last school in  $C'$  to receive an application from an acceptable student of  $A'$

in the Gale-Shapley algorithm. Since all  $c \in C'$  have rejected acceptable students from  $A'$ ,  $c$  had some student  $a$  on the waitlist when it received its last application. Then,  $(a, c)$  is the desired blocking pair because  $a$  is not in  $A'$  because if so, after having been rejected by  $c$ , he would have applied again to another member of  $C'$ , contradicting the fact that  $c$  received the last application. But  $a$  prefers  $c$  to his school under  $G S_{min}$  and since he is no better off under  $\mu$ , he prefers  $c$  to  $\mu(a)$ . On the other hand,  $a$  was the last student to be rejected by  $c$  so  $c$  must have rejected another student under  $\mu$  before it rejected  $a$ . Hence  $c$  prefers  $a$  to the last student in  $\mu(c)$ .

From Claim 1, we get a contradiction. ■

Now that we have discussed the features of the Gale-Shapley algorithm, we compare the performance of the Gale-Shapley and Chicago mechanisms. For this, we need to examine the behavior of the Chicago mechanism under the same minority-reserves conditions as the Gale-Shapley algorithm.

**Theorem 3.4.** *The matching obtained from the Chicago algorithm with minority reserves is not stable.*

Proof) It is sufficient to prove that the Chicago algorithm without minority reserves is not stable. Consider a set of students  $a_1, a_2, a_3$  and schools  $c_1, c_2$  such that

$$\begin{aligned} p(a_1) &= c_1, c_2, a_1 \\ p(a_2) &= c_2, c_1, a_2 \\ p(a_3) &= c_1, c_2, a_3 \\ p(c_1) &= a_1, a_3, a_2, c_1 \\ p(c_2) &= a_1, a_3, a_2, c_2 \end{aligned}$$

Then the resulting matching from the Chicago algorithm without minority reserves is  $\begin{pmatrix} c_1 & c_2 \\ a_1 & a_2 \end{pmatrix}$ , which is not stable since  $(c_2, a_3)$  is a blocking pair. ■

**Theorem 3.5.** *The matching obtained from the Chicago algorithm with minority reserves is not Pareto-efficient out of all stable matchings.*

Proof) Assume that there is a matching  $\mu$  such that all students are better off. Then there is a student  $a_1$  such that  $\mu(a_1) P_{a_1} C H(a_1)$ . Let us define  $c_1 = C H(a_1)$  and  $c_2 = \mu(a_1)$ . Since  $\mu$  strictly dominates  $C H$ , we know that  $\mu(c_2) \succ_{c_2} C H(c_2)$ , meaning that there exists a student  $a_2$  such that ranked  $c_2$  prefers  $a_2$ , and either  $a_2$  ranked  $c_2$  higher than  $a_1$  ranked  $c_2$  or  $a_1$  and  $a_2$  ranked  $c_2$  in the same ranking, but  $c_2$  prefers  $a_2$ . Denote  $r(a_i, c_j)$  as the ranking  $a_i$  gave to  $c_j$ , and inductively define  $c_{(n+1)} = \mu(a_n)$  and  $a_{(n+1)} = C H(\mu(a_n))$ . Then

$$\begin{aligned} r(a_{(n+1)}, c_{(n+1)}) &= r(C H(\mu(a_n)), \mu(a_n)) \\ &\leq r(a_n, \mu(a_n)) < r(a_n, c_n) \end{aligned}$$

, and by the method of infinite descent, we find that there is a contradiction. ■

**Theorem 3.6.** *The matching obtained from the Chicago algorithm with minority reserves is not strategy-proof.*

Proof) We continue with the example of students and schools given in 3.4:

$$\begin{aligned} p(a_1) &= c_1, c_2, a_1 \\ p(a_2) &= c_2, c_1, a_2 \\ p(a_3) &= c_1, c_2, a_3 \\ p(c_1) &= a_1, a_3, a_2, c_1 \\ p(c_2) &= a_1, a_3, a_2, c_2 \end{aligned}$$

The matching resulting from the Chicago algorithm is

$$\begin{pmatrix} c_1 & c_2 \\ a_1 & a_2 \end{pmatrix}$$

, which can be manipulated by  $a_3$  if he decides to report his preferences as  $P(a_3) = c_2, c_1, a_3$ . ■

The Chicago mechanism is neither stable nor strategy-proof when evaluated in the context of minority reserves within a school choice system. However, it is Pareto-optimal. When both the Chicago and Gale-Shapley mechanisms are subjected to truncated preferences, they are found to be neither stable nor Pareto-optimal, and both are manipulable. Therefore, the question arises as to which mechanism is more manipulable than the other. While it is possible that neither mechanism is more manipulable, if it can be demonstrated that the Gale-Shapley algorithm produces a more favorable matching than the Chicago algorithm under truncated preferences, it can be concluded that the Gale-Shapley algorithm is objectively superior to the Chicago algorithm in this context.

**Theorem 3.7.** *Suppose each student has a complete rank ordering and  $k > 1$ . The old Chicago Public Schools mechanism with minority reserves  $CHI_{min}^k$  is at least as manipulable as any weakly stable mechanism.*

Proof) First, fix a problem  $P$  and let  $\Phi$  be an arbitrary mechanism that is weakly stable. Suppose that  $CHI^k$  is not manipulable for problem  $P$ .

*Claim 1:* Any student assigned under  $CHI_{min}^k(P)$  receives her top choice school.

Proof. There must be a student that is assigned to a school she has not ranked first. If not, since each student has a complete rank order list,  $|I_t| > Q_t$  for all types  $t$  and  $k > 1$ , there must be a student  $a$  that is assigned to a school she has not ranked first. Consider the highest composite score student  $i$  who is unassigned and is in the same type as student  $a$ . Student  $i$  can rank school  $S$  first and will be assigned a seat there in the first round of  $CHI^k$  mechanism instead of some student who has not ranked school  $S$  first. That contradicts  $CHI^k$  is not manipulable for problem  $P$ .

*Claim 2:* The set of students who are assigned a seat under  $CHI^k(P)$  is equal to the set of top  $\Sigma_S q_S^t$  composite score students in type  $t$  and the next  $\Sigma_S q_S^0$  students who are not assigned a seat.

Proof. If not, there is a school seat assigned to a student  $y$  who does not have a top  $\Sigma_S q_S^t$  score in type  $t$  or to a student  $z$  who ranked lower than the next  $\Sigma_S q_S^0$  students.

1. Let student  $i$  be the highest scoring top  $\Sigma_S q_S^t$  student in type  $t$  who is not assigned. Since student  $i$  has a complete

rank order list, she can manipulate  $CHI^k$  by ranking student  $y$ 's assignment as her top choice again contradicting  $CHI^k$  is not manipulable for problem  $P$ .

2. Let student  $j$  be the highest scoring student in who ranked lower than the next  $\Sigma_S q_S^0$  students. Since student  $j$  has a complete rank order list, she can manipulate  $CHI^k$  by ranking student  $z$ 's assignment as her top choice again contradicting  $CHI^k$  is not manipulable for problem  $P$ .

*Claim 3.* In problem  $P$ , the matching obtained through  $CHI^k(P)$  is the unique weakly stable matching.

Proof. Let us define the term "top students" as the top  $\Sigma_S q_S^t$  composite score students in type  $t$  and the next  $\Sigma_S q_S^0$  students who are not assigned a seat. By Claims 1 and 2, it is possible to assign the top students a seat at their top choice school under  $P$  and  $CHI^k(P)$  picks that matching. Let  $\mu \neq CHI^k(P)$ . That means under  $\mu$  there exists a top student  $i$  who is not assigned to her top choice  $s$ . Pick the highest composite score such student  $i$ .

Since all higher score students are assigned to their top choices, either there is a vacant seat at her top choice  $s$  or it admitted a student with lower composite score. It is trivial that the pair  $(i, s)$  strongly blocks matching  $\mu$  in the former case, and in the latter, there is always a student ranked lower than  $i$  who is not in the quota of his type. Hence  $CHI^k(P)$  is the unique weakly stable matching under  $P$ . We are now ready to complete the proof. By Claim 3,  $\Phi(P) = CHI^k(P)$  and hence mechanism  $\Phi$  assigns all top students a seat at their top choices. None of the top students has an incentive to manipulate  $\Phi$  since each receives her top choice. Moreover, no other student can manipulate  $\Phi$  because regardless of their stated preferences,  $\Phi(P) = CHI^k(P)$  remains the unique weakly stable matching and hence  $\Phi$  picks the same matching for the manipulated economy. Hence, any other weakly stable mechanism is also not manipulable under  $P$ . ■

**Proposition 3.8** *Suppose there are at least  $k$  schools and let  $k > 1$ . The truncated old Chicago mechanism for minorities ( $CHI_{min}^k$ ) is more manipulable than the truncated Gale-Shapley mechanism ( $GS_{min}^k$ ) for minorities.*

Proof) If we look at a problem with three schools and three students whose preferences are truncated as the following:

$$\begin{aligned} p(a_1) &= c_1, c_2 \\ p(a_2) &= c_3, c_2 \\ p(a_3) &= c_1, c_3 \\ p(c_1) &= a_1, a_3, a_2, c_1 \\ p(c_2) &= a_1, a_3, a_2, c_2 \\ p(c_3) &= a_1, a_3, a_2, c_3 \end{aligned}$$

The Gale-Shapley mechanism yields the following matching:

$$\begin{pmatrix} c_1 & c_2 & c_3 \\ a_1 & a_2 & a_3 \end{pmatrix}$$

, which is strategy-proof. However, the Chicago mechanism results in

$$\begin{pmatrix} c_1 & c_2 & c_3 \\ a_1 & a_2 & a_2 \end{pmatrix}$$

, which is manipulable since  $a_3$  can falsely report his preferences as  $P(a_3) = c_3, c_2$  and be better off by being matched with  $c_3$ . Therefore,  $CHI_{min}^k$  is more manipulable than  $GS_{min}^k$ . ■

Hence, we can conclude that in a minority-reserve context, when preferences are truncated, the Chicago mechanism is more manipulable than the Gale-Shapley mechanism.

**Conjecture 3.9.** *We can find counterexamples in the proof above regardless of the number of schools and students, number of types, and quota for each school.*

Explanation) To do this, we first define  $q_{(i,j)}$  as the quota of type  $j$  for school  $i$  ( $i$  starts at 1,  $j$  starts at 0). For example,  $q_{1,5}$  is the quota of type 5 students for school 1. Also, define  $\Sigma_i q_{i,j}$  by  $Q_j (> |I_j|$  for  $j \leq 1$ ), which is the number of students in school  $i$ . We are curious whether we can always find a set of preferences for any  $t$  and  $q_{i,j}$ . This problem is yet to be solved. ■

## 4 Conclusion

The focus of our research was to compare the performance of two different mechanisms, the Gale-Shapley algorithm and the Chicago mechanism, in a school choice context. We evaluated whether these mechanisms possessed the properties of stability, Pareto-efficiency, and manipulability, and compared their performance when preferences are truncated.

Our findings indicated that when preferences are truncated, the Chicago mechanism is more manipulable than the Gale-Shapley algorithm. This has important implications for understanding the strengths and weaknesses of each mechanism in practical applications.

Furthermore, this study contributes to the existing body of research by filling a gap in the literature. We constructed a framework that enables researchers to assess the performance of matching mechanisms in minority reserves. Overall, this research provides valuable insights into the real-world applications of matching mechanisms and underscores the need for careful consideration of specific characteristics when selecting an appropriate mechanism.

## References

- Abdulkadiroğlu, A., Sönmez, T. (2003). School choice: A mechanism design approach. *American economic review*, 93(3), 729-747.
- Benabbou, N., Chakraborty, M., Ho, X. V., Sliwinski, J., Zick, Y. (2018, July). Diversity constraints in public housing allocation. In 17th International Conference on Autonomous Agents and MultiAgent Systems (AAMAS 2018).
- Ehlers, L., Hafalir, I. E., Yenmez, M. B., Yildirim, M. A. (2014). School choice with controlled choice constraints: Hard bounds versus soft bounds. *Journal of Economic theory*, 153, 648-683.
- Gale, D., Shapley, L. S. (1962). College admissions and the stability of marriage. *The American Mathematical Monthly*, 69(1), 9-15.
- Pathak, P. A., Sönmez, T. (2013). School admissions reform in Chicago and England: Comparing mechanisms

by their vulnerability to manipulation. *American Economic Review*, 103(1), 80-106.

Roth, A. E., Sotomayor, M. (1992). Two-sided matching. *Handbook of game theory with economic applications*, 1, 485-541.

Sönmez, T., Switzer, T. B. (2013). Matching with (branch-of-choice) contracts at the United States Military Academy. *Econometrica*, 81(2), 451-488.

# CONTRIBUTORS

First, we would like to express our deepest gratitude to the following contributors for helping create Singapore American School's very first pure and applied mathematics journal:

## TEACHER REVIEWERS

Mr. Saylar Craig, Mathematics Department

Mr. Jason Son, Mathematics Department

Ms. Darlene Poluan, Mathematics Department

Mr. Tim Zitur, Mathematics Department

from Singapore American School



## Contact

kang782455@sas.edu.sg

40 Woodlands Street 41, Singapore 738547

Singapore American School

Welcome to the launch of the SAS Mathematics Journal, the school's first-ever publication dedicated to showcasing the diverse and fascinating world of math!

This journal was brought to life through the hard work of our teacher reviewers and talented team of editors who share a passion for helping people understand and appreciate the power and beauty of math. With this journal, we aim to engage and inspire readers of all ages and levels of mathematical knowledge; whether you're a seasoned mathematician or just starting to explore this intricate field, there's something for everyone.

We're excited to embark on this journey, and we look forward to your feedback and ideas for future issues. Happy reading!

## STUDENT AUTHORS

### Editors-in-Chief

Gyulim Jessica Kang (11th grade, class of 2024)

Frank Xie (11th grade, class of 2024)

### Editors

Gaurav Goel (12th grade, class of 2023)

Morgan Ahn (11th grade, class of 2024)

Irene Choi (11th grade, class of 2024)

Hyeonseo Kwon (11th grade, class of 2024)

Akshay Agarwal (10th grade, class of 2025)

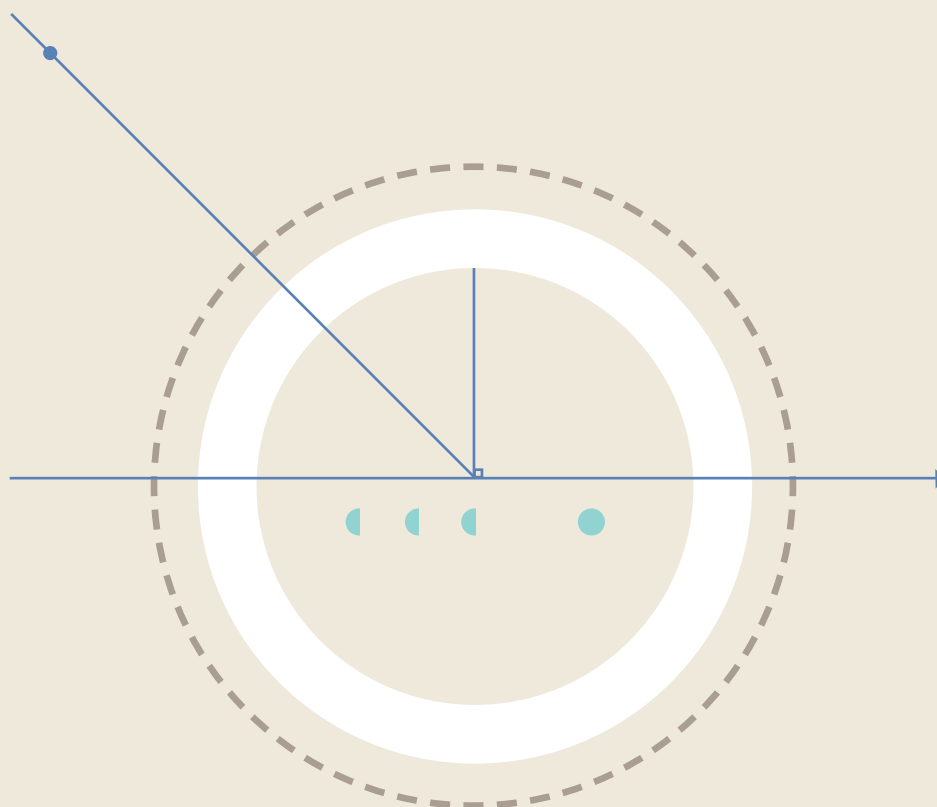
Benjamin Cheong (11th grade, class of 2024)

Sunghan Billy Park (10th grade, class of 2025)

Finding an Alternate Model to Malthusian  
Population Growth Model  
Evaluating Affirmative Action in School  
Choice

Application of Eigenvectors and Eigenvalues:  
SVD Decomposition in Latent Semantic Analysis

Creating a Machine Learning Pipeline to  
Perform Topological Data Analysis



2023

